REVIEWS OF GEOPHYSICS

VOLUME 5 NOVEMBER 1967 NUMBER 4

Dynamics of the Motion of a Phase Change Boundary to Changes in Pressure[1]

RICHARD J. O'CONNELL AND G. J. WASSERBURG

Charles Arms Laboratory of Geological Sciences
California Institute of Technology, Pasadena, California

Abstract. Because of the significance of both shallow and deep phase changes to geophysical problems, the dynamical response of a phase change to pressure loading was investigated. It was found that the characteristic behavior of the system may be analyzed in terms of simple parameters of the system by using analytic expressions that apply for the initial part and the final part of the motion of the phase boundary. These expressions are obtained from approximations based on generalizations of Neumann's solution for melting at a constant temperature or from simple physical approximations based on the over-all geometry of the model. The range of applicability of the approximations can be obtained from the approximations themselves. The analytic results compare very favorably with exact numerical solutions. The distribution of heat sources and convective heat transport are shown to be generally of minor importance on the motion of the phase boundary; the effect of convective heat transport can be estimated from the analytic approximation. The important parameters are the latent heat of the phase change and the difference in slope between the Clapeyron curve and the temperature distribution in the earth. In addition, the long-term motion depends primarily on the over-all geometry of the model and the boundary condition at depth. The analytic results indicate the time at which thermal blanketing by sediments becomes important and the effect of the rate of sedimentation on the response of the system; they also define slow and fast sedimentation and secular equilibrium. The effect of isostasy in conjunction with a shallow phase change is shown to be of major importance, and for certain cases the sediment thickness that can accumulate in a sedimentary basin may depend only on the sedimentation rate and not the initial depth of the basin. The analytic results permit a more physical discussion of the problem, since the functional dependence of the solution on the parameters may be seen. In addition, important results for a variety of models can be obtained by relatively simple calculations, without resorting to separate numerical solutions for each model considered.

[1] California Institute of Technology Contribution 1494.

NOTATION

t, time.
x, depth.
$T(x, t)$, temperature.
$M(t)$, location of phase boundary.
$b(t)$, location of lower boundary.
$-J(x, t)$, heat flux.
$P(x)$, pressure.
$\mathfrak{T}_c(P) = GP - F = T_c(x)$, Clapeyron temperature.
K_j, thermal conductivity in region 'j.'
ρ_j, density in region 'j.'
c_v, heat capacity at constant volume.
c_j, heat capacity c_v in region 'j.'
κ_j, thermal diffusivity in region 'j.'
A_j, heat production due to sources in region 'j.'
V_j, velocity in region 'j.'
L, latent heat of phase change.
S_j, entropy per gram of *phase* 'j.'
g, gravitational acceleration.
$\Theta(x, t) \equiv T(x, t) - T(x, 0)$, perturbation temperature.
$M_i \equiv M(0)$, initial location of phase boundary.
$M_f \equiv M(\infty)$, final location of phase boundary.
ΔP, pressure pulse.
$b_i \equiv b(0)$, initial location of lower boundary.
$b_f \equiv b(\infty)$, final location of lower boundary.
s, sediment thickness.
w, water depth.
$\tilde{\theta}, \tilde{\tau}, \tilde{\xi}$, tilde denotes approximation to corresponding quantity (θ, τ, ξ).

DIMENSIONLESS TERMS

$b_0 \equiv b(0)$
$T_0 \equiv [J(0, 0)/K_1]b_0$
$\xi \equiv x/b_0$, depth.
$\tau \equiv (\kappa_1/b_0^2)t$, time.
$\eta(\xi, \tau) \equiv T(x, t)/T_0$, temperature.
$\xi_m(\tau) \equiv M(t)/b_0$, location of phase boundary.
$\beta(\tau) \equiv b(t)/b_0$, location of lower boundary.
$\eta_c(\xi) \equiv T_c(P)/T_0$, Clapeyron temperature.
$\alpha_i \equiv \kappa_i/\kappa_1$, diffusivity.
$\sigma_i \equiv b_0^2 A_i/T_0 K_i$, heat sources.
$\nu \equiv (b_0/\kappa_1)V$, velocity.
$C \equiv L/c_1 T_0$, latent heat.
$\theta(\xi, \tau) \equiv \eta(\xi, \tau) - \eta(\xi, 0)$, perturbation temperature.
$\theta_c(\xi) \equiv \eta_c(\xi) - \eta(\xi, 0)$, reduced Clapeyron temperature.
$\gamma_i \equiv [J(0, 0)/K_i](b_0/T_0)$, temperature gradient.
$D \equiv (G\rho_1 g b_0/T_0) - \gamma_1$, reduced Clapeyron slope.
$E \equiv (F/T_0) - (G\,\Delta P/T_0)$, zero intercept of $\theta_c(\xi_m)$.
$W \equiv 1 - J(0, 0)/G\rho_1 g K_1$
$R \equiv \rho_s c_1 b_0/W K_1\, ds/dt$, sedimentary loading rate.
$r \equiv 4D/C\sqrt{\pi}$, rate constant for continuous sedimentation models.
$\tilde{\tau}^*$, see equation 36.
$\tilde{\tau}^{**}$, see equation 46.
$\tilde{\tau}_l$, see equation 44.
$\tilde{\tau}^\dagger$, see equation 48.
$\tilde{\tau}^{\dagger\dagger}$, see equation 49.
$\tilde{\tau}_B$, see equation 57.

1. INTRODUCTION

There is no doubt that phase changes are a significant feature of the earth's mantle; thus a response of a phase change to dynamical changes in pressure is of general geophysical interest. Although the discussion to be presented in this paper emphasizes shallow phase changes, the formal treatment developed is applicable to the more general problem.

The identification of the Mohorovicic discontinuity as a phase change has been shown to have important geological implications. *Lovering* [1958] and *Kennedy* [1959] have discussed such a phase change as a mechanism for uplifting or depressing relatively large areas of the earth's surface and have alluded to the pertinence of this mechanism to such questions as the formation of geosynclines, the elevation of plateaus, and the origin and permanence of mountain ranges.

The consequences of such a phase change result from the fact that the depth of the phase boundary is determined by the temperature and pressure in the earth; hence changes in either of these might change the equilibrium position of the phase boundary. If sediments are deposited on the surface, the resultant increase in pressure will tend to move the phase boundary upward, which, owing to the difference in density of the two phases, will cause the surface to subside. The conversion of a low density–high entropy phase to a high density–low entropy phase will result in the liberation of heat at the phase boundary. The removal of this extra heat will govern the rate of movement of the phase boundary.

Owing to the subsidence of the surface and the different thermal conductivities of the two phases, the new equilibrium position of the phase boundary may result in a final steady-state temperature distribution different from the initial distribution. This redistribution may extend to considerable depth and may therefore depend on thermal conditions deep in the earth. Since the new temperature distribution will partly determine the final equilibrium position of the phase boundary, it will affect its movement.

The presence of sediments on the formerly free surface will also affect the final temperature distribution, causing the temperature beneath the former surface to rise, which would tend to move the phase boundary deeper.

Thus there are basically two different effects: (1) an increase in pressure causes the surface to subside in response to the loading, and (2) the thermal blanketing of any deposited sediments would by itself cause the surface to rise in opposition to the loading. Modifying these two effects are (3) the fact that the latent heat must be removed from the vicinity of the phase boundary for the reaction to proceed, and (4) the final temperature distribution may require the redistribution of heat from the initial distribution.

MacDonald and Ness [1960] have already treated certain aspects of the dynamic problem; because of the possible importance of the problem, however, it was considered of interest to treat the problem in more detail in order to separate the effects of the various factors that together determine the solution.

Wetherill [1961] has treated some of the steady-state aspects of the problem, which predict the final location of the phase boundary after the deposition of a given thickness of sediments. He showed that, although the identification of the Moho as a single phase change cannot explain the differences between oceans and continents, response of a phase change to loading by sediments could result in considerable differences in crustal elevation. Further, the necessity to include isostasy in the solution to the dynamic problem was stressed, as well as the importance of the rate of erosion on uplifted regions. Finally, the possible importance of convective heat transport in the dynamic problem was pointed out.

Although the problem treated in this paper does not fully consider isostasy or

continuous sedimentation and erosion, it is still of considerable geophysical interest. The essential process that will be treated is the response of a phase change to changes in pressure; the effects of isostasy, sedimentation, and erosion will be primarily to modify the pressure response. Our first object is, therefore, to examine the response of a phase change to a given pressure pulse, and the dependence of this response on various parameters. To this end it is desirable to treat at first a highly simplified problem in order to separate various effects. We later consider the effect of the altered equilibrium temperature distribution on the movement of the phase boundary.

To formulate the problem in one dimension we represent the outer layers of the earth as an infinite plate of uniform thickness. We thus neglect the sphericity of the earth; this omission should not be serious, however, owing to the restricted thickness of the region considered (100–200 km).

The relevant equation is the equation of heat conduction

$$\rho c(DT/Dt) = \rho c[\partial T/\partial t + V(\partial T/\partial x)] = (\partial/\partial x)[K(\partial T/\partial x)] + A \qquad (1)$$

where T = temperature.
K = thermal conductivity.
ρ = density.
c = heat capacity.
A = rate of radioactive heat production.
V = velocity of medium.

The boundary conditions to be satisfied are:

(*a*) $T = 0$ at the earth's surface.

(*b*) a boundary condition must be applied at the bottom of the region, i.e. at some depth in the earth. The exact condition is not known; however, it should be contained between the following extremes:

(1) Constant temperature at the bottom of the region $x = b$. This means that the temperature in regions below the depth $x = b$ will be unaffected by changes at depths less than b.

(2) Constant heat flux at depth $x = b$. This means that changes in temperature at shallow depth might cause changes at all depths to the earth's center.

Since the process would actually take place only in a restricted segment of the earth, the temperature at depth would be controlled by lateral flow of heat. Constant flux at $x = b$ implies that heat flows laterally. Constant temperature implies that no heat flows laterally.

Knowledge of the effect of the choice of the boundary condition on the solution to the problem would indicate possible limitations of the solution obtained from this model.

(*c*) At the phase boundary $M(t)$, the temperature must be continuous and will be given by the Clapeyron curve, which gives the temperature at which the two phases may coexist at a given pressure. The liberation of the latent heat of reaction at the phase boundary requires

$$\left[K(x)\frac{\partial T}{\partial x}\right]_{x=M^-(t)} - \left[K(x)\frac{\partial T}{\partial x}\right]_{x=M^+(t)} = -L\rho\frac{dM(t)}{dt} \tag{2}$$

where L = latent heat of phase change and ρ = density of region in which the coordinate system is fixed. Thus there will be a discontinuity in the heat flux at the phase boundary due to the evolution of heat.

We will assume that the stress distribution is always hydrostatic. Conservation of mass across the phase boundary will determine the velocity in the field equation 1. In addition, heat sources must be conserved across the phase boundary.

There are two major sources of difficulty in the problem. The first is the nonlinear condition (2) at the phase boundary. The second is the nonlinear term for convective heat transport in the heat equation. This term could conceivably be neglected if it were small enough. If so, the search for an analytic solution would be greatly simplified. Thus it is of interest to determine the magnitude and importance of the term $V(\partial T/\partial x)$ in the field equation.

The approach in this paper will be to analyze the problem in certain limiting cases. We will then show that these cases exhibit a simple behavior, which can be characterized in terms of simple functions of the physical constants. These relationships will be applied to the more general case, and it will be shown that this can be treated semiquantitatively with the approximate analytical expressions obtained.

2. STEADY-STATE BEHAVIOR

Before discussing the dynamics of the motion of a phase boundary subject to loading, it is of interest to develop the properties of the steady-state systems. Consider a layered system of two phases (1, 2) in hydrostatic equilibrium containing no heat sources at equilibrium. Let the Clapeyron curve be a straight line defined by $\mathfrak{I}_e(P) = GP - F$, let the initial depth of the transition be M_i, and let the initial total thickness of the layers be $b(0)$. The mass per unit area between the surface and the base of the lower layer is $m \equiv \rho_1 M_i + \rho_2(b(0) - M_i)$. The initial temperature is given by

$$T_i(x) = \begin{cases} \dfrac{J_i x}{K_1} = \dfrac{J_i P(x)}{K_1\rho_1 g}; & 0 \le x \le M_i \\ \dfrac{J_i M_i}{K_1} + \dfrac{J_i(x - M_i)}{K_2} & \\ \qquad = \dfrac{J_i P(M_i)}{K_1\rho_1 g} + \dfrac{J_i[P(x) - P(M_i)]}{K_2\rho_2 g}; & M_i \le x \le b(0) \end{cases} \tag{3}$$

where $-J_i$ is the initial heat flux at the surface $x = 0$. The initial pressure as a function of depth is

$$P_i(x) = \begin{cases} \rho_1 g x & 0 \le x \le M_i \\ \rho_1 g M_i + \rho_2 g(x - M_i) & M_i \le x \end{cases} \tag{4}$$

The initial position of the phase boundary is given by

$$M_i = \frac{F}{\rho_1 g(G - J_i/K_1\rho_1 g)}$$

$$P_i(M_i) = \frac{F}{(G - J_i/K_1\rho_1 g)} \tag{5}$$

$$T_i(M_i) = \frac{J_i F}{K_1\rho_1 g(G - J_i/K_1\rho_1 g)}$$

If we assume for simplicity that $K_1\rho_1 = K_2\rho_2$, then on the (P, T) plane, the initial temperature T_i is a straight line of slope $J_i/K_1\rho_1 g$. This is shown in Figure 1. The point of intersection of $T_i[x(P)]$ and $\mathfrak{T}_c(P)$ is very sensitive to the difference between the Clapeyron slope $[d\mathfrak{T}_c(P)/dP] = G$ and the temperature slope $[dT_i(P)/dP] = J_i/K_i\rho_1 g$.

Let us now consider the new state that will obtain for this system at the instant that a sudden pressure pulse ΔP is applied and maintained. This means that the pressure of every piece of matter is increased by ΔP and the temperature at that

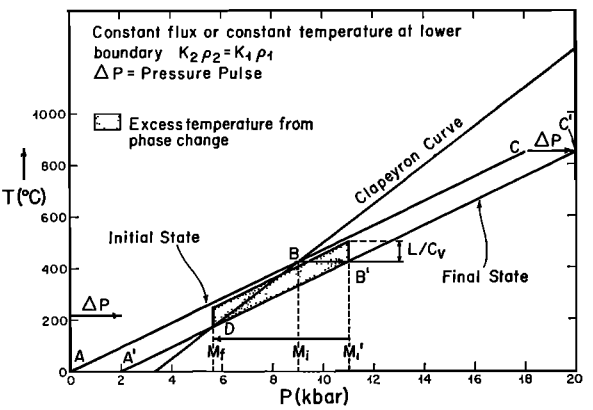

Fig. 1. Representation in the pressure-temperature plane of the effect of a pressure pulse ΔP on a phase change. The initial temperature distribution is shown by the line ABC. The phase boundary is originally at depth M_i, corresponding to point B. The pressure pulse increases the pressure at depth M_i; thus point B is moved to B' in pressure space, although the depth of the phase boundary is unchanged. The change in the temperature distribution due to the pressure pulse is represented by the translation of the line ABC into line $A'B'C'$ and of the point M_i to M_i'. The difference in pressure between the initial and final positions of the phase boundary corresponds to the arrow between M_i' and M_f. In order that the phase change move to its final position at M_f, the latent heat $L\rho(M_i - M_f)$ must be removed. The line displaced vertically by L/C_v is the increase in temperature that would occur if the phase change proceeded instantaneously in the region between M_f to M_i'.

instant remains constant. Hence, $P(x)$ is replaced by $P(x) - \Delta P$ in the expressions for $T(x)$.

$$T = \frac{J_i(P - \Delta P)}{K_1\rho_1 g}; \qquad P = \begin{cases} \rho_1 g x + \Delta P & 0 \leq x \leq M_i \\ \rho_1 g M_i + \rho_2 g(x - M_i) + \Delta P & M_i \leq x \leq b_i \end{cases} \tag{6}$$

This is the initial state translated by a distance ΔP in the (P, T) plane. In the (P, T) plane, the translated position of the initial phase boundary M_i is indicated by M_i' and corresponds to the motion of point B to B', as shown in Figure 1. If we assume the pressure pulse to be due to a load with no thermal impedance, then the final steady state will correspond to the translated line. The surface and bottom of the system correspond to points A' and C', respectively. The final equilibrium position of the phase change occurs at depth M_f, corresponding to point D in the diagram.

$$\begin{aligned} M_f &= M_i - \frac{G\,\Delta P}{\rho_1 g(G - J_i/K_1\rho_1 g)} = M_i\left(1 - \frac{G\,\Delta P}{F}\right) \\ P(M_f) &= P_i(M_i) - \frac{G\,\Delta P}{(G - J_i/K_1\rho_1 g)} = P_i(M_i)\left(1 - \frac{G\,\Delta P}{F}\right) \\ T(M_f) &= T_i(M_i) - \frac{GJ_i\,\Delta P}{K_1\rho_1 g(G - J_i/K_1\rho_1 g)} = T_i(M_i)\left(1 - \frac{G\,\Delta P}{F}\right) \end{aligned} \tag{7}$$

The fractional changes in the position, temperature, and pressure of the phase boundary at the new equilibrium position is thus $-(G\,\Delta P/F)$.

The difference between the new equilibrium temperature and the original unperturbed temperature as a function of position is defined by $\Theta(x, t) \equiv T(x, t) - T_i(x)$, and it is identically zero for the simple case under discussion.

The total heat energy per unit area that the system must lose to go from the initial to the final state is $L(M_f - M_j)\,\rho_1$. The temperature rise that a unit of matter would undergo if it instantaneously underwent the transition is L/c_v as shown in Figure 1. If $(L/c_vG) \geq \Delta P$, then no piece of matter will completely undergo the transition instantaneously, as this would drive it to a temperature above the Clapeyron curve. In this case the phase boundary will move at a rate determined by equation 2, if the transition is initiated at the initial interface, and the matter will never be superheated outside of its stability field. The possibility of mixtures of the two phases will not be considered here.

If the pressure pulse $\Delta P > (L/c_vG)$, there will exist a finite region that may spontaneously undergo the transition without intersecting the Clapeyron curve. If ΔP satisfies this condition, we will define the system to be overdriven. This is indicated by the region between M_i'' and M_i', corresponding to $P(M_i') - P(M_i'') = [(G\Delta P/F) - (L/c_vF)]\,P_i(M_i)$. M_i'' is the depth at which the Clapeyron curve intersects the top of the stippled region in Figure 1. The matter that is at pressures between $P(M_f)$ and $P(M_i'')$ is metastable and superpressured.

We have so far assumed that the agent causing the jump ΔP in pressure has no thermal impedance. If it has the same properties (i.e. ρ_1, K_1) as were initially above the phase boundary, then the final state will correspond to the initial state.

Immediately after the pressure pulse is applied, the phase boundary will move to shallower depths and lower pressures, approaching M_f, and will then reverse its motion and return to M_i. The addition of heat is then required to raise the temperature of the original material extending to the lower boundary, causing a long-term transient.

The behavior of the above system is greatly simplified because of the assumption that $K_1\rho_1 = K_2\rho_2$. We will now discuss the case in which the material properties are different in region 1, above the transition, and in region 2, below the transition. Let the lower boundary of region 2 be a distance $b(0)$ below the surface. We first consider the case in which the flux at the lower boundary is fixed. The initial temperature and pressure as a function of depth is given by equations 3 and 4, and the initial position and pressure at the phase boundary by equation 5. In the (P, T) plane, the initial temperature distribution consists of two straight line segments of slope $J_i/K_1\rho_1 g$ and $J_i/K_2\rho_2 g$ in regions 1 and 2, respectively. This is shown in Figure 2 for the case $K_2\rho_2 = 2K_1\rho_1$.

Immediately after the application of an increment ΔP in pressure, the T-P curve is translated to the right as stated earlier. The phase boundary moves to M_i', and the lower boundary $b(0)$ of region 2 moves from point C to C'. Since we have required that the flux at the lower boundary remain constant, the final state will have the same slope in regions 1 and 2 as the initial state. The difference between the final and initial states is markedly different than for the simple case where $\Theta(x, \infty) = 0$.

Here

$$\Theta(x, \infty) = T(x, \infty) - T_i$$

$$= \begin{cases} 0 & 0 \le x \le M_f \\ -J_i\left\{\frac{1}{K_1} - \frac{1}{K_2}\right\}(x - M_f) & M_f \le x \le M_i \\ -J_i\left\{\frac{1}{K_1} - \frac{1}{K_2}\right\}(M_i - M_f) & M_i \le x \le b(\infty) \end{cases} \tag{8a}$$

or as a function of pressure

$$\Theta = \begin{cases} 0 & \Delta P \le P \le P(M_f) \\ -J_i\left\{\frac{1}{K_1\rho_1 g} - \frac{1}{K_2\rho_2 g}\right\}[P - P(M_f)] & P(M_f) \le P \le P(M_i') \\ -J_i\left\{\frac{1}{K_1\rho_1 g} - \frac{1}{K_2\rho_2 g}\right\}[P(M_i') - P(M_f)] & P(M_i') \le P \le P(b(\infty)) \\ & = P_i(b(0)) + \Delta P \end{cases} \tag{8b}$$

P_f and M_f are given by equation 7.

Since the pressure on each unit of matter is assumed to be conserved after the pulse is applied, the time trajectories of each point are constrained to move vertically in the (P, T) plane. The propagation of the phase boundary under the assumptions given will proceed in the same manner as discussed for the simple

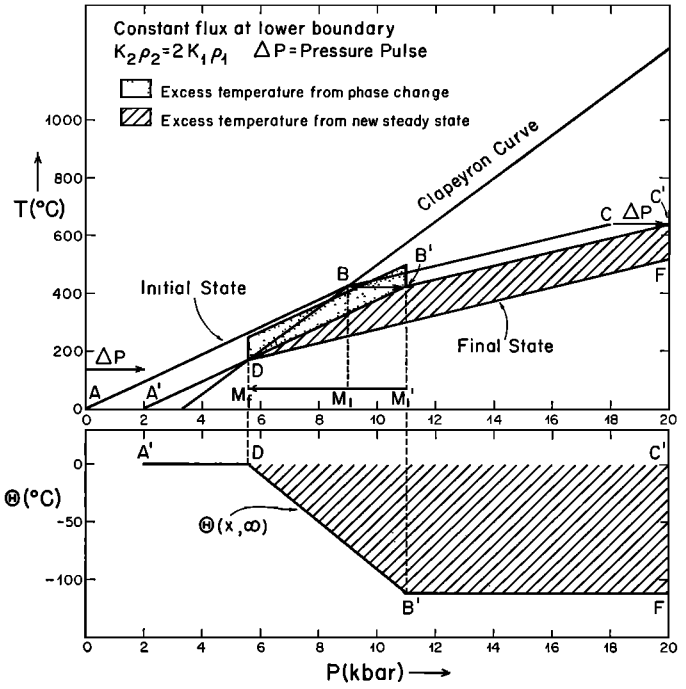

Fig. 2. Pressure temperature representation of the effects of a pressure pulse for constant flux at the lower boundary when the physical parameters of the two phases differ. The initial state shown by line *ABC* is translated to *A'B'C'*, owing to the pressure pulse. The final state is shown by line *A'DF*. Since the translated initial and final steady-state temperature distributions differ, the heat corresponding to the difference between the initial and final states (the hatched region) must be removed, as well as the latent heat, in order for the phase boundary to move from its initial position M_i' to its final position M_f. The lower curve shows the perturbation temperature $\Theta(x,\infty)$, which is the difference in temperature between the final and initial states $[\Theta(x,\infty) = T(x,\infty) - T(x,0)]$. $\Theta(x,\infty)$ is a continuous function comprised of three straight-line segments.

case $\rho_1 K_1 = \rho_2 K_2$. If the source of the pressure pulse has no thermal impedance, the excess heat per unit area corresponding to

$$-\int_{P(M_f)}^{P(b(0))+\Delta P} \Theta \frac{c_v\, dP}{g\rho}$$

must be removed in addition to the excess heat from the phase change.

If the source of the pressure pulse is a material of identical properties to region 1 and was initially at 0°C, then the phase boundary will move from M_i' toward M_f and then reverse and return to M_i; the final state will be the same as the initial state, except that heat will have to be added to the system to raise the temperature of the translated curve *A'B'C'* of Figure 2 to the temperature of curve *ABC*, the heat being provided from below the lower boundary. In either

case, if the load has thermal impedance or if $K_1 \neq K_2$, the system will have a long-time transient to achieve the final steady state.

So far we have emphasized the (P, T) representation of the system. The dependence on spatial coordinates is fundamentally different, since $T_i(x)$ does not change as $P \to P + \Delta P$, but $\mathfrak{I}_c(P)$ as an implicit function of x will be changed. In addition, the total depth $b(t)$ from the surface to the lower boundary depends on time, whereas the pressure is fixed in the matter. Mass conservation requires that the quantity $\rho_1 M(t) + \rho_2[b(t) - M(t)]$ be constant, so that the change in depth of the lower boundary for the preceding case with constant flux is

$$b(\infty) - b(0) = -G\,\Delta P \frac{(\rho_2 - \rho_1)}{\rho_2\rho_1 g(G - J_i/K_1\rho_1 g)} = -\frac{M_i(\rho_2 - \rho_1)}{\rho_2}\frac{G\,\Delta P}{F} \tag{9}$$

It follows that an (x, T) representation of the foregoing problem is analogous to the (P, T) representation, except that the Clapeyron curve is displaced instead of $T_i(x)$ and there is a shift in the end point $b(t)$. The trajectory of a unit of matter is thus not constrained to move vertically in the (x, T) plane, since the spatial coordinate of a unit of matter is not conserved.

The next case of steady-state behavior that we wish to consider here is for the case of the lower boundary at depth b at constant temperature $T(b(t)) = T_b$. Since the flux is not conserved, it is convenient to use the other variables to define the position of the phase boundary.

The equations governing the position of the phase boundary are

$$J_i = \frac{T(b)}{(b_i/K_2) + M_i[(1/K_1) - (1/K_2)]} \qquad J_f = \frac{T(b)}{(b_f/K_2) + M_f[(1/K_1) - (1/K_2)]}$$

$$\frac{J_f}{J_i} = \frac{1}{1 - [(M_i - M_f)/\rho_2[(\rho_2/K_1)] - (\rho_1/K_2)][J_i/T(b)]}$$

$$M_i = F \Big/ \left\{\frac{1}{2}\left[G\rho_1 g - \frac{T(b)K_2}{b_i K_1} - \frac{FK_2}{b_i K_1}\left(1 - \frac{K_1}{K_2}\right)\right]\right.$$
$$\left. + \frac{1}{2}\left[\left(G\rho_1 g - \frac{T(b)K_2}{b_i K_1} - \frac{FK_2}{b_i K_1}\left(1 - \frac{K_1}{K_2}\right)\right)^2 + 4G\rho_1 g\left(1 - \frac{K_1}{K_2}\right)\frac{FK_2}{b_i K_1}\right]^{1/2}\right\}$$

$$M_f = (F - G\,\Delta P) \Big/ \left\{\frac{1}{2}\left[G\rho_1 g - \frac{T(b)K_2\rho_2}{K_1 m}\right.\right.$$
$$\left. - \frac{(F - G\,\Delta P)}{m}\rho_2\frac{K_2}{K_1}\left(\left(1 - \frac{K_1}{K_2}\right) + \left(1 - \frac{\rho_1}{\rho_2}\right)\frac{K_1}{K_2}\right)\right] \tag{10}$$
$$+ \frac{1}{2}\left\{\left[G\rho_1 g - \frac{T(b)K_2\rho_2}{K_1 m} - \frac{(F - G\,\Delta P)}{m}\frac{\rho_2 K_2}{K_1}\left[\left(1 - \frac{K_1}{K_2}\right) + \left(1 - \frac{\rho_1}{\rho_2}\right)\frac{K_1}{K_2}\right]\right]^2\right.$$
$$\left. + 4(F - G\,\Delta P)\frac{G\rho_2\rho_1 g}{m}\frac{K_2}{K_1}\left[\left(1 - \frac{K_1}{K_2}\right) + \left(1 - \frac{\rho_1}{\rho_2}\right)\left(\frac{K_1}{K_2}\right)\right]\right\}^{1/2}\Bigg\}$$

$$T(M_i) = \frac{J_i M_i}{K_1} = \mathfrak{I}_c(P(M_i)) \qquad T(M_f) = \frac{J_f M_f}{K_1} = \mathfrak{I}_c(P(M_f))$$

$$m \equiv \rho_1 M_i + \rho_2(b_i - M_i) = \rho_1 M_f + \rho_2(b_f - M_f)$$

$$M_f^2\left(\frac{1}{K_1}-\frac{1}{K_2}\right)G\rho_1 g + M_f\left\{\frac{G\rho_1 g}{K_2}\left[b_i - \frac{(\rho_2-\rho_1)}{\rho_2}(M_i - M_f)\right]\right.$$
$$\left. - \frac{T(b)}{K_1} - \left(\frac{1}{K_1}-\frac{1}{K_2}\right)(-G\,\Delta P + F)\right\}$$
$$- \frac{1}{K_2}\left[b_i - \left(\frac{\rho_2-\rho_1}{\rho_2}\right)(M_i - M_f)\right](-G\,\Delta P + F) = 0$$

The expression for M_i is an explicit function of b_i and $T(b_i)$, and the expression for M_f is an implicit function of M_i through m.

If $(\rho_2/K_1) > (\rho_1/K_2)$ and $M_i > M_f$, the flux is increased and the temperature gradient is increased (see the expression for J_f/J_i). As a result, the temperature at the transition is increased above that which would obtain if $\rho_2 K_2 = \rho_1 K_1$, as in the first example. A schematic illustration of this case is shown in Figure 3. One of the fundamental effects of $(\rho_2/K_1) > (\rho_1/K_2)$ is that, to the low pressure side of point E (Figure 3), the temperature of the translated initial state is below the final state, and to the high pressure side of point E the reverse situation occurs. This means that in addition to the heat of the transition which must be removed,

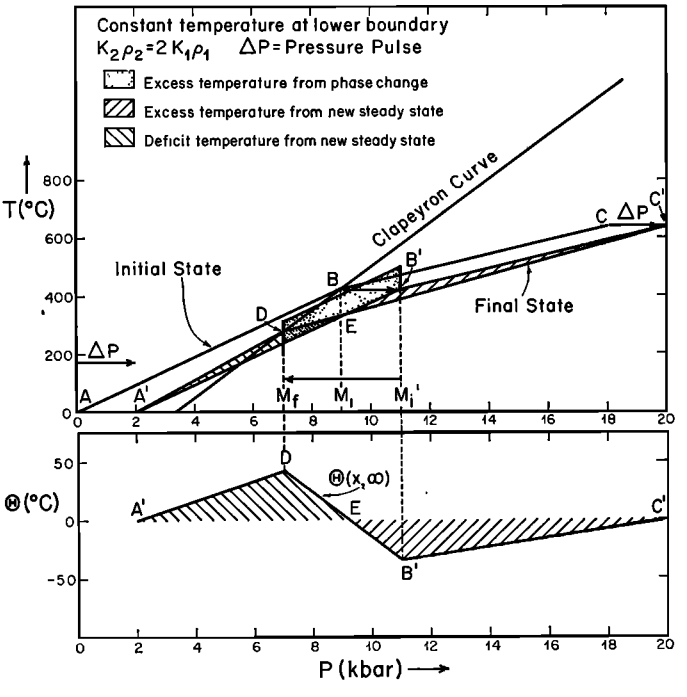

Fig. 3. Pressure temperature representation of the effect of a pressure pulse with a constant temperature at the lower boundary when the properties of the two phases differ. Besides the surplus heat in the region $EB'C'$, there is a heat deficit in the region $A'DE$ due to the difference between the translated initial state and the final state. The translated initial and final temperatures are the same at point E.

an additional amount of heat due to the excessive temperature must be removed from the right of point E. Some of this heat will go to the region to the left of E to fill in the temperature deficit. This has two major consequences. Firstly, a long-term temperature readjustment over the whole system must take place. Secondly, the kinetics of the motion of the phase boundary is somewhat enhanced because the heat lost at the front of the motion automatically tends to compensate for the difference between the initial and final states. This should be compared with the constant flux case where the system must radically alter the total heat content between initial and final states. Figure 3 shows $\Theta(x, \infty) = T_f - T_i$ for this case and illustrates the comments made above. Figure 4 shows a similar case in the (x, T) plane.

We have so far restricted the discussion to a source-free region. If sources of variable strength are present, the steady-state temperature distribution is defined by the field equation $(\partial/\partial x)[K(x)(\partial T(x)/\partial x)] + A(x) = 0$ and the boundary conditions. The position of the phase boundary is then defined by $T(M) = \mathfrak{I}_e(P(M))$,

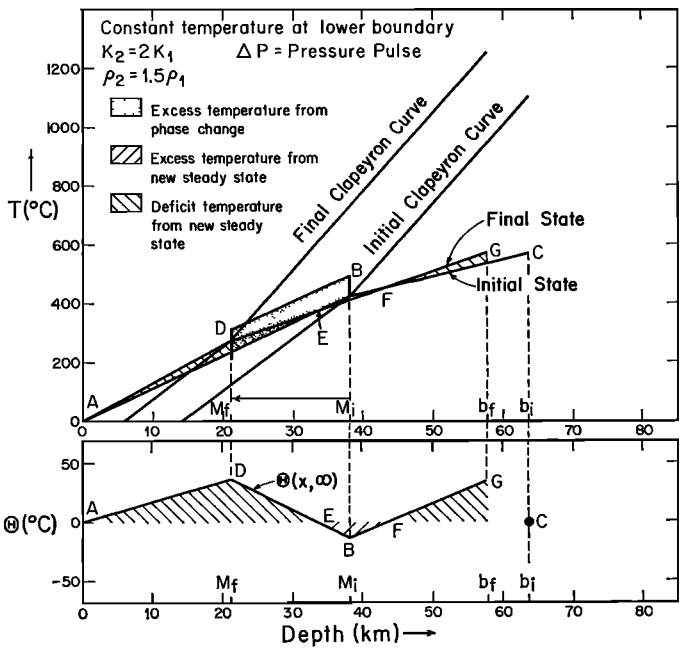

Fig. 4. A depth-temperature representation of the effect of a pressure pulse for constant temperature at the lower boundary. Both the densities and the conductivities in regions 1 and 2 are taken to be different. The initial temperature distribution is not changed by the pulse, but instead the Clapeyron curve is shifted. The initial and final Clapeyron curves are segmented in the (x,T) representation. The initial and final temperatures are given by the line segments ABC and ADG respectively. Points B and D correspond to the initial and final positions of the phase boundary. The lower boundary moves from C to G corresponding to depths b_i and b_f, respectively. Note that Θ is not defined in the region between G and C.

where $\mathfrak{I}_c(P)$ defines the Clapeyron curve. In investigating the possible positions of the phase boundary for various static loads, an additional constraint occurs from consideration of source conservation in regions into which the phase boundary may be displaced. Let $-$ and $+$ denote the low and high pressure side of the phase boundary, respectively; then $[A(M^-)/\rho(M^-)] = [A(M^+)/\rho(M^+)]$, i.e. A/ρ is continuous across the moving phase boundary in the direction of motion.

With regard to the phase transition, it is of course possible to utilize a simple two-layer model for ρ, K, c and to use an arbitrary source distribution subject to the above constraint. For the purpose of exhibiting the effects of sources, we will discuss the case of a simple two-layer model with $A_1/\rho_1 = A_2/\rho_2$.

The temperature distribution is then

$$T(x) = \begin{cases} \dfrac{J(0)x}{K_1} - \dfrac{A_1x^2}{2K_1}; & 0 \le x \le M \\ \dfrac{J(0)M}{K_1} - \dfrac{A_1M^2}{2K_1} + \left(\dfrac{J(0)}{K_2} - \dfrac{A_1M}{K_2}\right)(x - M) - \dfrac{A_1\rho_2}{2\rho_1K_2}(x - M)^2; & M \le x \le b \end{cases} \tag{11}$$

Here $J(0)$ is the flux at $x = 0$. The initial and final temperature distributions can be found by setting M equal to M_i and M_f, respectively, and $J(0)$ equal to J_i and J_f, respectively. For case of known flux, the expression for M is

$$M = \frac{F - G\,\Delta P}{\frac{1}{2}\rho_1 g\left\{\left(G - \dfrac{J(0)}{K_1\rho_1 g}\right) + \left[\left(G - \dfrac{J(0)}{K_1\rho_1 g}\right)^2 + 2(F - G\,\Delta P)\dfrac{A_1}{K_1\rho_1^2 g^2}\right]^{1/2}\right\}} \tag{12}$$

M_i can be obtained by setting $\Delta P = 0$ in the above equation. The effect of the sources is to decrease the depth M at which the phase transition takes place for a given flux.

As will be shown, the two-layer model does not fully exhibit the more general problem with sources because of the condition of source conservation.

More generally for an N layer model, where layer n lies between X_{n-1} and X_n, the temperature distribution is given by

$$T_n(x) = T_{n-1}(X_{n-1}) + \frac{J_{n-1}(X_{n-1})}{K_n}(x - X_{n-1}) - \frac{A_n}{2K_n}(x - X_{n-1})^2$$

$$X_{n-1} \le x \le X_n \quad \text{and} \quad X_0 \equiv 0$$

and

$$J_n(X_n) \equiv J_0(0) - \sum_{i=1}^{n}(X_i - X_{i-1})A_i \qquad n \ge 1$$

$T_n(x)$ is the temperature distribution in layer n which has material properties A_n and K_n.

For a two-layer model, the system is highly constrained, since the source strength in region 1 determines the strength in region 2. The simplest multilayer model which is not 'overconstrained' is with four layers. In the two neighboring regions in which the phase boundary may move, the relative source strengths are

fixed by the conservation condition. In the other two regions the source strengths may have arbitrary values. However, if the phase boundary M is at X_1 or X_2 and the sources in layers 3 and 4 are similar, then it is probably unnecessary to distinguish 3 and 4. Thus a three-layer model is sufficient for an approximate description of a system in which M is located at X_1, when A_1 and A_2 are similar in strength ($A_1/\rho_1 = A_2/\rho_2$) and A_3 is distinctly different, or when M is located at X_2 and A_1 and A_2 are distinct in strength, but A_2 and A_3 are similar ($A_2/\rho_2 = A_3/\rho_3$). These cases can correspond to M located in a high-source region or a low-source region.

In comparing the initial and final states of a system, it should be noted that the physical parameters in the regions $0 \leq x \leq M$ remain unchanged as a function of x. However, for $x \geq M$, the parameters will change, owing to the translational motion of material. This applies to the source strengths A_n as well as the conductivities. The function $\Theta(x, \infty) = T_f(x) - T_i(x)$ will contain several regions with discontinuities both in slope and in curvature due to the translation of the boundaries between the regions.

For a three-layer model with M at depth X_1 and for constant flux the expression for $\Theta(x, \infty) = T_f(x) - T_i(x)$ is, assuming $M_f \leq M_i$

$$\Theta(x, \infty) = T_{1f}(x) - T_{1i}(x) = 0 \qquad 0 \leq x \leq M_f$$

$$\Theta(x, \infty) = T_{2f}(x) - T_{1i}(x) = -J(0)\left(\frac{1}{K_1} - \frac{1}{K_2}\right)(x - M_f) + A_1 M_f{}^2\left(\frac{1}{K_2} - \frac{1}{2K_1} - \frac{\rho_2}{2\rho_1 K_2}\right) + \frac{A_1 M_f x}{K_2}\left(\frac{\rho_2}{\rho_1}\right) + \frac{A_1 x^2}{2}\left(\frac{1}{K_1} - \frac{\rho_2}{\rho_1 K_2}\right) \qquad M_f \leq x \leq M_i$$

$$\Theta(x, \infty) = T_{2f}(x) - T_{2i}(x) = -J(0)(M_i - M_f)\left(\frac{1}{K_1} - \frac{1}{K_2}\right) + \frac{A_1}{2K_1}(M_i{}^2 - M_f{}^2) - \frac{A_1}{K_2}[M_i{}^2 - M_f{}^2 - (M_i - M_f)x] + \frac{\rho_2 A_1}{2K_2\rho_1}[M_i{}^2 - M_f{}^2 - 2(M_i - M_f)x] \qquad M_i \leq x \leq X_{2f}.$$

$$\Theta(x, \infty) = T_{3f}(x) - T_{2f}(x) \qquad X_{2f} \leq x \leq X_{2i}$$

$$\Theta(x, \infty) = T_{3f}(x) - T_{3i}(x) \qquad X_{2i} \leq x \leq X_{3f}$$

where $\rho_1 M_i + \rho_2(X_{2i} - M_i) = \rho_1 M_f + \rho_2(X_{2f} - M_f)$ from the conservation of matter. The values of M_i and M_f are determined from the same equation 12 as the one-layer model for this case. The above equations may be compared with equations 10 for the source-free cases. The case with sources is shown in Figure 5.

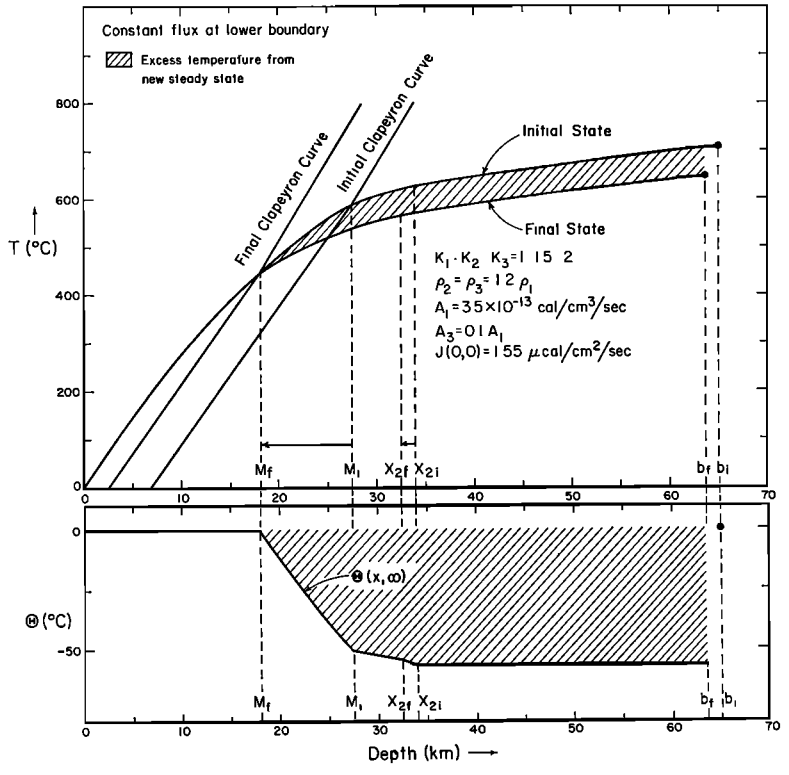

Fig. 5. Depth-temperature diagram similar to Figure 4 except for a three-layer model with sources and constant flux at the lower boundary. The boundary between layers 2 and 3, X_2, moves from X_{2i} to X_{2f} as the phase boundary moves from M_i to M_f. Note that there are discontinuities in $\partial\Theta/\partial x$ at both X_{2i} and X_{2f} due to the translation of the material in the region $X > M$. In addition $\partial^2\Theta/\partial x^2$ does not vanish for $M_f < x < M_i$ and $X_f < x < X_i$, owing to the different source strengths in the different layers. Nevertheless, the curvature is small in these two regions.

The discontinuities in $\Theta(x, \infty)$ due to the different conductivities in the different regions are apparent in Figure 5.

3. THE DYNAMIC PROBLEM

Formulation. In this section we treat the formulation of the dynamic problem in one dimension. We first exhibit the relevant equations and boundary conditions; we then reduce them to a convenient dimensionless form and introduce a dimensionless perturbation temperature relative to the initial steady state. These transformations in themselves result in a great simplification of the problem and allow significant general conclusions to be drawn.

For simplicity we consider a two-layer model with constant uniform properties, subject to a sudden pressure pulse. The geometry of the model is shown below.

$x = 0$—— surface

Region 1: $\rho_1, c_1, K_1, A_1, V_1 \equiv 0$; phase 1

$x \downarrow$ $M(t)$——

Region 2: $\rho_2, c_2, K_2, A_2, V_2$; phase 2

$b(t)$——

The surface of the earth is taken as $x = 0$, the phase boundary is at $x = M(t)$, corresponding to a point on the Clapeyron curve, and the lower boundary condition is imposed at $x = b(t)$, which is fixed in the matter in region 2. Since the coordinates are fixed in region 1, the velocity vanishes in this region.

We assume that the two phases coexist only among the plane $x = M(t)$; thus we do not consider mixtures of two phases along the Clapeyron curve. This implies that a new phase does not nucleate away from the plane $x = M(t)$.

The heat equation thus becomes

$$\begin{aligned} \frac{\partial T}{\partial t} &= \frac{K_1}{\rho_1 c_1}\frac{\partial^2 T}{\partial x^2} + \frac{A_1}{\rho_1 c_1} && 0 \le x \le M(t) \\ \frac{\partial T}{\partial t} + V_2\frac{\partial T}{\partial x} &= \frac{K_2}{\rho_2 c_2}\frac{\partial^2 T}{\partial x^2} + \frac{A_2}{\rho_2 c_2} && M(t) \le x \le b(t) \end{aligned} \tag{13}$$

The boundary equations become

$$T(0, t) = 0 \tag{14a}$$

$$T(b(t), t) = \text{constant}, \quad \text{or} \tag{14b}$$

$$J(b(t), t) = K_2\frac{\partial T}{\partial x}\bigg|_{x=b(t)} = \text{constant}$$

$$K_1\frac{\partial T}{\partial x}\bigg|_{x=M^-(t)} - K_2\frac{\partial T}{\partial x}\bigg|_{x=M^+(t)} = -L\rho_1\frac{dM(t)}{dt} \tag{14c}$$

$$T(M(t), t) = \mathfrak{Z}_c(P) \qquad \text{Clapeyron curve} \tag{14d}$$

The Clapeyron curve $\mathfrak{Z}_c(P)$ is the integral of the Clausius Clapeyron equation

$$(d\mathfrak{Z}_c/dP) = [(1/\rho_1) - (1/\rho_2)]/(S_1 - S_2) \tag{15}$$

where P = pressure and S_i = entropy per gram of phase i.

We now assume that the Clapeyron curve may be adequately represented by $\mathfrak{Z}_c(P) = GP - F$ and defining $T_c(x) = \mathfrak{Z}_c(P(x))$ we have

$$T_c(x) = G\rho_1 gx + G\,\Delta P - F \tag{16}$$

where g = acceleration due to gravity and ΔP = pressure pulse. The intersection of this curve for $\Delta P = 0$ with $T(x, 0)$ defines the initial position $M(0)$ of the phase boundary.

Similarly, the latent heat of the phase change L in (14c) is

$$L = T_c(S_1 - S_2) \tag{17}$$

which we take as constant. This assumption is not compatible with (15) ,if ρ_1 and ρ_2 are constant; however, this approximation should introduce no significant error unless $T(M_i) - T(M_f)$ is large.

Conservation of mass and heat sources requires

$$V_2 = [(\rho_2 - \rho_1)/\rho_2]\, dM/dt \tag{18a}$$

$$b(t) = b(0) - [(\rho_2 - \rho_1)/\rho_2](M(0) - M(t)) \tag{18b}$$

$$A_1/\rho_1 = A_2/\rho_2 \tag{18c}$$

We now introduce the dimensionless parameters, with $b_0 = b(0)$ and with T_0 an arbitrary temperature scaling factor.

$$\xi \equiv \frac{x}{b_0}, \qquad \tau \equiv \frac{K_1}{\rho_1 c_1 b_0^2}\, t, \qquad \eta(\xi, \tau) \equiv \frac{T(x, t)}{T_0}, \qquad \gamma_i \equiv \frac{J(0, 0) b_0}{K_i T_0}$$

$$\alpha \equiv \frac{K_2 \rho_1 c_1}{K_1 \rho_2 c_2}, \qquad \xi_m(\tau) \equiv \frac{M(t)}{b_0}, \qquad \beta(\tau) \equiv \frac{b(t)}{b_0}, \qquad C \equiv \frac{L}{c_1 T_0} \tag{19}$$

$$\sigma_i \equiv \frac{b_0^2 A_i}{T_0 K_i}, \qquad \eta_c(\xi) \equiv T_c(x)/T_0, \qquad \nu \equiv \frac{b_0}{\kappa_1} V_2$$

The equations become

$$\frac{\partial \eta}{\partial \tau} = \frac{\partial^2 \eta}{\partial \xi^2} + \sigma_1 \qquad 0 \le \xi \le \xi_m \tag{20a}$$

$$\frac{\partial \eta}{\partial \tau} = \alpha \frac{\partial^2 \eta}{\partial \xi^2} - \nu \frac{\partial \eta}{\partial \xi} + \alpha \sigma_2 \qquad \xi_m \le \xi \le \beta(\tau) \tag{20b}$$

subject to the boundary conditions

$$\eta(0, \tau) = 0 \tag{21a}$$

$$\eta(\beta(\tau), \tau) = \text{constant}, \quad \text{or} \tag{21b}$$

$$\left.\frac{\partial \eta}{\partial \xi}\right|_{\xi = \beta(\tau)} = \text{constant}$$

$$\left.\frac{\partial \eta}{\partial \xi}\right|_{\xi = \xi_m^-} - \frac{K_2}{K_1} \left.\frac{\partial \eta}{\partial \xi}\right|_{\xi = \xi_m^+} = -C \frac{d\xi_m}{d\tau} \tag{21c}$$

$$\eta(\xi_m(\tau), \tau) = \eta_c(\xi_m) = \frac{G \rho_1 g b_0}{T_0} \xi_m + \frac{G\, \Delta P}{T_0} - \frac{F}{T_0} \tag{21d}$$

as well as the conservation equations

$$\nu = [(\rho_2 - \rho_1)/\rho_2]\, d\xi_m/d\tau \tag{22a}$$

$$\beta(\tau) = 1 - [(\rho_2 - \rho_1)/\rho_2](\xi_m(0) - \xi_m(\tau)) \tag{22b}$$

$$K_1 \sigma_1/\rho_1 = K_2 \sigma_2/\rho_2 \tag{22c}$$

We define the perturbation temperature $\theta(\xi, \tau)$ and the reduced Clapeyron curve $\theta_c(\xi)$ to be

$$\theta(\xi, \tau) \equiv \eta(\xi, \tau) - \eta(\xi, 0)$$
$$\theta_c(\xi) \equiv \eta_c(\xi) - \eta(\xi, 0) \tag{23}$$

The reduced Clapeyron curve $\theta_c(\xi)$ depends only on the difference between $\eta_c(\xi)$ and $\eta(\xi, 0)$.

Both $\eta(\xi, 0)$ and $\eta(\xi, \tau)$ are continuous; hence $\theta(\xi, \tau)$ will be continuous. Continuity of heat flux requires that $\partial\eta(\xi, \tau)/\partial\xi$ and $\partial\eta(\xi, 0)/\partial\xi$ have discontinuities at $\xi_m(\tau)$ and $\xi_m(0)$, respectively. Hence $\partial\theta(\xi, \tau)/\partial\xi$ will have discontinuities at these two points.

From the initial condition of thermal equilibrium, it may be seen that

$$\left.\frac{\partial\eta(\xi, 0)}{\partial\xi}\right|_{\xi=\xi_m^-(0)} - \frac{K_2}{K_1}\left.\frac{\partial\eta(\xi, 0)}{\partial\xi}\right|_{\xi=\xi_m^+(0)} = 0$$
$$\eta(0, 0) = 0, \qquad \left.\frac{\partial\eta(\xi, 0)}{\partial\xi}\right|_{\xi=0} = \gamma_1 \tag{24}$$

For the case $\xi_m(\tau) \leq \xi_m(0)$, the problem as formulated for $\theta(\xi, \tau)$ is

$$\frac{\partial\theta}{\partial\tau} = \frac{\partial^2\theta}{\partial\xi^2}; \qquad 0 \leq \xi \leq \xi_m(\tau) \qquad \text{(region 1)} \tag{25a}$$

$$\frac{\partial\theta}{\partial\tau} = \alpha\frac{\partial^2\theta}{\partial\xi^2} - \nu\left[\frac{\partial\theta(\xi, \tau)}{\partial\xi} + \frac{\partial\eta(\xi, 0)}{\partial\xi}\right] + \alpha(\sigma_2 - \sigma_1);$$
$$\xi_m(\tau) \leq \xi \leq \xi_m(0) \qquad \text{(region 3)} \tag{25b}$$

$$\frac{\partial\theta}{\partial\tau} = \alpha\frac{\partial^2\theta}{\partial\xi^2} - \nu\left[\frac{\partial\theta(\xi, \tau)}{\partial\xi} + \frac{\partial\eta(\xi, 0)}{\partial\xi}\right]; \qquad \xi_m(0) \leq \xi \leq \beta(t) \qquad \text{(region 2)} \tag{25c}$$

subject to boundary conditions

$$\theta(0, \tau) = 0 \tag{26a}$$

$$\theta(\beta(\tau), \tau) = \eta(\beta(0), 0) - \eta(\beta(\tau), 0) \quad \text{or}$$
$$\left.\frac{\partial\theta(\xi, \tau)}{\partial\xi}\right|_{\xi=\beta(\tau)} = \left.\frac{\partial\eta(\xi, 0)}{\partial\xi}\right|_{\xi=\beta(0)} - \left.\frac{\partial\eta(\xi, 0)}{\partial\xi}\right|_{\xi=\beta(\tau)} \tag{26b}$$

$$\left.\frac{\partial\theta}{\partial\xi}\right|_{\xi=\xi_m^-(\tau)} - \frac{K_2}{K_1}\left.\frac{\partial\theta}{\partial\xi}\right|_{\xi=\xi_m^+(\tau)}$$
$$+ \left.\frac{\partial\eta(\xi, 0)}{\partial\xi}\right|_{\xi=\xi_m^-(\tau)} - \frac{K_2}{K_1}\left.\frac{\partial\eta(\xi, 0)}{\partial\xi}\right|_{\xi=\xi_m^+(\tau)} = -C\frac{d\xi_m}{d\tau} \tag{26c}$$

$$\left.\frac{\partial\theta}{\partial\xi}\right|_{\xi=\xi_m^-(0)} - \left.\frac{\partial\theta}{\partial\xi}\right|_{\xi=\xi_m^+(0)}$$
$$= -\left.\frac{\partial\eta(\xi, 0)}{\partial\xi}\right|_{\xi=\xi_m^-(0)} + \left.\frac{\partial\eta(\xi, 0)}{\partial\xi}\right|_{\xi=\xi_m^+(0)}; \qquad \tau > 0 \tag{26d}$$

$$\theta(\xi_m(\tau), \tau) = \theta_c(\xi_m) \equiv \frac{G\rho_1 g b_0}{T_0}\xi_m + \frac{G\,\Delta P(\tau)}{T_0} - \frac{F}{T_0} - \eta(\xi_m, 0) \tag{26e}$$

$$\theta(\xi, 0^+) = 0, \qquad \xi \neq \xi_m(0) \tag{26f}$$

The conservation equations (22) remain unchanged.

A comparison of the original field equations 13 with those obtained for the dimensionless perturbation temperature (25) shows that the equations for θ require the distinction of three regions, owing to the conditions 26*c* and 26*d* whereas the equations for T require only a distinction of two regions.

Region 3 arises for two reasons: (1) We have subtracted $\eta(\xi, 0)$, which has a discontinuous first derivative at $\xi_m(0)$, from $\eta(\xi, \tau)$. This leads to condition 26*d*. The extra term in condition 26*c* arises similarly. Both are due solely to different conductivities in regions 1 and 2.

(2) Heat sources are redistributed, owing to the volume change at the phase boundary, giving rise to a source term in the heat equation in region 3.

In spite of the complexity due to the addition of a third region with associated boundary conditions, it is obvious that field equations 25 are considerably simplified as compared with (13). There are no source terms in either regions 1 or 2. The source term appears only as the difference $\alpha(\sigma_2 - \sigma_1)$ in region 3, i.e., in the region between the initial and final position of the phase boundary. From this consideration for the two-layer model, it is evident that the presence of sources is of small importance in the dynamic equations, unless region 3 becomes large. As was seen in the discussion of the steady-state case, the presence of sources affects the initial and final positions of the phase boundary. The final steady-state temperature in region 3 will have a change in curvature, which will be small unless $\sigma_2 - \sigma_1$ is large and, in fact, will vanish if $\rho_2/K_2 = \rho_1/K_1$, as can be seen from (22*c*). This leads to the conclusion that the distribution of sources is of small importance in determining the dynamics of motion and the perturbation in the temperature.

This conclusion must be somewhat weakened for the case of multilayer or continuous models. Because of our choice of Eulerian coordinates for the representation of the problem, the source intensity must be considered as a function of time. The general equations corresponding to (13) for a nonuniform continuous medium with arbitrary time-independent sources are unchanged in the region $(0 \leq x \leq M(t))$, and hence the source term will still vanish in the perturbation temperature formulation. In some other regions for $x > M(t)$, there will be differences in source terms due to the effects of translation and the phase transition. It follows that the strong conclusion drawn for the model with two homogeneous layers must be weakened somewhat for the more realistic multi or continuous layer models.

However, following the argument given for the homogeneous two-layer model, we still conclude that for small motions of the phase boundary, the effects of the source distribution on the dynamics of the systems will still be small unless the differences between the source strengths is large.

Returning to the two-layer problem as formulated in (25) and (26), it is evident that the major complexities remain. These are the nonlinear condition (26*c*) at the phase boundary and the nonlinear term for convective heat transport in the heat equation in regions 2 and 3. In addition, it can be seen that the differences in thermal properties complicate the boundary conditions. From the above discussion it would appear that sources should not dominate the geophysical problem considered here. The important issue is the motion of the phase boundary,

which is governed by the nonlinear boundary condition 26c, and the Clapeyron curve.

The gutted problem. To isolate the effect of this nonlinear boundary condition, the following simplifications were made to define the gutted problem: (1) sources are neglected, $\sigma_1 \equiv 0$; (2) the thermal parameters in regions 1 and 2 are taken to be identical; (3) the densities of the two phases are set equal in the field equation and conservation equations; hence the velocity in region 2 vanishes and the lower boundary $\beta(\tau) = \beta(0) = 1$; and (4) the reduced Clapeyron curve is given by $\theta_c(\xi) = D\xi - E$; $0 < E < D$; thus the phases are assumed to have different densities only in the Clausius Clapeyron equation.

The gutted problem so defined may be summarized

$$\frac{\partial \theta}{\partial \tau} = \frac{\partial^2 \theta}{\partial \xi^2} \qquad 0 \leq \xi < \xi_m, \quad \xi_m < \xi \leq 1, \quad \tau > 0 \tag{27a}$$

$$\theta(0, \tau) = \theta(1, \tau) = 0, \qquad \tau \geq 0 \tag{27b}$$

$$\left.\frac{\partial \theta}{\partial \xi}\right|_{\xi=\xi_m^+(\tau)} - \left.\frac{\partial \theta}{\partial \xi}\right|_{\xi=\xi_m^-(\tau)} = C\frac{d\xi_m(\tau)}{d\tau} \tag{27c}$$

$$\theta(\xi_m(\tau), \tau) = D\xi_m(\tau) - E, \qquad \tau \geq 0 \tag{27d}$$

$$\theta(\xi, 0) = 0, \qquad \xi \neq \xi_m(0); \qquad \theta(\xi_m(0), 0) = D\xi_m(0) - E \tag{27e}$$

$$C, D, E \text{ constants}, \quad 0 < E < D; \quad 0 < \xi_m(0) < 1, \quad C > 0 \tag{27f}$$

$$D \equiv \frac{G\rho_1 g b_0}{T_0} - \frac{J(0,0)b_0}{K_1 T_0} \qquad E \equiv \frac{F}{T_0} - \frac{G\,\Delta P}{T_0}$$

$$C \equiv \frac{L}{c_1 T_0}$$

In comparing (25), (26), and (27), major simplifications are evident, including the disappearance of region 3. These simplifications make the problem more susceptible to analysis and permit the identification of characteristic parameters of the motion.

Some of the characteristics of the gutted problem are given in the appendix. It is shown (appendix 1) that, if $\xi_m(0) > E/D$, then (1) $E/D \leq \xi_m(\tau) < \xi_m(0)$, and (2) $\xi_m = E/D$ is the only equilibrium position for $\xi_m(\tau)$. Thus the phase boundary is constrained to move only in the region between the initial position and the zero of the reduced Clapeyron curve $\theta_c(\xi_m) = 0$, which is the final equilibrium position.

We may note here that the boundary condition (26c) can be rewritten in integral form: Integrating equation 26a

$$\int_0^1 \frac{\partial \theta}{\partial \tau}\,d\xi = \int_0^{\xi_m} \frac{\partial^2 \theta}{\partial \xi^2}\,d\xi + \int_{\xi_m}^1 \frac{\partial^2 \theta}{\partial \xi^2}\,d\xi = \left.\frac{\partial \theta}{\partial \xi}\right|_{\xi=\xi_m-} - \left.\frac{\partial \theta}{\partial \xi}\right|_{\xi=0} + \left.\frac{\partial \theta}{\partial \xi}\right|_{\xi=1} - \left.\frac{\partial \theta}{\partial \xi}\right|_{\xi=\xi_m+}$$

Using (26c), we then obtain

$$C\frac{d\xi_m}{d\tau} = -\frac{d}{d\tau}\int_0^1 \theta\,d\xi - \left.\frac{\partial \theta}{\partial \xi}\right|_{\xi=0} + \left.\frac{\partial \theta}{\partial \xi}\right|_{\xi=1}. \tag{28}$$

This expression is equivalent to the requirement that heat energy be conserved.

The characteristic behavior of the gutted problem is shown in Figure 6. The initial temperature distribution $\theta(\xi, 0)$ is zero everywhere except at $\xi = \xi_m(0)$, where $\theta(\xi_m(0), 0) = D\xi_m(0) - E$ and the phase transition is initiated. As the phase boundary moves, the temperature pulse becomes wider. The temperature of the phase boundary is constrained to lie on the reduced Clapeyron line of slope D. Because the boundary conditions require that the temperature at the ends be zero, the temperature θ rises from the end points to a point $\theta(\xi_m(\tau), \tau) = D\xi_m(\tau) - E$ on the reduced Clapeyron line and is restricted to lie below the reduced Clapeyron curve to the right of the phase boundary.

The temperature at the phase boundary continually decreases until the end point $\xi_m(\infty) = E/D$ is reached, and the perturbation temperature $\theta(\xi, \infty)$ is everywhere zero. As shown in appendix 1, the curvature of the perturbation temperature is always negative just behind the phase boundary. For the initial motion, the curvature in front of the pulse is positive and then becomes negative for long times.

This problem is essentially similar to the classical Stefan problem with these major exceptions: the temperature at the phase boundary is not constant, the thermodynamically unstable region is finite, and the displacement of the phase boundary is bounded.

Generalized Stefan problem. Many of the essential aspects of the gutted problem may be found by consideration of a modification of Neumann's solution to the Stefan problem as given by *Carslaw and Jaeger* [1959, chapter 11]. We will present the solution to this problem in dimensionless form and use it to define the asymptotic behavior of the gutted problem for short times. This discussion will be followed by a treatment for long times. These results will then permit the a priori assignment of values for the dimensionless parameters that characterize the problem and the dependence of the solution on these quantities.

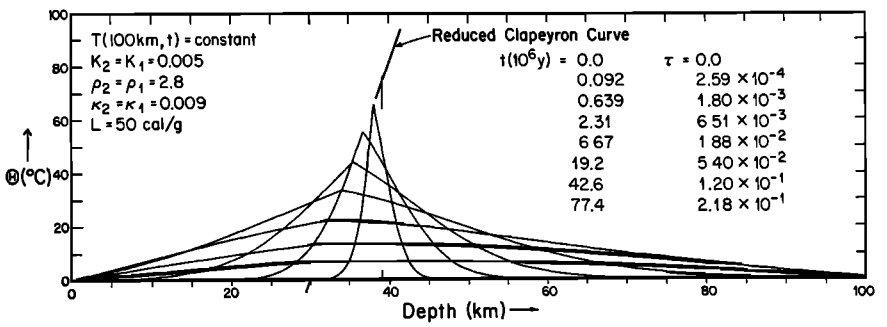

Fig. 6. Profiles of the perturbation temperature $\Theta(x,t)$ at selected times for the gutted problem obtained by the numerical solution for model 1. Each curve is the distribution at a specific time t or an equivalent dimensionless time τ, starting with $t = \tau = 0$. At $\tau = 0$, the temperature is zero everywhere except at M_4 and is represented in the figure as an interrupted vertical line at a depth of 39 km. The peaks of all the profiles lie on the reduced Clapeyron curve, a portion of which has been omitted for clarity. $\Theta(x,\infty)$ is zero everywhere.

Consider a supercooled liquid phase 1 ($-\infty < \xi < \xi_m(0)$) initially in contact with a solid phase 2 ($\xi_m(0) < \xi < +\infty$). The two phases have identical parameters. Let us suppose that the initial temperature of both phases is zero and that the equilibrium temperature at which these two phases coexist is θ_s. Let C be the dimensionless heat liberated by the transition ($1 \rightarrow 2$). Then the solution to the problem, if the liquid begins freezing at the interface $\xi_m(0)$, is

$$\theta(\xi, \tau) = \frac{\theta_s}{(1 - \operatorname{erf} \lambda)}\left[1 + \operatorname{erf}\left(\frac{\xi - \xi_m(0)}{2\tau^{1/2}}\right)\right]; \quad \xi \leq \xi_m(\tau)$$
$$\theta(\xi, \tau) = \frac{\theta_s}{(1 + \operatorname{erf} \lambda)}\left[1 - \operatorname{erf}\left(\frac{\xi - \xi_m(0)}{2\tau^{1/2}}\right)\right]; \quad \xi \geq \xi_m(\tau) \tag{29}$$

$$\xi_m(\tau) - \xi_m(0) = -2\lambda\tau^{1/2} \tag{30}$$

where λ is the root of the transcendental equation

$$n(\lambda) \equiv \tfrac{1}{2}\pi^{1/2}\lambda e^{\lambda^2}[1 - (\operatorname{erf} \lambda)^2] = \theta_s/C \tag{31}$$

The function $n(\lambda)$ is shown in Figure 7, and it has a maximum value of 1 as

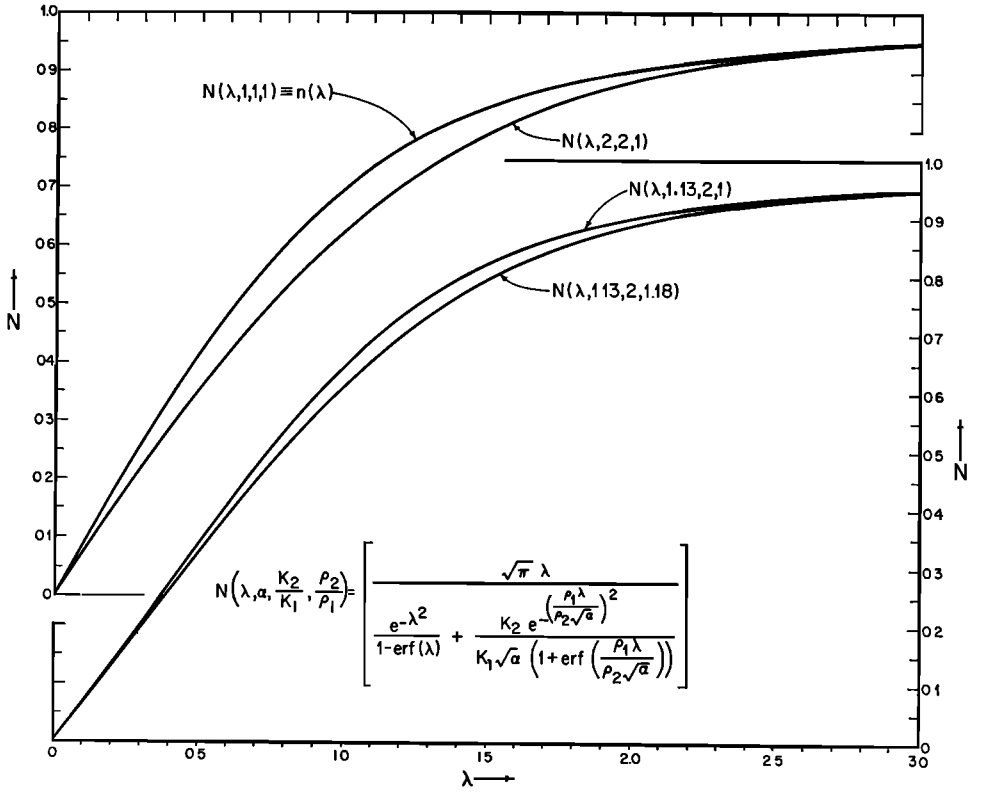

Fig. 7. The characteristic function $N(\lambda, \alpha, K_2/K_1, \rho_2/\rho_1)$ versus λ for the Stefan problem for various values of the arguments α, K_2/K_1, ρ_2/ρ_1. The characteristic function $n(\lambda)$ for the gutted problem is equal to $N(\lambda, 1, 1, 1)$. The two curves on the left should be read on the left-hand scale, the other curves on the right-hand scale. The scales on both sides are equal and offset by an integral number of scale divisions.

$\lambda \to \infty$. The temperature is bounded by $0 \leq \theta \leq \theta_s$, and the curvature is

$$\frac{\partial^2 \theta}{\partial x^2} \begin{cases} >0, & \xi \leq \xi_m(\tau) \\ <0, & \xi = \xi_m{}^+(\tau) \end{cases}.$$

These results are a special case of the theorem given in appendix 1. The heat flux at the lead edge of the phase boundary exceeds the flux at the back edge, as may be seen by

$$-\frac{\partial \theta}{\partial x}\bigg|_{\xi=\xi_m^-} \Big/ \frac{\partial \theta}{\partial x}\bigg|_{\xi=\xi_m^+} = \frac{1 + \operatorname{erf} \lambda}{1 - \operatorname{erf} \lambda} > 1$$

The half-width $(\xi_{1/2}{}^+ - \xi_{1/2}{}^-)$ of the temperature perturbation as defined by

$$\theta(\xi_{1/2}{}^-, \tau) = \theta_s/2 \qquad \xi_{1/2}{}^- < \xi_m$$
$$\theta(\xi_{1/2}{}^+, \tau) = \theta_s/2 \qquad \xi_{1/2}{}^+ > \xi_m$$

is

$$(\xi_{1/2}{}^+ - \xi_{1/2}{}^-) = \frac{[\xi_m(0) - \xi_m(\tau)]}{\lambda} \{\operatorname{erf}^{-1} [\tfrac{1}{2} + \tfrac{1}{2} \operatorname{erf} \lambda] + \operatorname{erf}^{-1} [\tfrac{1}{2} - \tfrac{1}{2} \operatorname{erf} \lambda]\} \tag{32}$$

and therefore increases in proportion to the displacement or to $\tau^{1/2}$.

This problem corresponds to the gutted problem for an infinite region and for a constant transition temperature $\theta_c(\xi) = \theta_s$. Let us now consider the case of the gutted problem with a variable temperature $\theta_c(\xi_m)$ at the phase boundary. For the initial motion of the phase boundary, the relative change in $\theta_c(\xi_m)$ will be small. Hence the motion of the phase boundary should approximately be as though the temperature at the phase boundary were constant, and, in particular, the initial singularity in $d\xi_m/d\tau$ exhibited by the Neumann solution must also characterize the gutted problem.

If we substitute $\theta_c(\xi_m)$ for θ_s in equation 29 and thus interpret θ_c to be an explicit function of ξ_m and only an implicit function of time, we obtain the function $\tilde{\theta}_{SA}$, which is a solution to the heat flow equation and which satisfies the condition $\tilde{\theta}_{SA}(\xi_m, \tau) = \theta_c(\xi_m)$. Here

$$\begin{aligned} \tilde{\theta}_{SA} &\equiv \frac{\theta_c(\xi_m)}{[1 - \operatorname{erf} \lambda(\xi_m)]} \left[1 + \operatorname{erf}\left(\frac{\xi - \xi_m(0)}{2\tau^{1/2}}\right)\right] \qquad \xi \leq \xi_m(\tau) \\ \tilde{\theta}_{SA} &\equiv \frac{\theta_c(\xi_m)}{[1 + \operatorname{erf} \lambda(\xi_m)]} \left[1 - \operatorname{erf}\left(\frac{\xi - \xi_m(0)}{2\tau^{1/2}}\right)\right] \qquad \xi \geq \xi_m(\tau) \end{aligned} \tag{33}$$

where we have defined $\lambda = \lambda(\xi_m)$ so that equation 30 becomes

$$\xi_m(\tau) - \xi_m(0) = -2\lambda(\xi_m)\tau^{1/2} \tag{34a}$$

The boundary condition 27c becomes

$$\begin{aligned} -2C \frac{d}{d\tau} [\lambda(\xi_m)\tau^{1/2}] &= -\frac{C\lambda(\xi_m)}{\tau^{1/2}} - 2C\tau^{1/2} \frac{d\lambda(\xi_m)}{d\xi_m} \frac{d\xi_m}{d\tau} \\ &= -\frac{\theta_c(\xi_m)}{\tau^{1/2}(\pi^{1/2})} \left[\frac{2e^{-\lambda^2}}{(1 + \operatorname{erf} \lambda(\xi_m))(1 - \operatorname{erf} \lambda(\xi_m))}\right]. \end{aligned} \tag{34b}$$

It should be noted that the boundary condition 27 can be numerically integrated directly for a given approximation $\tilde{\theta}$ to the temperature field

$$C\frac{d\xi_m}{d\tau} \approx \frac{\partial\tilde{\theta}}{\partial\xi}\bigg|_{\xi_m+} - \frac{\partial\tilde{\theta}}{\partial\xi}\bigg|_{\xi_m-}$$

Boundary condition 34*b* may be rewritten in the form

$$n(\lambda) = \frac{\theta_c(\xi_m)}{C}\left[1 - \frac{d\log\lambda}{d\log(\xi_m(0) - \xi_m(\tau))}\right] \tag{35}$$

It is evident that (33) and (35) are not exact solutions to the generalized Stefan problem and that a particular functional form for the temperature field is assumed. Nonetheless, they satisfy the field equations and obey the constraint $\theta_c(\xi_m) = \tilde{\theta}_{SA}(\xi_m, \tau)$ and have the characteristic singularity of the simple Stefan problem. It therefore appears useful to apply this general Stefan-type approximation (SA) to the gutted problem. This functional form must be valid in the neighborhood of $\tau = 0$ because of the singularity that obtains at this time. If $|(d\log\lambda)/[d\log(\xi_m(0) - \xi_m)]| \ll 1$, then the time derivative of λ is negligible compared with $d\xi_m/d\tau$, and we may obtain the roots $\lambda(\xi_m)$ from the simple equation $n(\lambda) = \theta_c(\xi_m)/C$. Within the scheme of the SA an estimate of the error, resulting from neglecting the term $(d\log\lambda)/[d\log(\xi_m(0) - \xi_m)]$, may be obtained by evaluating this from the expression

$$\frac{d\log\lambda}{d\log(\xi_m(0) - \xi_m)} \approx \frac{(\xi_m - \xi_m(0))D}{\lambda C[dn(\lambda)/d\lambda]}.$$

When this term is neglected we define the general Stefan approximation to be of type 1 (SA1).

From physical considerations, it would appear that the approximation SA1 does not take into account the redistribution of heat behind the phase boundary. That is, the temperature behind the phase boundary is always less than $\theta_c(\xi_m)$ in the SA1 approximation. This suggests that the instantaneous velocity calculated from SA1 is too great.

Another estimate of the solution that will tend to compensate for this effect is to include the apparent excess heat behind the phase boundary $D[\xi_m(0) - \xi_m(\tau)]$ with the latent heat C. This yields a second Stefan approximation SA2, where the expression for the temperature remains unchanged but C is replaced by $C + D[\xi_m(0) - \xi_m(\tau)]$ in the characteristic equation 35.

Termination of Stefan-like behavior. From the equation

$$\frac{d\xi_m}{d\tau}\left(D - \frac{\partial\theta}{\partial\xi}\bigg|_{\xi=\xi_m}\right) = \frac{\partial^2\theta}{\partial\xi^2}\bigg|_{\xi=\xi_m}$$

given in appendix 1, it is evident that at a time τ^* and position ξ_m^*, when $(\partial\theta/\partial\xi)_{\xi-m} = D$, there is an inflection point at ξ_m^- at the phase boundary, and the curvature changes sign from positive to negative. This is a fundamental change in the nature of $\theta(x, \tau)$; it cannot happen in the Stefan approximation and is proof that the solution is not exact. This condition when applied to the Stefan problem thus gives

a criterion for the change from behavior predicted by the Stefan approximation to a behavior where $(\partial^2\theta/\partial\xi^2) < 0$ over the major part of the space.

Inserting $\tilde{\theta}_{SA}$ into the above expression, we obtain an estimate $\tilde{\tau}^*$ of the time τ^* when the curvature of θ changes sign and when the Stefan approximation would deviate from the correct solution. Thus

$$\left.\frac{\partial\theta}{\partial\xi}\right|_{\xi_m-} \cong \left.\frac{\partial\tilde{\theta}_{SA}}{\partial\xi}\right|_{\xi_m-} = D = \frac{\theta_c(\xi_m{}^*)e^{-\lambda^{*2}}}{(1 - \operatorname{erf}\lambda^*)(\pi)^{1/2}(\tilde{\tau}^*)^{1/2}}$$

or

$$(\tilde{\tau}^*)^{1/2} = \frac{(D\xi_m(0) - E)}{D\{\pi^{1/2}(1 - \operatorname{erf}\lambda^*)e^{\lambda^{*2}} + 2\lambda^*\}} = \frac{(D\xi_m(0) - E)}{Dp(\lambda^*)} \tag{36}$$

and

$$\begin{aligned}\xi_m{}^* \equiv \xi_m(\tilde{\tau}^*) &= \xi_m(0) - \frac{2\lambda(D\xi_m(0) - E)}{D\{(\pi)^{1/2}(1 - \operatorname{erf}\lambda^*)e^{\lambda^{*2}} + 2\lambda^*\}} \\ &= \xi_m(0) - \frac{2\lambda^*(D\xi_m(0) - E)}{p(\lambda^*)D}\end{aligned} \tag{37}$$

where

$$p(\lambda) \equiv (\pi)^{1/2}(1 - \operatorname{erf}\lambda)e^{\lambda^2} + 2\lambda. \tag{38}$$

The value of λ^* to be used in (36) and (37) is determined from the characteristic equation for SA1

$$h_1(\lambda^*) \equiv n(\lambda^*) + \lambda^{*2}(\operatorname{erf}\lambda^* + 1) = \frac{D\xi_m(0) - E}{C} \tag{39}$$

or for SA2

$$h_2(\lambda^*) \equiv \frac{n(\lambda^*) + \lambda^{*2}(\operatorname{erf}\lambda^* + 1)}{1 - \lambda^{*2}(\operatorname{erf}\lambda^* + 1)} = \frac{D\xi_m(0) - E}{C} \tag{40}$$

The values of λ^* and $(\tau^*)^{1/2}$ for case 1 are less than the respective values for SA2. It would appear that the estimates of τ^* and $\xi_m{}^* \equiv \xi_m(\tau^*)$ determine the end of the Stefan behavior in terms of the constants of the problem. Graphs of the functions of $h_i(\lambda)$ and $p(\lambda)$ are presented in Figure 8. In terms of the dimensional parameters of the system, the termination of the Stefan behavior is therefore given by

$$\begin{aligned}h_i(\lambda^*) &= \frac{\{G\rho_1 g - [J(0, 0)/K_1]\}M(0) + G\,\Delta P - F}{L/c_1} \\ (\tilde{t}^*)^{1/2} &= \left(\frac{\rho_1 c_1}{K_1}\right)^{1/2}\left[\frac{M(0) - M(\infty)}{p(\lambda^*)}\right] \\ M(0) - M(t^*) &\cong 2\lambda^*(\tilde{\tau}^*)^{1/2}b_0 = 2\lambda^*\left(\frac{K_1}{\rho_1 c_1}\right)^{1/2}(\tilde{t}^*)^{1/2}\end{aligned} \tag{41}$$

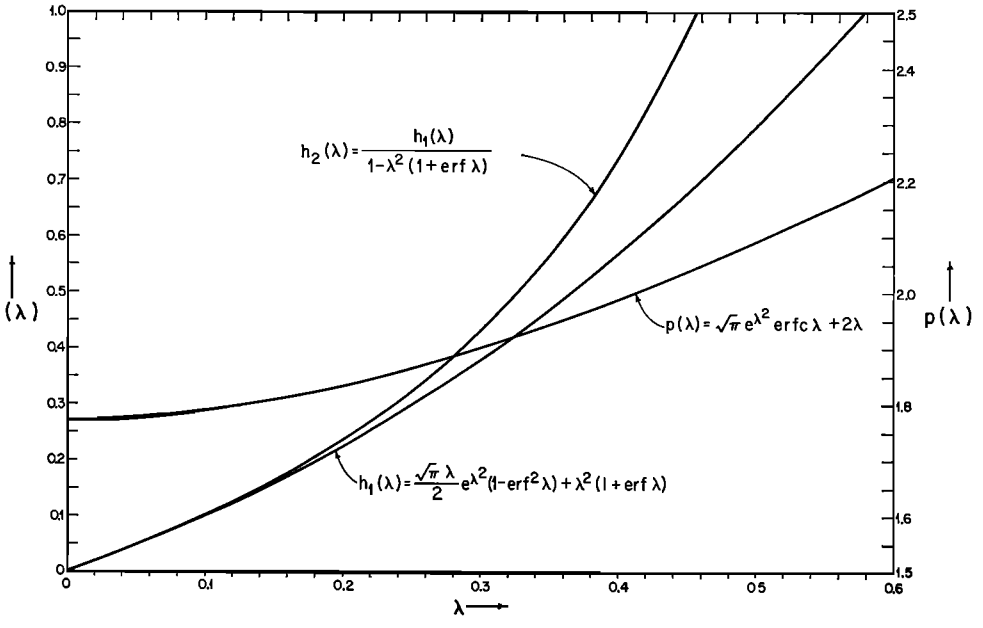

Fig. 8. The functions $p(\lambda)$, $h_1(\lambda)$, $h_2(\lambda)$ versus λ. The value of $\tilde{\lambda}_i^*$ is determined from $h_i(\tilde{\lambda}_i^*) = (1/C)[D\xi_m(0) - E]$. $\tilde{\tau}^*$ is then determined by $\tilde{\tau}_i^{*1/2} = [\xi_m(0) - E/D]/p(\tilde{\lambda}_i^*)$. h_i is read on the on the left-hand scale and p on the right-hand scale.

Long-time behavior. In the previous section the effects of the boundaries at $\xi = 0$ and $\xi = 1$ were neglected. At times when these are important, the SA type of treatment is clearly not applicable. The boundaries will be significant when the energy liberated at the moving phase boundary has diffused over the entire region and caused the temperature field to rise uniformly from the exterior boundaries to the phase boundary, rather than in the type of sharply peaked temperature distribution that characterizes the initial motion.

An estimate for the long-time behavior of $\xi_m(\tau)$ can be obtained by approximating the temperature $\theta(\xi, \tau)$ with a quasi-steady-state distribution (QSSA)

$$\begin{aligned} \tilde{\theta}_{SS}(\xi, \tau) &\equiv \left(\frac{D\xi_m(\tau) - E}{\xi_m(\tau)}\right)\xi \qquad 0 \le \xi \le \xi_m(\tau) \\ \tilde{\theta}_{SS}(\xi, \tau) &\equiv \left(\frac{D\xi_m(\tau) - E}{1 - \xi_m(\tau)}\right)(1 - \xi) \qquad \xi_m(\tau) \le \xi \le 1 \end{aligned} \tag{42}$$

Inspection of Figure 6, showing the temperature distribution for the gutted problem, indicates the essential validity of this approximation for sufficiently long times. Substituting $\tilde{\theta}_{SS}$ into the integral form of the boundary condition 28 yields

$$C\frac{d\xi_m}{d\tau} = -\frac{D}{2}\frac{d\xi_m}{d\tau} - \frac{D(\xi_m - E/D)}{\xi_m(1 - \xi_m)}$$

The first term on the right-hand side of this equation is due to the change in temperature of the phase transition and the resulting change in the total distribution.

The second term corresponds to the heat flux out of the region at the boundaries. If we had used the differential form of the boundary condition (27*c*), we would have neglected the first term.

For the long times under consideration, $\partial^2\theta/\partial\xi^2 = (\partial\theta/\partial\tau) < 0$, whereas for the approximation used $\partial^2\tilde{\theta}_{ss}/\partial\xi^2 = \partial\tilde{\theta}_{ss}/\partial\tau = 0$. Thus we have under-estimated the magnitude of $\partial\theta/\partial\xi$ at the boundaries. The effect of $\partial^2\theta/\partial\xi^2$ in the integral should be very small. Hence we expect that the approximation $\tilde{\theta}_{ss}$ will underestimate the velocity of the phase boundary.

If, as ξ_m approaches E/D, $[1/(\xi_m - E/D)]\ (d\xi_m/d\tau) \to -1/\tau_l = \text{constant}$, it follows that the asymptotic behavior is exponential. From $\tilde{\theta}_{ss}$ we obtain

$$\xi - E/D \cong \text{constant} \exp\left\{\frac{-\tau}{[(C/D) + \frac{1}{2})(E/D)(1 - (E/D)]}\right\}. \tag{43}$$

We expect that the long-term behavior for the gutted problem will exhibit this functional form. This can be characterized by the dimensionless relaxation time

$$\tau_l \approx \bar{\tau}_l = [(C/D) + \tfrac{1}{2})(E/D)(1 - (E/D)] \tag{44}$$

In this time the distance of the phase boundary from its final position will reduce by a factor $1/e$.

For $C = 0$, the movement will be controlled by the decay of the temperature distribution alone. This may be compared with the long-term relaxation of a slab of unit thickness with zero surface temperature and constant initial temperature which has a dimensionless relaxation time $1/\pi^2$. The analogous form of the gutted problem is the symmetrical case $E/D = \frac{1}{2}$, which yields $\bar{\tau}_l = \frac{1}{8}$. The difference of these two values is an indication of the accuracy of the quasi-steady-state temperature approximation used.

In terms of the geophysical parameters

$$\bar{t}_l = \frac{\rho_1 c_1}{K_1}\left\{\frac{L/c_1}{b_0[G\rho_1 g - (J(0, 0)/K_1)]} + \frac{1}{2}\right\}M_f[b_0 - M_f] \tag{45}$$

Taking the values of the parameters $K_1/\rho_1 c = 0.01$ cm^2/sec, $b_0 = 100$ km, $M_f = 30$ km, $L/c_1 = 75$°C, we see that the latent heat will not dominate unless $G\rho_1 g - (J(0, 0)/K_1) \leq 1.5$°C/km; thus, neglecting the latent heat, $\bar{t}_l = 33 \times 10^6$ years. This is approximately the thermal relaxation time for the slab between $x = 0$ and $x = 30$ km, and it therefore appears that the long-term effects for cases of this type are little influenced by the thermodynamic parameters.

The time at which the motion of the phase boundary becomes exponential is defined as τ^{**}. This will be approximately the time at which the temperature distribution becomes essentially linear. We may estimate this time τ^{**} after which the long-term behavior predicted by the QSSA will apply by considering the limiting case of a slab with ends at zero temperature which was initally at a constant temperature. The linear behavior will dominate when all but the lead time-dependent terms in the Fourier representation of the solution are negligible [*Carslaw and Jaeger*, 1959, p. 100]. This will certainly be the case for $\pi^2\tau/(1 - \xi_m)^2 > 2$ for which the deviation from a linear distribution is less than 10%.

Hence

$$\tau^{**} \approx \bar{\tau}^{**} = 2(1 - E/D)^2/\pi^2 \tag{46}$$

For times approaching τ^{**}, the QSSA should be a very good approximation. We have assumed above that the phase boundary is closer to $\xi = 0$ than to $\xi = 1$. If this is not the case, then the above expression for τ^{**} should be modified accordingly.

If the phase boundary is far enough removed from the boundaries of the region, so that we may regard it as infinite, we can obtain an estimate of the limiting behavior as ξ_m approaches E/D from the Stefan approximation.

For small values of λ, $n(\lambda) \approx (\pi^{1/2}/2)\ \lambda$. Then $\lambda = (2/\pi^{1/2})\ (D/C)\ [\xi_m - (E/D)]$ and $d\xi_m/d\tau = -\lambda/\tau^{1/2} = (-2/\pi^{1/2})\ (D/C)\ (\xi_m - E/D)\tau^{-1/2}$. Hence

$$\xi_m - E/D \approx \text{constant exp}\ [-(4/\pi^{1/2})(D/C)\tau^{1/2}] \tag{47}$$

This type of long-term behavior may be of significance for a phase change deep in a planetary interior, for instance.

4. NUMERICAL RESULTS

Since exact analytic solutions to the problems defined in the last section have not been found, the problems were solved numerically. An implicit method using standard finite difference equations was used in an iterative scheme to determine the motion of the phase boundary (appendix 2). The solution obtained was stable with respect to changes in the space and time steps. The method was also used to solve the Stefan problem for short times.

The numerical solutions to the gutted problem and the Stefan problem were obtained using both the integral and differential forms of the boundary conditions. The solutions by either of the two methods were in satisfactory agreement for both cases, indicating that no serious errors were accumulated in the partial derivatives near the phase boundary.

The solutions so obtained enabled us to determine the validity of the approximations to the gutted problem, to identify the more important parameters, and to extend the approximations to more complex cases.

The parameters of the models for which numerical solutions have been obtained are given in Tables 1 and 2. The models generally increase successively in complexity in order to illustrate the dependence of the solution on the parameters of the model.

In general these models have been constructed to represent some specific aspects of the problem in a reasonable manner; they are not intended to be taken as realistic representations of the complete geophysical problem. Thus, the parameters used are usually in the range of geophysical interest, although their exact values may have been chosen to facilitate comparisons among different models.

In discussing the numerical results we will compare the temperature distribution, position of the phase boundary, and the various parameters τ^*, τ^{**}, τ_l, $\xi_m(\tau^*)$, etc., with the estimates obtained from the approximate theory given in

TABLE 1. Parameters Describing Models

Parameter	Model: Units	1	2	3	4	5	6	7	8	9	10	11	12	13	14	15	16	17	18–20
K_1	$\frac{\text{cal}}{\text{cm/sec °C}}$	0 005	0.005	0.005	0.005	0.005	0 005	0.005	0.005	0.005	0.005	0.005	0 005	0.005	0.005	0 005	0.005	0.005	0 005
K_2		0 005	0.005	0.005	0.010	0.010	0 010	0.010	0.010	0.010	0.010	0 010	0.005	0.010	0.010	0 010	0.010	0 010	0.005
κ_1	$\frac{\text{cm}^2}{\text{sec}}$	0.0089	0 0089	0.0089	0 0089	0 0089	0 0089	0.0089	0.0089	0.0089	0.0089	0.0089	0.0089	0.0089	0 0089	0 0089	0 0089	0.0089	0.0089
κ_2		0.0089	0 0089	0.0089	0 018	0 018	0.018	0.018	0.018	0.010	0 010	0 010	0 0089	0 018	0 010	0 010	0.010	0.010	0.0089
ρ_1	g/cm³	2.8	2 8	2.8	2 8	2 8	2.8	2.8	2 8	2 8	2 8	2.8	2 8	2.8	2 8	2 8	2 8	2 8	2.8
ρ_2		2.8	2 8	2.8	2 8	2.8	2 8	2 8	2.8	2.8	3.3	3.3	2.8	3.3	3 3	3.3	3 3	3.3	2.8
$J(0, 0)$	$\frac{\mu\text{cal}}{\text{cm}^2\text{ sec}}$	0.62	0 62	0 62	0.62	0.62	0 62	0 62	0.62	0.62	0.62	0.62	0.62	0.62	1.01	1 50	0 53	0.19	0.62
$b(0)$	km	100	100	100	100	100	200	100	100	100	100	100	95	95	100	100	100	100	100
B_0C_0*		T	T	J	J	T	T	T	T	T	T	T	T	T	T	T	T	T	T
G	°C/kbar	75	75	75	75	75	75	75	60	75	75 ·	75	75	75	75	75	100	75	75
F	°C	320	320	320	320	320	320	320	160	320	320	320	320	320	167	170	274	658	320
ΔP	kbar	1.0	1 0	1 0	1.0	1 0	1 0	1 0	1 0	1 0	1 0	1.0	1.0	1.0	1.0	1 0	0.75	1.0	0
L	cal/g	50	15	15	15	15	15	30	15	15	15	15	15	15	15	15	15	15	15
V_2†		0	0	0	0	0	0	0	0	0	0	finite	finite	finite	finite	finite	finite	finite	0
A_i/ρ_i	$\frac{10^{-13}\text{ cal}}{\text{g sec}}$	0	0	0	0	0	0	0	0	0	0	0	0	0	0 36	1 25	0	0	0
$\dot{J}(b(0), 0)$	$\frac{\mu\text{cal}}{\text{cm}^2\text{ sec}}$	0.62	0.62	0 62	0 62	0.62	0 62	0 62	0.62	0.62	0.62	0.62	0.62	0.62	0.0	0.05	0.53	0.19	0 62
Sediments	km	0	0	0	0	0	0	0	0	0	0	0	3.64	3.64	0	0	0	0	0

* Boundary condition at lower boundary. T: constant temperature; J: constant flux.

† Velocity in lower layer. If finite, $V_2 = [(\rho_2 - \rho_1)/\rho_2]dM(t)/dt$.

TABLE 2. Dimensionless Parameters Describing Models

Model	b, km	T_0, °C*	C	D	E	$\xi_m(0)$	$\xi_m(\infty)$	γ_1	t/τ, 10^6 yr
1	100	1000	0.250	0.8193	0.245	0.3906	0.2991	1.24	355
2	100	1000	0.075	0.8193	0.245	0.3906	0.2991	1.24	355
3	100	1000	0.075	0.8193	0.245	0.3906	0.2991	1.24	355
4	100	1000	0.075	0.8193	0.245	0.3906	0.2991	1.24	355
5	100	1000	0.075	0.8193	0.245	0.3906	0.3238	1.24	355
6	200	2000	0.0375	0.8193	0.1225	0.1953	0.1573	1.24	1420
7	100	1000	0.150	0.8193	0.245	0.3906	0.3238	1.24	355
8	100	1000	0.075	0.4096	0.100	0.3906	0.3047	1.24	355
9	100	1000	0.075	0.8193	0.245	0.3906	0.3238	1.24	355
10	100	1000	0.075	0.8193	0.245	0.3906	0.3268	1.24	355
11	100	1000	0.075	0.8193	0.245	0.3906	0.3268	1.24	355
12	100†	1000	0.075	0.8193	0.245	0.3906	0.3335	1.24	355
13	100†	1000	0.075	0.8193	0.245	0.3906	0.3454	1.24	355
14	100	1000	0.075	‡	0.092	0.3906	0.3244	‡	355
15	100	1000	0.075	§	0.095	0.3925	0.3550	§	355
16	100	1000	0.075	1.6755	0.583	0.3925	0.3550	1.063	355
17	100	1000	0.075	1.6755	0.583	0.3925	0.3507	0.384	355
18–20	100	1000	0.075	0.8193	0.320‖	0.3906	¶	1.24	355

* These values for T_0 have been arbitrarily chosen to make comparison between different models easier. T_0 is not necessarily the temperature at the lower boundary.

† Note, however, that the lower boundary condition was fixed at $x = 95$ km. The discrepancy is due to the sediments on the surface.

‡ Compare model 11, which is a no-source approximation for this model.

§ Compare models 16 and 17, which are no-source approximations for this model.

‖ $E(0)$, since E is time dependent.

¶ Not determined, since E is time dependent.

section 3. It will be seen that the Stefan and long time approximations are extremely successful. In the subsequent discussion the approximate theory will be extended to apply to more complicated cases as they arise.

Gutted problem. We will first consider the numerical results for the most elementary cases that correspond to the gutted problem. Models 1 and 2 are examples of the gutted problem, and model 3 is a slight variation of it.

As we are neglecting sources in these cases, it is necessary to neglect the heat that would be produced by them. For this reason the artifically low value of 0.62 μcal/cm^2 sec is used for the surface heat flux $J(0, 0)$. A Clapeyron curve was chosen which is compatible with the results of *Ringwood and Green* [1964]. This yields a depth for the phase boundary that is near that of the continental Moho. The initial temperature distribution and Clapeyron curve for models 1, 2, and 3 may be seen in Figure 9*a*. Some results for model 3 which illustrate the nature of the temperature distribution are presented in Figure 9*b*, which shows the actual temperature and perturbation temperature after the motion has gone 60% of the total possible displacement. The shape of the perturbation temperature ⊛ illustrates the 'short time' behavior discussed in the section on the gutted problem. Its similarity with the form for the generalized Stefan problem is evident. The

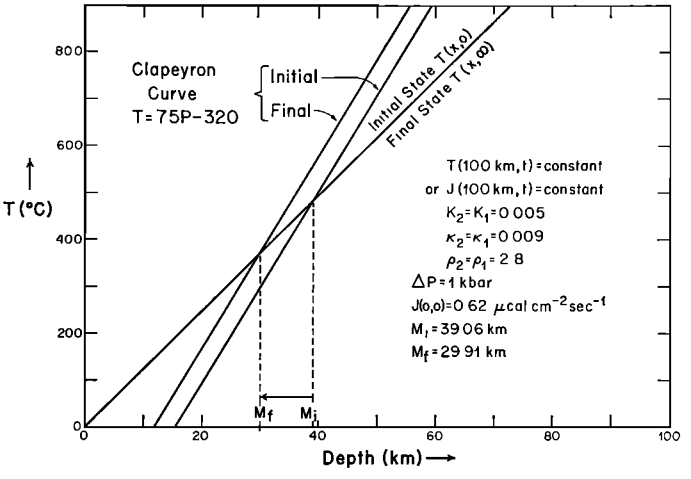

Fig. 9*a*. Initial and final temperature distribution and Clapeyron curves for models 1, 2, and 3. For constant temperature at the lower boundary, the problem reduces to the gutted problem.

general effect of this phase transition is to generate a narrow region of anomalously high temperature.

The development of the temperature distribution with time for model 1 is shown in Figure 6. The initial sharp peak decreases in height and becomes broader with time until it is limited by the effects of the boundaries. The illustration shows segments of the reduced Clapeyron curve. This line passes through the points of the temperature profile where there is a discontinuity in the slope. The singularity in the initial temperature is shown by the interrupted vertical line.

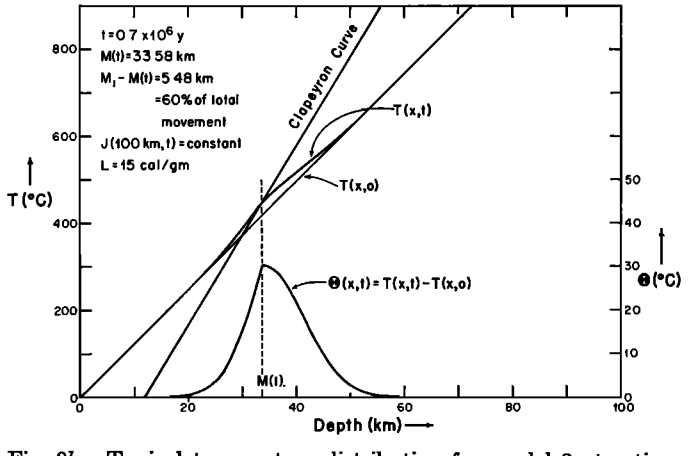

Fig. 9*b*. Typical temperature distribution for model 3 at a time t after the pressure pulse was applied, showing the relation between the temperature $T(x,t)$, the initial temperature $T(x, 0)$, the final Clapeyron curve, and the perturbation temperature $\Theta(x, t)$.

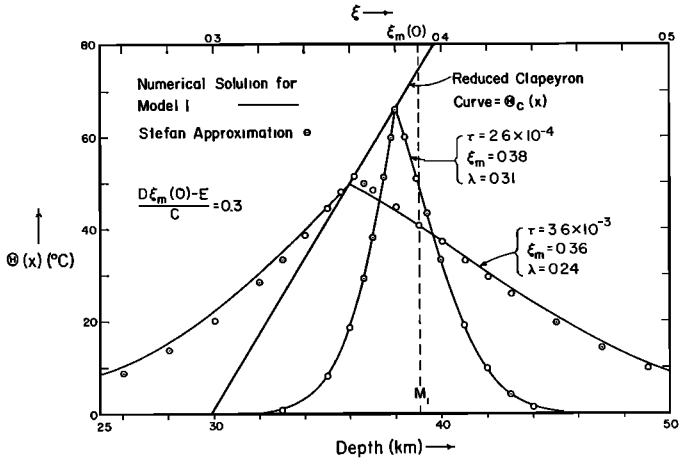

Fig. 10. Profiles of the perturbation temperature comparing the Stefan approximation (SA1) and the numerical solution for model 1 at the same time, for two different times. The solid curves show the numerical solution; the separate points indicate the Stefan approximation.

A comparison of the shapes of the temperature profile for the gutted problem and the Stefan approximation SA1 at two different times may be seen in Figure 10. The agreement for $\tau = 2.6 \times 10^{-4}$ is remarkably good. Since for this model $(1/C)\,[D\xi_m(0) - E] = 0.3$, the initial value of λ and the initial velocity are not too great, and we would not except the Stefan approximation to be in serious error. The agreement for $\tau = 3.6 \times 10^{-3}$ is not so good as in the previous case, primarily because there is a slight error in the time dependence of the location of the phase boundary using the Stefan approximation. With this error taken into consideration, the agreement may be regarded as very satisfactory.

The position of the phase boundary with time is shown in Figure 11. This figure shows two curves: (1) the logarithm of the displacement from the *initial* position versus the logarithm of time in order to illustrate the behavior for times when the position of the boundary changes rapidly; and (2) the logarithm of the distance of the boundary from its *final* position in order to illustrate the behavior when the position changes slowly with time.

Examination of the first curve shows that the slope $[d \log (\xi_m(0) - \xi_m(\tau))]/(d \log \tau)$ is initially slightly greater than $\frac{1}{2}$ and decreases smoothly as time increases, until it equals zero when the phase boundary attains its equilibrium position. In spite of the changing slope, the departure of the curve from a straight line of slope $= \frac{1}{2}$ is quite small for the first 20–25% of the motion.

Several points for the Stefan approximation are shown, and it may be seen that the agreement between the numerical solution and the approximation is satisfactory. The point (ξ_m^*, τ^*) at which the Stefan behavior begins to break down is shown as well. The Stefan approximation remains good well beyond this point even though the criterion that determines equation 36 is violated. Thus the change in curvature of the temperature distribution at this time is a subtle

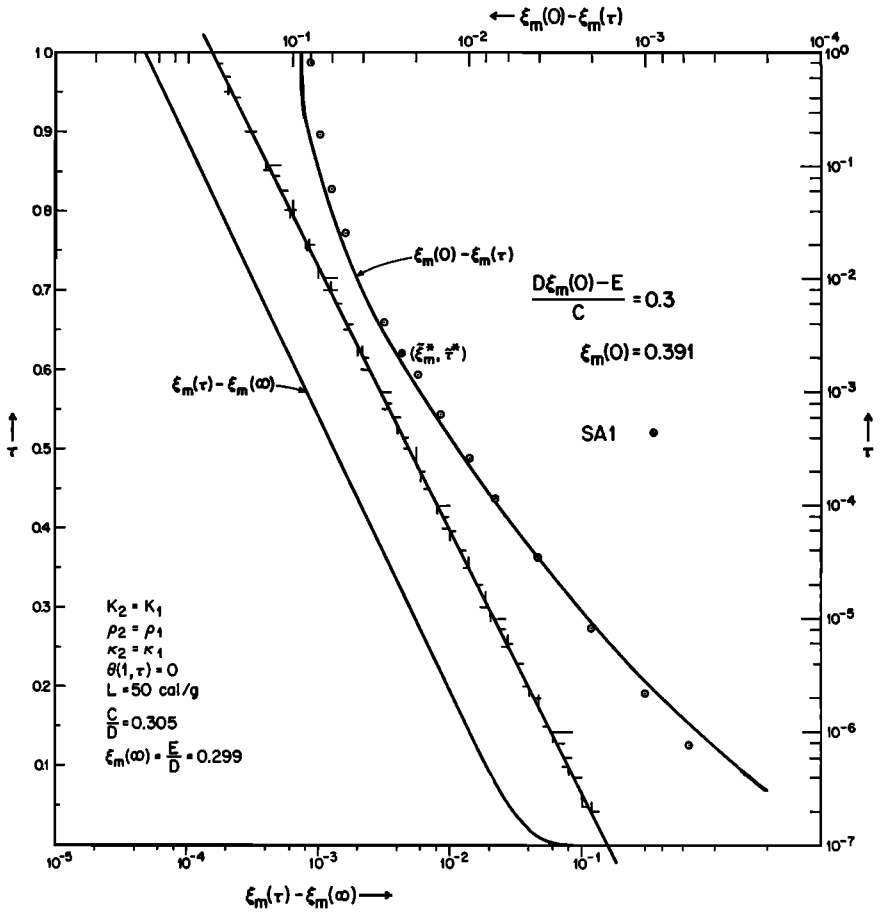

Fig. 11. Model 1. The curve on the right shows the nature of the initial motion of the phase boundary as shown by a plot of log $(\xi_m(0) - \xi_m(\tau))$ versus log τ. Selected points for the Stefan approximations are indicated. These include $(\xi_m(\bar{\tau}_1^*), \bar{\tau}_1^*)$ as calculated from the Stefan approximation. The curve on the left shows the nature of the long-term motion as shown by a plot of log $(\xi_m(\tau) - \xi_m(\infty))$ versus τ. Note that the two curves are separated by the heavy diagonal line with tick marks and have different scales.

criterion and does not appear to have a serious influence on the solution. This may be confirmed by examination of Figure 6, where the general shape of the temperature profile is the same after τ^* ($\tau = 6.51 \times 10^{-3}$) as before ($\tau = 1.80 \times 10^{-3}$). It would thus appear that the approximation SA1 continues to be accurate until the effects of the boundaries of the region significantly interfere.

The above comparison between the numerical results and the Stefan approximation indicates that the criterion at τ^* provides a very strict limit to the cessation of Stefan behavior and should be generally applicable in predicting the range of application of the Stefan approximation.

The preceding discussion was concerned with the motion of the phase boundary for times such that the boundaries of the region were not felt. The

motion of the phase boundary for long times is best shown by the curve on the left of Figure 11, which shows the logarithm of the distance of the phase boundary from its final position plotted against time. The curve is linear for long times in agreement with the exponential behavior predicted by the quasi-steady-state approximation (QSSA); the departure from linearity is due to the nonapplicability of the quasi-steady-state approximation. This may be confirmed by examination of the temperature profiles for $\tau < 0.02$. The logarithmic derivative $(d/d\tau)$ as $\tau \to \infty$, $d[\log(\xi_m - E/D)]/d\tau = 1/\tau_l$ for model 1 is given in Table 3 and may be compared with that calculated from QSSA, also in Table 3. The agreement between the actual and theoretical values is quite satisfactory considering the simplicity of the theoretical model.

An estimate of the time τ^{**} when the QSSA is dominant was here defined for the numerical solution when the logarithmic slope

$$\frac{1}{(\xi_m(\tau) - \xi_m(\infty))} \frac{d\xi_m(\tau)}{d\tau}$$

last departed by 20% from the asymptotic value as $\tau \to \infty$. The comparison of the theoretical and numerical values may be seen in Table 3.

In model 1 we have considered a case in which the term $d(\log \lambda)/d[\log(\xi_m(0) - \xi_m)]$ in (35), which is neglected in the SA1 approximation, has not been very large. We next consider the limiting case $(1/C)\ [D\xi_m(0) - E] = 1.0$ in model 2. This corresponds to the maximum pressure pulse which can be applied without overdriving the system and for which in the corresponding Stefan case $\lambda(\xi_m(0)) \to \infty$.

A representative example of the temperature distribution may be seen in Figure 9*b*. The peak is not as pointed as it would be for model 1, which may be attributed to the more rapid motion of the phase boundary for this case. Nevertheless, the general shape of the curve is similar to that for model 1.

The location of the phase boundary with time may be seen in Figure 12, which is analogous to Figure 11 for model 1. The general shape of the curves are, of course, similar for the two cases.

This model provides a more severe test for the Stefan approximation because of the singularity in λ. Comparison of SA1 with the numerical results for times significantly after $\tau = 0$ indicates that it is a fairly reasonable approximation to the temperature field. A comparison between the positions of the phase boundary calculated from the Stefan approximation (SA1 and SA2) and the numerical results are also shown in Figure 12.

It may be seen that for the initial motion $(\xi_m(0) - \xi_m(\tau)) \lesssim 0.01$, $\lambda \gtrsim 1.5$), the position of the phase boundary as calculated from either SA1 or SA2, overestimates the displacement. Both Stefan approximations are intrinsically unsatisfactory because their error lies primarily in approximating the temperature field. Exact integration of equation 34*b* would result in an even greater motion of the phase boundary for short times. This is undoubtedly because the motion of the phase boundary is so rapid that it is controlled to a large extent by the decay of the former temperature peak. For short times, SA2 is the better approximation for this case because it includes some of the effects of the redistribution of heat.

TABLE 3. Time and Position Criteria Obtained from Both the Stefan Approximation and Numerical Solution

Model	τ^*	$\xi_m(\tau^*)$	$\bar{\tau}_1{}^*$	$\tilde{\xi}_m(\bar{\tau}_1{}^*)$	$\tau_2{}^*$	$\tilde{\xi}_m(\bar{\tau}_2)$	$\bar{\tau}\dagger$	$\tilde{\xi}_m(\bar{\tau}\dagger)$	$\bar{\tau}\dagger\dagger$	$\tilde{\xi}_m(\bar{\tau}\dagger\dagger)$	τ_l	$\bar{\tau}_l$	τ^{**}	$\bar{\tau}^{**}$
1	0.00252	0.3635	0.00241	0.3659	0.00243	0.3672	...	...	...	...	0.1510	0.1688	0.1060	0.0996
2	0.00106	0.3429	0.00176	0.3420	0.00200	0.3497	...	...	...	...	0.1148	0.1240	0.1129	0.0996
3	0.00106	0.3429	0.00176	0.3420	0.00200	0.3497	...	...	...	...	0.4260	0.2817	0.3488	0.2987
4	0.00126	0.3458	0.00172	0.3406	0.00191	0.3467	3.15×10^{-4}	0.3555	0.00154	0.3396	0.5003	0.4403	0.0481	0.1493
5	0.00126	0.3458	0.00172	0.3406	0.00191	0.3467	3.15×10^{-4}	0.3555	0.00154	0.3396	0.0875	0.1036	0.0241	0.0463
6	0.00032	0.1729	0.00043	0.1703	0.00048	0.1734	7.88×10^{-5}	0.1778	0.00039	0.1698	0.0828	0.0837	0.0567	0.0719
7	0.00184	0.3559	0.00213	0.3543	0.00218	0.3563	6.15×10^{-4}	0.3651	0.00236	0.3515	0.0967	0.1151	0.0415	0.0463
8	0.00412	0.3321	0.00477	0.3175	0.00513	0.3248	3.12×10^{-4}	0.3560	0.00116	0.3522	0.1008	0.1196	0.0276	0.0490
9	0.00145	0.3470	0.00171	0.3405	0.00188	0.3458	4.52×10^{-4}	0.3526	0.00155	0.3392	0.1362	0.1100	0.0370	0.0819
11	0.00156	0.3467	0.00170	0.3401	0.00187	0.3453	...	...	...	...	0.1119	...	0.025	...

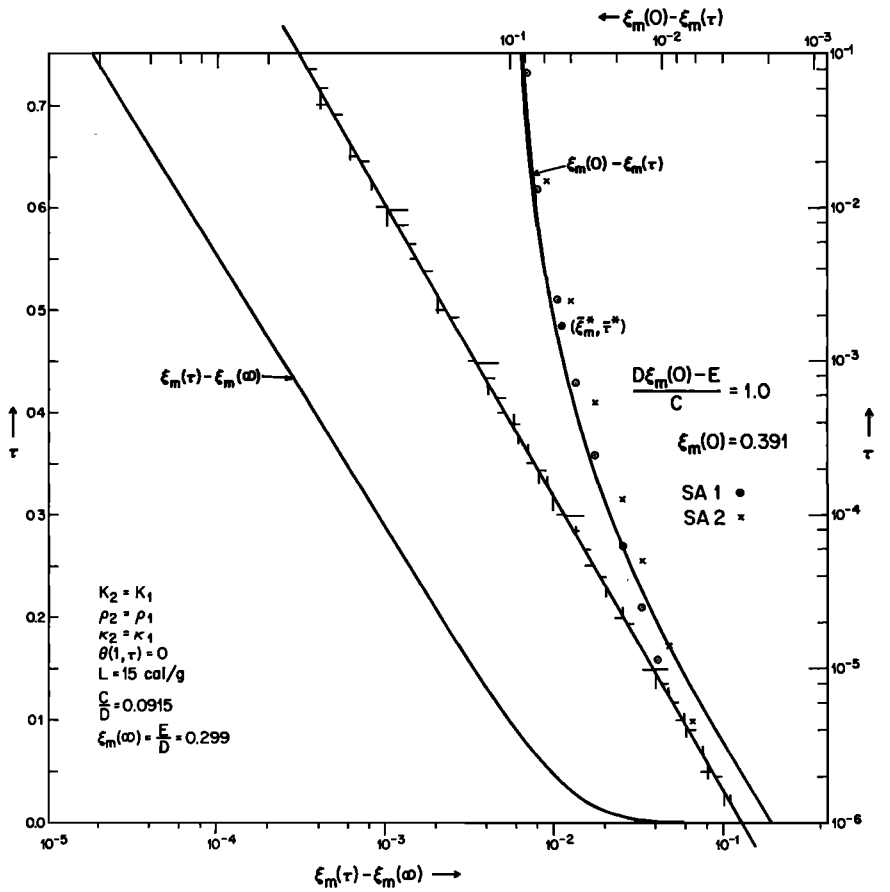

Fig. 12. Model 2. Log-log and semi-log plots showing the nature of motions of the phase boundary for model 2. See Figure 11. The only difference between models 1 and 2 is the values of the latent heat.

Nevertheless, it too will be in error as $\tau \rightarrow 0$, because implicit in the Stefan approximation is the assumption that the instantaneous temperature distribution is not influenced by the change in temperature at the phase boundary. However, for very short times the effect of the change in temperature at the phase boundary becomes large, and the neglect of this effect results in noticeable error. Nevertheless, for $\tau > 10^{-5}$, the Stefan approximation is reasonably good. For $\xi_m(0) - \xi_m(\tau) \gtrsim 0.015$, SA1 is the better approximation, never departing from the actual solution by greater than 0.005 in ξ, and remaining close to the actual solution for the latter two-thirds of the motion. The point (ξ_m^*, τ^*) is also shown, and, as was the case for model 1, the Stefan approximation remains good well beyond this point.

The long-term behavior, represented by the linear portion of the curve on the left of Figure 11, begins at nearly the same time for model 2 as for model 1; it obtains for a smaller fraction of the total displacement, however, owing to the faster motion of the phase boundary. Owing to the relatively small latent heat

in model 2, the long-term decay is controlled almost completely by the decay of the temperature distribution. In model 1 on the other hand, the latent heat was sufficient to affect the long-term behavior, as may be seen by the smaller logarithmic derivative $1/\tau_l$ as given in Table 3. For either model the agreement between τ_l and $\bar{\tau}_l$ is satisfactory.

We have seen that the motion of the phase boundary may be quite accurately predicted for short times and for long times. However, between the time before which the boundaries of the region are not felt and the time beyond which the boundaries are completely felt is usually a period of transition between these two types of behavior. The duration in time or the length of this transition region will depend on all the parameters of the problem, and predicting the motion of the boundary in this region may be a difficulty. Nevertheless, the curves in Figures 11 and 12 in this region are smoothly varying, and one might expect to reasonably approximate the curves by continuing the Stefan approximation and then utilizing the exponential behavior for the long-term behavior.

Model 3 is identical to model 2, except that the lower boundary condition (27*b*) $\theta(1, \tau) = 0$ is replaced by

$$\left.\frac{\partial \theta}{\partial \xi}\right|_{\xi=1} = 0$$

Thus the short-term behavior is identical to that of model 2, and the only difference is in the long-term behavior.

A typical temperature curve is shown in Figure 9*b*, and, since the effect of the lower boundary is not yet apparent, this curve applies equally to either model 2 or 3. The motion of the phase boundary is not shown, as it differs from that for model 2 only for long times.

We may construct a quasi-steady-state solution for this case in the same manner as was done for the constant temperature boundary condition.

$$\tilde{\theta}_{ss}(\xi, \tau) = \begin{cases} \dfrac{D\xi_m - E}{\xi_m}\xi; & 0 \le \xi \le \xi_m \\ D\xi_m - E; & \xi_m \le \xi \le 1 \end{cases}$$

Insertion of $\tilde{\theta}_{ss}$ into (28) yields

$$\frac{1}{(\xi_m - E/D)}\frac{d\xi_m}{d\tau} = \frac{1}{\dfrac{E}{D}\left[\dfrac{C}{D} + 1 - \dfrac{1}{2}\dfrac{E}{D}\right]} \equiv \frac{1}{\bar{\tau}_l} \quad \text{as} \quad \xi_m \to E/D$$

The relaxation time for

$$\left.\frac{\partial \theta}{\partial \xi}\right|_{\xi=1} = 0$$

is considerably larger than for the gutted problem for $\theta(1, \tau) = 0$, as can be seen by comparison with equation 44.

The approximate ($\bar{\tau}_l$) and actual (τ_l) relaxation times for case 3 are given in Table 3. The agreement is satisfactory.

The time τ^{**} after which logarithmic behavior should certainly obtain may be estimated in a manner analogous to that used for models 1 and 2. This yields $\tau^{**} \approx [6(1 - E/D)^2]/\pi^2$. As may be seen from the theoretical and actual values for τ^{**} in Table 3, the agreement is satisfactory.

The comparisons of the results obtained by the numerical solution of the gutted problem with those obtained from elementary physical considerations show them to be in reasonable agreement, and we conclude that the essential behavior of the generalized Stefan problem for regions with matched thermal constants is well understood. It may be noted that the important parameters are the ratios C/D and $E/D = \xi_m(\infty)$. C and E are the dimensionless latent heat and zero intercept of the Clapeyron curve and may be estimated fairly well for realistic models. The parameter D is the difference between the Clapeyron slope and initial temperature gradient and is probably one of the more uncertain and critical parameters to be estimated in constructing realistic geophysical models.

Unmatched thermal constants. We now turn to cases in which the thermal conductivities of the two phases differ. Differences in thermal conductivities cause the initial and final temperature distribution to differ, and they generate a long-term transient in the temperature distribution for the whole region, as was discussed in the section on the static problem. The relevant equations for the dynamic problem are (25) and (26) in which we will neglect convective heat transport ($\nu \equiv 0$) and sources ($\sigma \equiv 0$). The initial dimensionless steady-state temperature distribution will be

$$\eta(\xi, 0) = \gamma_1 \xi \qquad 0 \leq \xi \leq \xi_m(0)$$

$$\eta(\xi, 0) = \gamma_2 \xi + \delta_2 \qquad \xi_m(0) \leq \xi \leq 1$$

where $K_2\gamma_2 = K_1\gamma_1$ and $\delta_2 \equiv \xi_m(0)\ (\gamma_1 - \gamma_2)$ by (24). (For $T_0 = (J(0, 0)/K_1)b_0$, $\gamma_1 = 1$. However, since T_0 could be chosen otherwise, we shall continue to use γ_1.)

The form of the Stefan problem for the case in which the two phases have different thermal properties is

$$\theta(\xi, \tau) = \frac{\theta_S}{(1 - \operatorname{erf} \lambda)}\left[1 + \operatorname{erf}\left(\frac{\xi - \xi_m(0)}{2\tau^{1/2}}\right)\right] \qquad \xi \leq \xi_m(\tau)$$

$$\theta(\xi, \tau) = \frac{\theta_S}{[1 + \operatorname{erf}(\lambda/\alpha^{1/2})]}\left[1 - \operatorname{erf}\left(\frac{\xi - \xi_m(0)}{2(\alpha\tau)^{1/2}}\right)\right] \qquad \xi \geq \xi_m(\tau)$$

$$\xi_m(0) - \xi_m(\tau) = 2\lambda\tau^{1/2}$$

where λ is the root of

$$N(\lambda, \alpha, K_2/K_1, 1) = \lambda\pi^{1/2}\left\{\frac{\exp(-\lambda^2)}{1 - \operatorname{erf}\lambda} + \frac{K_2 \exp[-(\lambda^2/\alpha)]}{K_1\alpha^{1/2}[1 + \operatorname{erf}(\lambda/\alpha^{1/2})]}\right\}^{-1} = \frac{\theta_S}{C}$$

The function $N(\lambda, \alpha, K_2/K_1, 1)$ is a special case of (54) and is shown in Figure 7 for the values of the arguments used in this paper. The symbol N used for this function is in honor of Franz Neumann who first presented the solution to this type of problem [*Neumann*, 1860]. With this solution we may thus construct

Stefan approximations as in the case of the gutted problem by substituting $\theta_c(\xi_m)$ for θ_s and by regarding λ as a function of ξ_m. The Stefan approximation for the case with unmatched thermal constants does not have a discontinuity in the gradient at $\xi_m(0)$; hence it does not satisfy equation 26*d*. If $K_2 = K_1$ or $\partial\eta(\xi, 0)/\partial\xi = 0$, this Stefan approximation will satisfy the field equations and boundary conditions in the same way that it did for the gutted problem.

Because of the fact that the thermal constants of the two phases differ, equations 25 and 26 are rather complicated in comparison with the gutted problem. These complications arise because the temperature has a discontinuous gradient at certain points. In the definition of $\theta(\xi, \tau) \equiv \eta(\xi, \tau) - \eta(\xi, 0)$ we have subtracted $\eta(\xi, 0)$, which has a discontinuous gradient at $\xi_m(0)$, from $\eta(\xi, \tau)$, which has a discontinuous gradient at $\xi_m(\tau)$. Hence discontinuities in $\partial\theta/\partial\xi$ will exist at $\xi_m(\tau)$ and $\xi_m(0)$. Except at these two points, $\partial\theta/\partial\xi$ will be continuous everywhere, as can be seen in Figure 13*a*. The resultant perturbation temperature distribution is thus quite different than that for the three previous cases, and the final distribution, $\theta(\xi, \infty)$, is not identically zero everywhere. The equation for $d\xi_m/d\tau$ now includes the term $[1 - (K_2/K_1)]\ [\partial\eta(\xi, 0)/\partial\xi]$, and at the initial position of the phase boundary, equation 26*d* applies. The term

$$\left(1 - \frac{K_2}{K_1}\right) \frac{\partial\eta(\xi, 0)}{\partial\xi}\bigg|_{\xi=\xi_m-(\tau)}$$

in (26*c*) is a constant and therefore does not dominate the behavior near the singularity in $d\xi_m/d\tau$. The initial behavior in all regions will therefore be like the initial behavior of the gutted problem. If $K_2 > K_1$, the term

$$\left(1 - \frac{K_2}{K_1}\right) \frac{\partial\eta(\xi, 0)}{\partial\xi}\bigg|_{\xi=\xi_m-(\tau)}$$

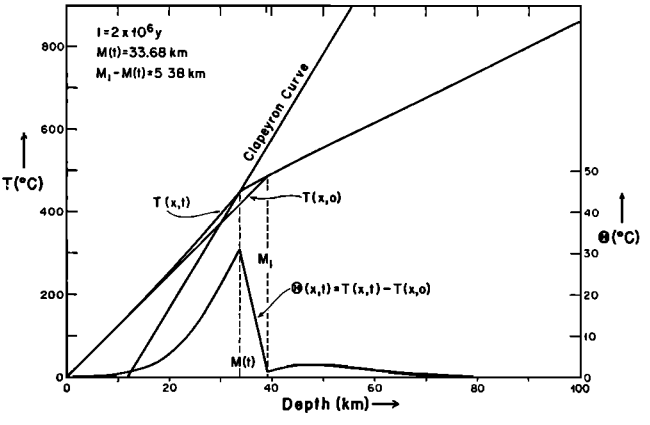

Fig. 13*a*. Model 4 and model 5 with conductivity difference ($K_2 \neq K_1$). Initial temperature and temperature after 2×10^6 years. The two models are indistinguishable at this time. The lower curve shows $\Theta(x, t)$ at the same time. Note the discontinuities in $\partial\Theta/\partial x$ at $x = M_i$ and $x = M(t)$.

is negative and acts like a heat source; thus it tends to decrease the magnitude of the velocity of the phase boundary. The additional term in (26*d*) has the same magnitude but is of different sign, and it acts like a sink at the boundary $\xi_m(0)$. If we attempt to extend the Stefan approximation to treat this case, the natural extension would be to replace C in equation 26*c* by

$$C + \left(\frac{K_2}{K_1} - 1\right) \frac{\partial \eta(\xi, 0)}{\partial \xi}\bigg|_{\xi=\xi_m(\tau)} \frac{[\xi_m(0) - \xi_m(\tau)]}{2\lambda^2}$$

which is analogous to SA2. We shall not use this, however, in the ensuing discussion.

We may estimate the time $\tau^\dagger$ at which the term

$$\left(\frac{K_2}{K_1} - 1\right) \frac{\partial \eta(\xi, 0)}{\partial \xi}\bigg|_{\xi=\xi_m-(0)}$$

in equation 26*d* has a significant effect on the temperature. This will certainly be the case when the flux from the Stefan approximation is equal to the jump in flux at the boundary $\xi_m(0)$:

$$-\frac{K_2}{K_1} \frac{\partial \tilde{\theta}_{SA}}{\partial \xi}\bigg|_{\xi=\xi_m(0)} = \left(\frac{K_2}{K_1} - 1\right) \frac{\partial \eta(\xi, 0)}{\partial \xi}\bigg|_{\xi=\xi_m-(0)}$$

This yields, using SA1

$$(\tau^\dagger)^{1/2} = \frac{\xi_m(0) - E/D}{q_1(\lambda, \alpha, \Delta\gamma/D)} \tag{48}$$

where

$$q_1(\lambda, \alpha, \Delta\gamma/D) = [1 + \operatorname{erf}(\lambda/\alpha^{1/2})]\pi^{1/2}\alpha^{1/2}(\Delta\gamma/D) + 2\lambda; \qquad \Delta\gamma \equiv \gamma_1 - \gamma_2$$

and λ is the root of

$$q_2(\lambda, \alpha, \Delta\gamma/D, K_2/K_1) = [D\xi_m(0) - E]/C$$

where

$$q_2(\lambda, \alpha, \Delta\gamma/D, K_2/K_1) = \frac{N(\lambda, \alpha, K_2/K_1, 1)q_1(\lambda, \alpha, \Delta\gamma/D)}{(\Delta\gamma/D)[1 + \operatorname{erf}(\lambda/\alpha^{1/2})]\pi^{1/2}\alpha^{1/2}}$$

For small enough λ we may approximate q_1 by

$$q_1(\lambda, \alpha, \Delta\gamma/D) \approx \pi^{1/2}(\Delta\gamma/D)\alpha^{1/2} + 2[1 + (\Delta\gamma/D)]\lambda - (2\Delta\gamma/3\alpha D)\lambda^3$$

For the parameters used in this paper, the error incurred in using this approximation is less than 2.5%. The function q_2 is shown in Figure 14 for values of the arguments used in this paper.

As has been seen in Figures 2 and 3, the heat due to the difference between the initial and final temperature distributions may be quite significant. Hence we may expect that the redistribution of this heat will be a major feature of the problem and will govern the motion of the phase boundary when the singularity is no longer dominant and possibly before the effect of the lower boundary becomes evident. We may estimate the time $\tau^{\dagger\dagger}$ beyond which this will be the case by equating the transport of heat away from the phase boundary for the

Stefan approximation with the effective flux source

$$-\left(1-\frac{K_2}{K_1}\right)\frac{\partial\eta(\xi,0)}{\partial\xi}\bigg|_{\xi=\xi_m-(\tau)}$$

at the phase boundary. This corresponds to the velocity of the phase boundary being zero if the temperature distribution in the neighborhood of the phase boundary is given by the Stefan approximation. Although this value of $\tau^{\dagger\dagger}$ will correspond to a value of $\xi_m(\tau^{\dagger\dagger})$ from the Stefan approximation, which will be physically realizable, we should not expect either the Stefan approximation for ξ_m or θ to be a good approximation to the actual values at this time. This criterion yields, using SA1

$$(\tau^{\dagger\dagger})^{1/2} = (K_1/K_2)(C\lambda/\Delta\gamma) \tag{49}$$

where λ is the root of

$$q_3(\lambda, \alpha, \Delta\gamma/D, K_2/K_1)$$
$$\equiv N(\lambda, K_2/K_1, \alpha, 1) + (K_1 2D/K_2\,\Delta\gamma)\lambda^2 = [D\xi_m(0) - E]/C$$

This function is shown in Figure 14.

Since the final temperature distribution and location of the phase boundary depend strongly on the lower boundary condition, numerical solutions were first obtained for two cases: constant flux (model 4) and constant temperature (model 5) at the lower boundary, which was fixed at 100-km depth. In both models $K_2 = 2K_1$.

The temperature distributions for model 4 at selected times are shown in Figure 13*b*. For extremely short times these are almost identical to those of the gutted problem. The discontinuity in

$$\frac{\partial\theta}{\partial\xi}\bigg|_{\xi=\xi_m(0)}$$

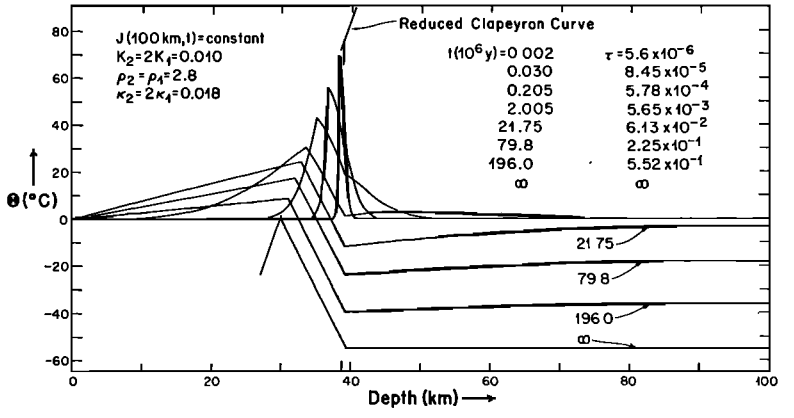

Fig. 13*b*. Model 4. Perturbation temperature at selected times for the case with constant flux at the lower boundary. The initial pulse develops similarly to that in Figure 6 but is changed later by the development of the discontinuity in $\partial\Theta/\partial x$ at $M(0) = 39$ km. Note the long-term transient and final steady state.

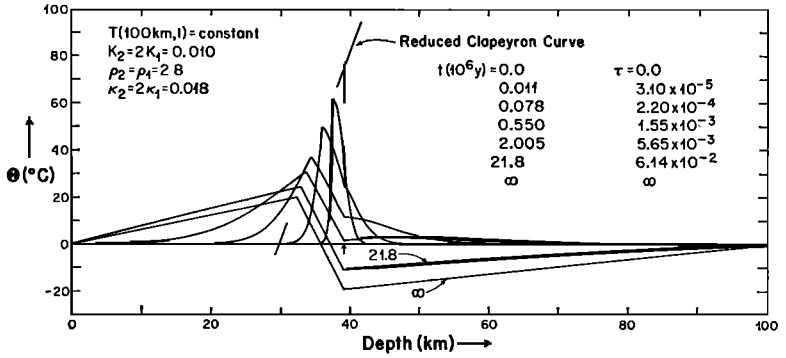

Fig. 13*c*. Model 5. Perturbation temperatures for the case with constant temperature at the lower boundary. Note the limited long-term transient and final steady state.

is apparent at $\tau = 6 \times 10^{-4}$ in the third temperature profile. This may be compared with the estimate for $\tau^{\dagger}$ of 3×10^{-4} in Table 3. The position of the phase boundary may also be compared. The value for $\tau^{\dagger\dagger}$ is also given in Table 3. By this time the discontinuities in the temperature distribution are well developed, and the incipient behavior of the long-term motion has begun to manifest itself. The effect of the discontinuity on the temperature may be seen in the last five temperature profiles, in which the long-term transient obviously dominates. Through profile 4 the temperature everywhere exceeds the initial steady state;

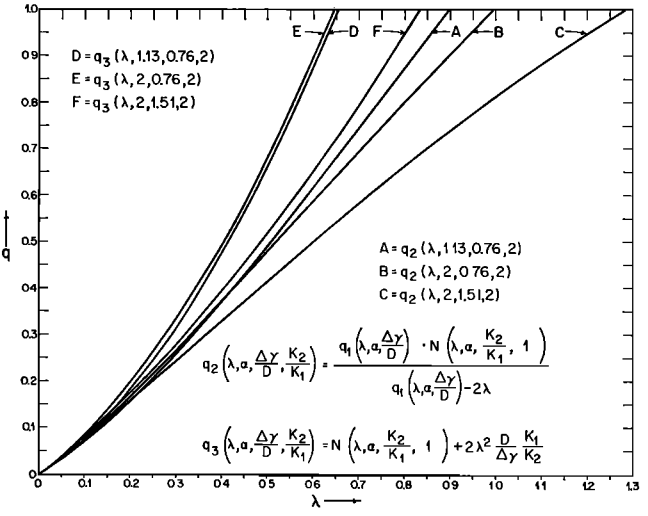

Fig. 14. Graphs of the functions q_2 and q_3 for selected values of the arguments. These functions define $(\tau\dagger)^{1/2}$ and $(\tau\dagger\dagger)^{1/2}$, $\lambda\dagger\dagger$ and $\lambda\dagger$. $\lambda\dagger\dagger$ is the root of q_3 $(\lambda\dagger\dagger, \alpha, \Delta\gamma/D, K_2/K_1) = (D\xi_m(0) - E)/C$ and $(\tau\dagger\dagger)^{1/2} = C\lambda K_1/K_2\,\Delta\gamma$. $\lambda\dagger$ is the root of q_2 $(\lambda\dagger, \alpha, \Delta\lambda/D, K_2/K_1) = (D\xi_m(0) - E)/C$ and $(\tau\dagger)^{1/2} = (\xi_m(0) - E/D)/q_1$ $(\lambda\dagger, \alpha, \Delta\lambda/D)$ (see text for q_1).

subsequent to this time ($\sim\tau^{\dagger\dagger}$) the temperature for part of the region is less than the initial state and greater than the final state.

The motion of the phase boundary for model 4 is shown in Figure 15*a*. Comparison of the numerical results shows that the motion is nearly identical with that of the gutted problem for $\tau < \tau_1^{\dagger}$. The departure after that time is apparently due to the influence of the discontinuity in

$$\left.\frac{\partial\theta}{\partial\xi}\right|_{\xi=\xi_m(0)}$$

and the dominance of the long-term transient for $\tau > \tau_1^{\dagger}$.

It should be pointed out that in models 1, 2, and 3, the Stefan approximation, where applicable, appears to be nearly an exact solution. For model 4, while the Stefan approximation appears to be a reasonable one, it is not an accurate representation for θ for sizeable displacements, as can be seen from the estimate for $\xi_m(\tau^{\dagger})$ and $\xi_m(\tau^{\dagger\dagger})$.

The long-term motion may be estimated in a manner analogous to that used

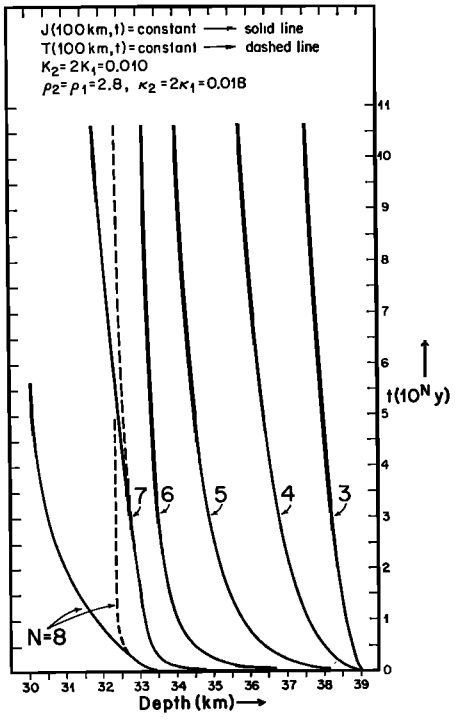

Fig. 15*a*. Models 4 and 5. The position of the phase boundary versus times, comparing the effects of constant flux or constant temperature at the lower boundary (c.f. Figure 13*b*, *c*). Note that the curves for different values of N correspond to different time scales.

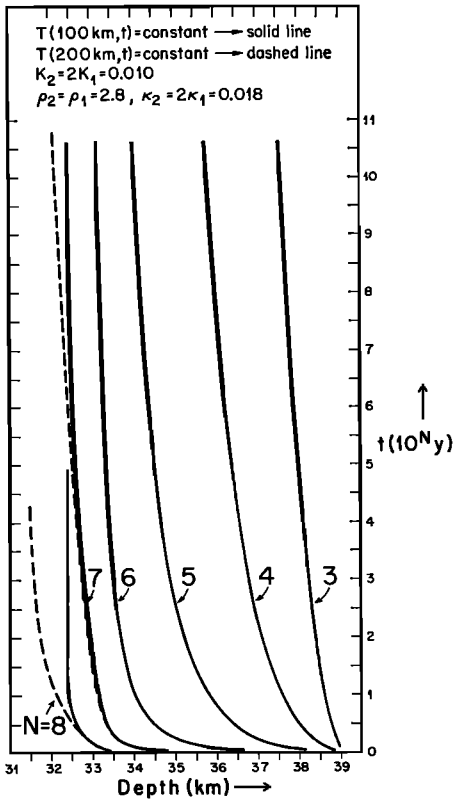

Fig. 15*b*. Models 5 and 6, illustrating the effect of the depth at which the lower boundary condition is applied. Note that the long-term motion for model 6 is intermediate to those of models 4 and 5.

in the previous cases. For a case with constant flux at the lower boundary, this yields a relaxation time

$$\bar{\tau}_l = \frac{E}{D}\left\{\frac{C}{D} + \frac{E}{D}\left[\frac{\gamma_1}{D} + \frac{1}{2}\right]\left[1 - \frac{2\gamma_1}{\gamma_2\alpha}\right] + \frac{\gamma_1}{\gamma_2\alpha}\left[1 + \frac{\gamma_1}{D} - \frac{\gamma_2}{D}\left(1 - \frac{E}{D}\right)\right]\right\} \tag{50}$$

which is given in Table 3. As can be seen in Figure 15*a*, there is a very prominent long-term transient, as would be expected from the steady-state discussion and the magnitude of τ_l for this case.

The time τ^{**}, after which the above long-term behavior should obtain, is given by

$$\bar{\tau}^{**} = 2(1 - E/D)^2/\alpha\pi^2 \tag{51}$$

which is analogous to equation 46. This is given in Table 3.

We now consider model 5, which is identical to model 4, except that the lower boundary condition is taken as constant temperature rather than as constant flux at the lower boundary.

The governing equations for case 5 are, of course, identical to those of case 4, except for the change in the lower boundary condition. Hence, the same criteria for the breakdown of Stefan behavior at $\tau = \tau^{\dagger}$ and $\tau = \tau^{\dagger\dagger}$ apply, and the only difference between the two cases occurs for long-term behavior governed by the lower boundary condition.

The final equilibrium position of the phase boundary for this case is given by the root of

$$(D + \gamma_1)\left(\frac{\gamma_1}{\gamma_2} - 1\right)\xi_m^2 + \left[D + \gamma_1 - \frac{\gamma_1}{\gamma_2}\eta(1, 0) - \left(\frac{\gamma_1}{\gamma_2} - 1\right)E\right]\xi_m - E = 0 \tag{52}$$

Thus for this case $\gamma_1 \neq \gamma_2$ (or $K_1 \neq K_2$), $\xi_m(\infty)$ will *not* be E/D, as in the previous cases. For this reason the Stefan approximation is not internally consistent in that $\xi_{m\,SA}$ may be less than $\xi_m(\infty)$. The formal equations of the Stefan approximation which are used for estimates of $\tau^{\dagger}$, $\tau^{\dagger\dagger}$ may be subject to more error than in the previous cases, and $\xi_{m\,SA}(\tau^{\dagger\dagger})$ may lie outside of the accessible region for ξ_m. In addition, the long-term behavior for this case may be significantly different from that of the cases where $\xi_m(\infty) = E/D$.

Construction of a quasi-steady-state temperature distribution with the correct limiting end point $\xi_m(\infty)$ yields

$$\frac{1}{(\xi_m(\tau) - \xi_m(\infty))}\frac{d\xi_m}{d\tau}$$

$$\rightarrow \frac{2\xi_m(\infty)(D + \gamma_1)\left[\frac{\gamma_1}{\gamma_2} - 1\right] - E\left[\frac{\gamma_1}{\gamma_2} - 1\right] + D + \gamma_1 - \frac{\gamma_1}{\gamma_2}\eta(1, \tau)}{\left[C + ((D+\gamma_1)\xi_m(\infty) - \tfrac{1}{2}E)\left(1 - \frac{\gamma_1}{\gamma_2\alpha}\right) + \frac{\gamma_1}{2\gamma_2\alpha}(D + \gamma_1 - \eta(1, 0))\right][1 - \xi_m(\infty)]\xi_m(\infty)}$$

$$= \frac{-1}{\bar{\tau}_l} \quad \text{as} \quad \xi_m \rightarrow \xi_m(\infty) \tag{53}$$

Comparison of the actual and approximate values may be seen in Table 3.

The long-term relaxation time for this case is considerably less than that for model 4. In addition, the distance the phase boundary must move is less for this case than for model 4.

The development of the temperature distribution with time is shown in Figure 13*c*. Prior to 20×10^6 years the temperature distribution for this case is nearly identical to that for model 4 (cf. Figure 12*b*); after that time the two models diverge. Model 5 attains equilibrium fairly rapidly, in contrast to model 4 whch approaches equilibrium quite slowly.

This may also be seen in Figure 15*a*, which shows the motion of the phase boundary for both cases. The long transient for model 4 is apparent. On the other hand, in model 5, the phase boundary nearly reaches its final position before the long-term behavior becomes evident; in fact, for this case a long-term transient is essentially nonexistent in relation to the total displacement of the phase boundary. This illustrates the primary effect of the lower boundary condition on the problem. For constant temperature at the lower boundary $b(t)$, equilibrium is approached by internally redistributing the excess heat from $\xi > \xi_m$ to the region $\xi < \xi_m$, which has a heat deficit compared with the final state. In contrast, for constant flux at $b(t)$, there is no region that has a lower temperature than the final steady state; hence the excess of heat cannot be compensated for internally and must escape at the boundary $\xi = 0$, which leads to a major long-term transient.

In the preceding models the thickness of the region was 100 km and the phase boundary was originally near the center of the region. To evalute the effects of distance to the lower boundary, we have investigated model 6, in which the lower boundary is at 200 km, at which the temperature is constant.

The motion for short times will be the same as in cases 4 and 5; the only difference will be the long-term behavior and the final position of the phase boundary.

The long-term relaxation time will be given by equation 50, as it was for model 5. Note, however, that, since b_0 is different for the two models, the scale factor relating dimensionless time τ to real time t will not be the same for the two cases. As can be seen in Table 3, the relaxation time for model 6 is nearer that for model 4 (constant flux at 100 km) than that for model 5 (constant T at 100 km). The final position of the phase boundary will be intermediate between those for models 4 and 5. In the limit $b_0 \to \infty$ for the same initial steady state, the final position of the phase boundary will be E/D for either boundary condition.

The motion of the phase boundary is shown in Figure 15*b*, where it is compared with model 5. Comparison with Figure 15*a* will demonstrate that this case is intermediate between models 4 and 5.

Comparison of the effects of different boundary conditions and the depth at which they apply shows that the boundary conditions do not affect the short-term behavior; they do, however, significantly affect the long-term behavior, both in terms of the rates of movement of the phase boundary and its final position. In the consideration of a realistic geophysical problem including the thermal impedance of the material causing the pressure pulse, sedimentation and erosion

rates (particularly the latter), and isostasy, it is clear that the choice of the lower boundary condition may be primary in determining the elevation and duration of positive surface relief. The proper lower boundary condition that describes the actual geophysical conditions is not obvious to the authors.

In model 5 the pressure pulse was the maximum that could be applied without overdriving the system. To better illuminate the response when $(1/C)$ $(D\xi_m(0) - E) < 1$, model 7 was investigated. In model 7 the latent heat was taken as 30 cal/g, rather than 15 cal/g, as in model 5. Otherwise, the models are identical. The short-term behavior for this model agrees with that predicted by the Stefan approximation, as can also be seen in Table 3. As in the comparison between models 1 and 2 for the gutted problem, the greater latent heat significantly slows the phase boundary in the region of Stefan behavior. The long-term behavior is, however, little affected by the larger latent heat, as is expected, since the primary process is the redistribution of the heat of the initial temperature distribution.

All the preceding models have had the same reduced Clapeyron curve $D\xi_m - E$, which partly determined: (1) the total displacement of the phase boundary $\xi_m(0) - \xi_m(\infty)$; (2) the initial temperature at the phase boundary $D\xi_m(0) - E$; (3) the criteria τ^* and $\tau^\dagger$ for cessation of Stefan behavior; and (4) the long-term relaxation time τ_l.

As an illustration of the effect of the Clapeyron slope, model 8 was constructed such that the reduced Clapeyron slope was reduced to one-half of its value in the previous models. In order to keep $\xi_m(0)$ unchanged (for purposes of comparison with previous models), it was necessary to alter E as well. All other parameters were unchanged from model 5. The numerical and theoretical results are presented in Table 3. The agreement is as expected from previous cases. It should be noted that the short-term motion is slower than in model 5, owing to the smaller initial perturbation temperature at the phase boundary, and that the long-term transient is more prominent, owing primarily to the larger total displacement of the phase boundary for this model.

In all the models that have so far been considered, we have taken $\alpha = K_2/K_1$. Since α appears only in the field equations, whereas K_2/K_1 appears in the boundary conditions, it was considered desirable to consider a case for $\alpha \neq K_2/K_1$. This was done in model 9. A Stefan solution has been presented that approximates this model and may therefore be compared with the numerical solution. The motion of the phase boundary compared with that for model 5 is shown in Figure 16. The motion for model 9 is initially faster than that for model 5, because the smaller diffusivity of model 9 reflects a larger heat capacity ($\kappa = K/\rho c$). Thus more heat may be released into the region behind the phase boundary for the same rise in temperature as for model 5. The fact that model 9 lags behind model 5 for longer times ($t \gtrsim 7 \times 10^4$ yr) is due to the redistribution of the heat that was originally behind the phase boundary. Again this is a reflection of the greater latent heat of model 9. The approximate solutions for both short and long times are again in good agreement with the numerical results.

Convective heat transport. We have so far discussed only the most elementary cases in which we neglected convective heat transfer and the presence of heat sources. We now turn to the investigation of the effects of including convec-

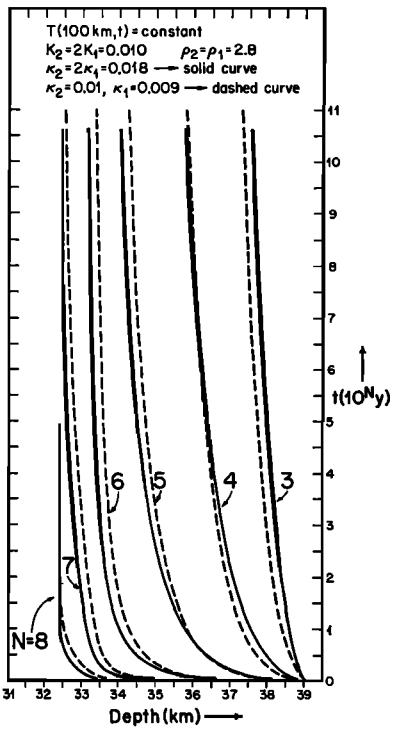

Fig. 16. Models 5 and 9. The effect of the thermal diffusivity of the lower layer on the motion of the phase boundary. Although both curves have the same endpoint, there are slight differences in the detailed motion of the phase boundary.

tive heat transfer, which is expressed by the term

$$\nu\left(\frac{\partial\theta(\xi,\tau)}{\partial\xi}+\frac{\partial\eta(\xi,0)}{\partial\xi}\right)$$

in the field equations 25 and the motion of the lower boundary $\beta(\tau)$. Thus the difference in density of the two phases will no longer be neglected, and the mass in the region $0 < \xi < \beta(\tau)$ will be conserved. In the ensuing discussion we will assume $K_2 > K_1$.

For short times less than τ^{**}, as defined in (51), the effect of the lower boundary $\beta(\tau)$ will be insignificant and we need only investigate the effect of the convective term in the field equation. Owing to the nonlinearity of the field equations with the convective term included, it is no longer possible to consider the perturbation temperature $\theta(\xi, \tau)$ separately from the initial steady state, as is indicated by the presence of the term $[\partial\eta(\xi, 0)/\partial\xi]$ in the field equations 25.

Initially the velocity of the phase boundary and the temperature gradients in the neighborhood of the phase boundary are singular, and $[\partial\theta(\xi, \tau)/\partial\xi]$ will dominate the convective term in the field equations in the neighborhood of the phase boundary. We may investigate this term by appealing once again to the Stefan approximation. A solution to the generalized Stefan problem, including convected heat, may be obtained from the form given by *Carslaw and Jaeger* [1959, p. 290]:

$$\theta_{SA}(\xi, \tau) = \frac{\theta_c(\xi_m)}{1 - \operatorname{erf}\lambda}\left[1 + \operatorname{erf}\frac{\xi - \xi_m(0)}{2\tau^{1/2}}\right]; \qquad \xi \leq \xi_m(\tau)$$

$$\theta_{SA}(\xi, \tau) = \frac{\theta_c(\xi_m)}{1 + \operatorname{erf}(\lambda\rho_1/\alpha^{1/2}\rho_2)}\left\{1 - \operatorname{erf}\left[\frac{\xi - \xi_m(0)}{2(\alpha\tau)^{1/2}} + \frac{\lambda(\rho_2 - \rho_1)}{\rho_2\alpha^{1/2}}\right]\right\} \qquad \xi \geq \xi_m(\tau)$$

$$\xi_m(0) - \xi_m(\tau) = 2\lambda(\xi_m)\tau^{1/2}$$

where λ is the root of

$$N(\lambda, \alpha, K_2/K_1, \rho_2/\rho_1)$$

$$\equiv \lambda\pi^{1/2}\left\{\frac{e^{-\lambda^2}}{1 - \operatorname{erf}\lambda} + \frac{K_2}{K_1}\frac{e^{-(\lambda\rho_1/\alpha^{1/2}\rho_2)^2}}{\alpha^{1/2}[1 + \operatorname{erf}(\lambda\rho_1/\alpha^{1/2}\rho_2)]}\right\}^{-1} = \frac{\theta_c}{C}(\xi_m) \qquad (54)$$

This is an exact solution to the problem defined in (25) and (26) if (1) $\sigma_2 = \sigma_1$; (2) $[\partial\eta(\xi, 0)/\partial\xi] = 0$; (3) $\theta(\xi_m, \tau) =$ constant; and (4) the region is infinite. Owing to the initial singularity in $d\xi_m/d\tau$, condition 2 is nearly satisfied near the phase boundary for short times for all cases.

The function $N(\lambda, \alpha, K_2/K_1, \rho_2/\rho_1)$ is shown in Figure 7 and compared with $N(\lambda, \alpha, K_2/K_1, 1)$ for equivalent arguments. It is evident from the similarity of the two curves that the term $\nu(\partial\theta/\partial\xi)$ in the field equation has little effect on the velocity or position of the phase boundary for a 20% difference in density. In region 1, at a given time, the effect of convected heat does not change the functional form of the temperature distribution but only the magnitude of the perturbation, because of the change in the value of the root of $N(\lambda, \alpha, K_2/K_1, \rho_2/\rho_1)$ as compared with $N(\lambda, \alpha, K_2/K_1, 1)$. In region 2 the spatial temperature distribution will be altered owing both to the scaling due to the change in the characteristic root and to the motion of colder material toward the phase boundary. This will tend to decrease the width of the temperature peak to the right of the phase boundary and corresponds to a translation of the temperature distribution by $[2\lambda(\rho_2 - \rho_1)/\rho_2]\,\tau^{1/2}$.

As has been stated, the singularity in $[\partial\theta(\xi, \tau)]/\partial\xi$ at $\tau = 0$ makes $[\partial\eta(\xi, 0)]/\partial\xi$ or any other finite term negligible in the immediate neighborhood of the phase boundary for the initial motion. At points somewhat removed from the immediate vicinity of the phase boundary, however, the terms $[\partial\theta(\xi, \tau)]/\partial\xi$ and $[\partial\eta(\xi, 0)]/\partial\xi$ may cancel for some given points in space and time. As seen from the Stefan problem, such 'accidental' cancellations should not significantly affect the actual solution to the problem, since the effect of convective heat transport is small for the cases considered here.

At distances from the phase boundary where the temperature is little affected by the heat released at the phase boundary, $[\partial\eta(\xi, 0)]/\partial\xi$ will become the dominant term in the field equation. In the limiting case at point ξ_i, where the temperature is invariant

$$\left.\frac{D\eta(\xi, \tau)}{D\tau}\right|_{\xi=\xi_i} = 0$$

and

$$\left.\frac{[\partial\theta(\xi, \tau)]/\partial\tau}{\nu\{[\partial\eta(\xi, 0)]/\partial\xi + [\partial\theta(\xi, \tau)]/\partial\xi\}}\right|_{\xi=\xi_i} = -1$$

will apply. Thus $[\partial^2\theta(\xi, \tau)]/\partial\xi^2 = 0$ and the time dependence of the temperature is completely dominated by the convective term. This will apply at the lower boundary $\xi_i = \beta(\tau)$, if $\eta(\beta(\tau), \tau) =$ constant. If the lower boundary condition is constant flux, then

$$\frac{\partial\theta(\beta(\tau), \tau)}{\partial\xi} = \frac{\partial\eta(\beta(0), 0)}{\partial\xi} - \frac{\partial\eta(\beta(\tau), 0)}{\partial\xi}$$

If there are no sources, it follows that $[\partial\theta(\beta(\tau),\tau)]/\partial\xi = 0$; hence again the term $[\partial\eta(\xi, 0)]/\partial\xi$ completely dominates the convective term. In these cases the changes in temperature are totally due to the translation of the initial temperature distribution.

The principal effect of the motion of the lower boundary is its effect on the final equilibrium position of the phase boundary and the final temperature distribution; even this, however, is slight for geophysically reasonable models.

From the preceding discussion it can be seen that the neglect of the convective heat transport results in two effects: (1) the temperature distribution in the immediate neighborhood of the phase boundary will be altered and the motion of the phase boundary will be too slow; (2) the total movement of the phase boundary, $\xi_m(0) - \xi_m(\infty)$, will be slightly overestimated and the final temperature will be too low. The magnitude of these errors will, of course, depend on the values of the parameters used. For the geophysical situation considered in this paper, the errors appear to be unimportant, especially considering the uncertainties in the lower boundary condition and the values of the parameters.

It may be noted that, if the nonlinear terms in the field equation are neglected, but the lower boundary $\beta(\tau)$ is moved so that the matter conservation equations are satisfied, and the correct boundary conditions are applied at that point, then the system will approach the proper final equilibrium state. This approximation effectively generates, however, an anomalous transient in the temperature distribution corresponding to a heat source or sink depending on the sign of the velocity. This may be understood by referring to Figure 17*a*. In the region between $M(t)$ and $b(t)$, the nonzero value of Θ is primarily due to convected heat. If this means of heat transport is neglected, the final temperature distribution in this region will have to be attained solely by conduction, which will generate a long-term transient.

In order to show the effects discussed in the preceding paragraphs, numerical solutions were obtained. In both models 10 and 11 the parameters are identical with those of model 9. In model 10 the lower boundary $\beta(\tau)$ was moved to satisfy mass conservation in the region $0 \leq \xi \leq \beta(\tau)$, and the temperature at $\beta(\tau)$ was kept constant. The convective term $\nu\{[\partial\theta(\xi, \tau)]/\partial\xi + [\partial\eta(\xi, 0)]/\partial\xi\}$ in the field equation was *neglected*. Model 11 is identical to model 10 except that the convective heat transport is *not* neglected. The position of the phase boundary with time for each case is shown in Figure 18. It should be noted that both cases have the same final equilibrium states.

The temperature distributions in the vicinity of the phase boundary at a relatively short time are shown in Figure 17*b* for both cases. It may be seen that the phase boundary for the model including the convective term has traveled slightly

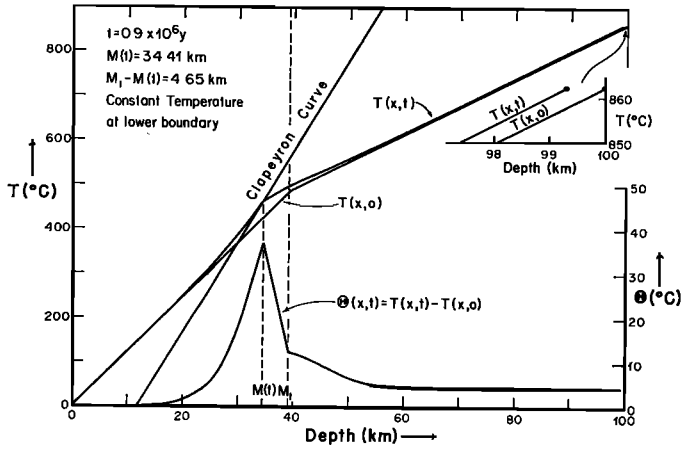

Fig. 17*a*. Model 11. Initial temperature and temperature after 0.9 m.y., showing the effect of convective heat transport. The upper detail shows the effects due to the convective heat transport. The nonzero value of Θ for depths greater than 60 km is almost entirely due to the translation of the initial steady state in this region.

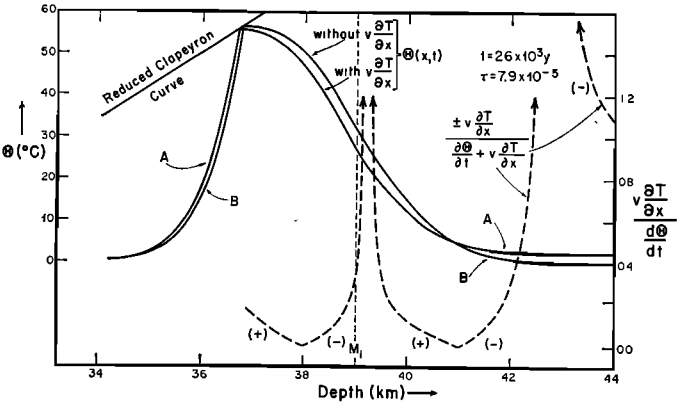

Fig. 17*b*. Curve A shows the temperature in the neighborhood of the phase boundary for model 11 for short times. Curve B is for model 10, in which convective heat has been neglected but the lower boundary moved to conserve mass. The dashed curve shows the ratio of the convective term $V\ \partial T/\partial x$ to the total time derivative of the temperature $D\Theta/Dt = \partial\theta/\partial t + V\ (\partial T/\partial x)$. This ratio is less than 0.2 near the phase boundary except for an isolated point and becomes dominant in the region approaching the lower boundary. The + and − signs correspond to branches of the dashed curve where $V\ (\partial T/\partial x)/(D\Theta/Dt)$ is positive or negative, respectively.

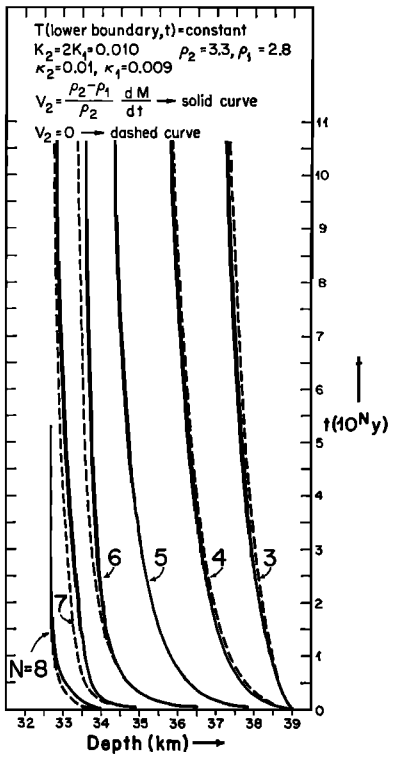

Fig. 18. Effect of convective heat on the motion of the phase boundary. In model 10 (dashed line), convective heat is neglected but mass is conserved by moving the lower boundary. In model 11 convective heat is not neglected. The difference between the two curves for long times is due to the anomalous long-term transient that results from the neglect of convective heat in model 10. In general the difference between the two curves is small.

farther than for the model neglecting the convective term. In addition, the temperature immediately behind the phase boundary is lower for the former case, owing to the motion of 'colder' material toward the phase boundary. Farther behind the phase boundary, the temperature for the case with convective heat transport is greater than for the other case. This is due to the term $\nu[\partial\eta(\xi, 0)]/\partial\xi$ and is a result of the translation of the whole region $\xi_m \leq \xi \leq \beta$ toward the phase boundary.

Also shown in Figure 17*b* is the ratio of the convective term $V\ (\partial T/\partial x)$ to the total time derivative $D\Theta/Dt = (\partial\Theta/\partial t) + V\ (\partial T/\partial x)$ for model 10. Since the velocity vanishes identically in front of the phase boundary, this ratio also vanishes. Immediately behind the phase boundary the convective term is up to twenty per cent of $D\Theta/Dt$. The singularities in the ratio at depths of 39.2 and 42.3 km are due to the vanishing of $D\Theta/Dt$ and do not have a noticeable effect on the temperatures at these points. At depths greater than 43 km the neglected convective term would account for all the temperature, as is seen by comparing the temperature for model 11 in this region. At the point $\beta(\tau)$ (which may be seen in Figure 17*a*), the ratio is -1, as required by the invariance of the temperature at the lower boundary.

Thermal blanketing and reversals. In all the preceding discussion we have assumed that the pressure pulse ΔP has no thermal impedance. As discussed in the section on static behavior, the initial effect of a thermal blanket is insignifi-

cant, and the phase boundary will rise in response to the pressure pulse and move toward the position M_f as determined for no thermal impedance. However, the upper boundary conditions must finally dominate and cause the phase boundary to move toward the true equilibrium position, which may involve a reversal of motion. The time and position at which such a reversal occurs is of deep significance, since these factors determine the depth of maximum subsidence and the time at which the motion of the surface will reverse and uplift will begin. The time and position of reversal in conjunction with erosion rates, will govern the height and duration of positive relief.

Although it is not the purpose of this paper to discuss the detailed geophysical problem, including the effects of sedimentation and erosion rates, we can point out the basic effects that will result and the characteristic constants of the motion. We will present a discussion of the more complete geophysical problem in another paper.

Let us consider a sediment layer of thickness $s = \Delta P/\rho g$ at zero temperature deposited instantaneously on the surface $x = 0$. The top of the sediments will then be at $x = -s$. The temperature distribution immediately after the deposition of the sediments will be

$$T(x, 0) = 0 \qquad -s \leq x \leq 0$$

$$T(x, 0) = \frac{J(0, 0)}{K_1} x \qquad 0 \leq x \leq M(0)$$

$$T(x, 0) = \frac{J(0, 0)}{K_2} (x - M(0)) + \frac{J(0, 0)}{K_1} M(0) \qquad M(0) \leq x \leq b(0)$$

Subsequent to deposition, the temperature of the sediments and the material beneath the sediments will rise because of the flux from beneath, which is comprised of the initial flux and the flux due to the latent heat released by the phase change. The temperature gradient in the region $0 \leq x \leq M(t)$ will therefore be decreased, which will slow the motion of the phase boundary.

For short times the effect of the thermal blanketing will be small in the region of the phase boundary, and the initial motion of the phase boundary will be essentially Stefan-like in behavior as shown in Figure 19*a*. Eventually, however, the temperature distribution in the region $-s \leq x \leq M(t)$ will become substantially different from that for Stefan behavior, owing to the effects of the boundaries, which differ from those discussed in the previous sections because of the thermal blanketing caused by the sediments between $-s \leq x \leq 0$.

We may estimate when the effects of the thermal blanketing will become significant by considering the superposition of the solution to the thermal blanketing alone superposed on the solution for Stefan behavior.

As the problem is intrinsically nonlinear, this approach is not exact. As before, however, we assume that a good approximation for ξ_m is obtained if the approximation for θ is a solution to the field equations, satisfies the initial conditions satisfies the boundary condition at ξ_m, and approximately satisfies the other boundary conditions. We will first formulate the problem exactly and then obtain approximations for θ.

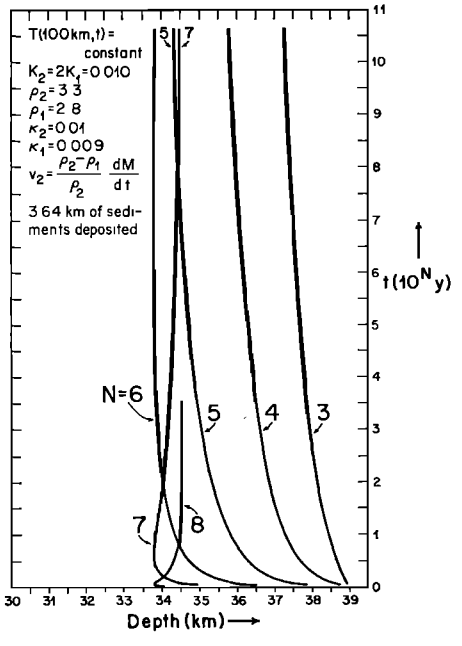

Fig. 19*a*. The motion of the phase boundary for model 13 in which sediments have been instantaneously placed on the surface at time = 0. The effect of the sediments is not apparent much before the motion reverses direction at 7×10^6 years, as can be seen by comparison with model 11.

In terms of the perturbation temperature θ, the problem for the thermal blanketing may conveniently be formulated by defining

$$\eta(\xi, 0) = \gamma_1 \xi \qquad \xi_s \leq \xi \leq 0; \qquad \xi_s \equiv -s/b_0$$

This extends the initial temperature distribution into the region where the sediments will be deposited such that $\partial\eta(\xi, 0)/\partial\xi$ is continuous, thus assuring that $\partial\theta(\xi, \tau)/\partial\xi$ will be continuous in the region $\xi_s \leq \xi \leq \xi_m(\tau)$ for $\tau > 0$.

The initial perturbation temperature distribution is thus

$$\begin{aligned} \theta(\xi, 0) &= -\gamma_1 \xi \qquad && \xi_s \leq \xi \leq 0 \\ \theta(\xi, 0) &= 0 \qquad && 0 \leq \xi \leq \beta(0), \quad \xi \neq \xi_m(0) \\ \theta(\xi_m(0), 0) &= \theta_c(\xi_m(0)) \end{aligned} \tag{55}$$

The boundary condition at the surface becomes $\theta(\xi_s, \tau) = -\gamma_1 \xi_s$. This initial state may be seen in Figure 19*b*.

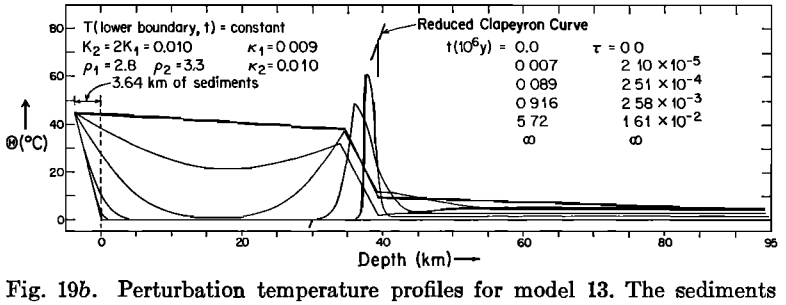

Fig. 19*b*. Perturbation temperature profiles for model 13. The sediments initially have the perturbation temperature shown to the left of $x = 0$. The phase boundary reverses its motion at $\tau = 0.0192$, just after the time of the second to last profile. The last profile shows the final steady state.

We will here consider the case where ξ_s is small relative to ξ_m. If we then neglect some of the heat initially in the sediments, i.e. $\theta(\xi, 0) = -\gamma_1\xi \cong 0$, $\xi_s < \xi \leq 0$ then

$$\begin{aligned} \theta(\xi_s, 0) &= -\gamma_1\xi_s \\ \theta(\xi, 0) &= 0 \qquad\qquad \xi_s \leq \xi \leq \beta(0), \quad \xi \neq \xi_m(0) \\ \theta(\xi_m(0), 0) &= \theta_c(\xi_m(0)) \end{aligned}$$

an approximate solution for short times will be given by [*Carslaw and Jaeger*, 1959, p. 310]

$$\tilde{\theta}_R(\xi, \tau) \equiv \tilde{\theta}_{SA}(\xi, \tau) + \tilde{\theta}_B(\xi, \tau)$$

$\tilde{\theta}_B$ is the solution for a slab of thickness $\xi_m - \xi_s$, initially at zero temperature, whose boundaries at ξ_s and ξ_m are maintained at temperatures of $-\gamma_1\xi_s$ and 0, respectively. Thus

$$\tilde{\theta}_B(\xi, \tau) = \frac{\gamma_1 s}{b_0} \sum_{n=0}^{\infty} \left\{ \operatorname{erfc}\left[\frac{(2n+1)(\xi_m - \xi_s) - \xi_m + \xi}{2\tau^{1/2}}\right] - \operatorname{erfc}\left[\frac{(2n+1)(\xi_m - \xi_s) + \xi_m - \xi}{2\tau^{1/2}}\right]\right\}$$

for $\xi_s \leq \xi \leq \xi_m(\tau)$ and

$$\tilde{\theta}_B(\xi, \tau) = 0$$

for $\xi_m(\tau) \leq \xi \leq \beta(\tau)$.

$\tilde{\theta}_B$ satisfies the initial condition $\tilde{\theta}_B = 0$ everywhere except at $\xi = \xi_s$, and $\tilde{\theta}_B(\xi_s, \tau) = -\gamma\xi_s$. Hence $\tilde{\theta}_R = \tilde{\theta}_B + \tilde{\theta}_{SA}$ satisfies the initial conditions and the boundary condition $\tilde{\theta}_R(\xi_m, \tau) = \tilde{\theta}_c(\xi_m)$. The boundary condition $\theta(\xi_s, \tau) = -\gamma_1\xi_s$ is in error by the amount $\tilde{\theta}_{SA}(\xi_s, \tau)$ and that at $\beta(\tau)$ is in error by $\tilde{\theta}_{SA}(\beta(\tau), \tau)$.

Inserting $\tilde{\theta}_R$ into the condition at the moving boundary $\xi_m(\tau)$ yields

$$-C\frac{d\xi_m}{d\tau} \approx Q(\xi_m, \lambda) \equiv \frac{1}{\pi^{1/2}\tau^{1/2}} \left\{ \frac{\theta_c \exp(-\lambda^2)}{1 - \operatorname{erf}\lambda} + \frac{\gamma_1\theta_c \exp(-\lambda^2/\alpha)}{\gamma_2(1 + \operatorname{erf}\lambda/\alpha^{1/2})} + 2\gamma_1\xi_s \sum_{n=0}^{\infty} \exp\left[-\frac{(2n+1)^2(\xi_m - \xi_s)^2}{4\tau}\right]\right\} \tag{56}$$

Setting $\lambda = [\xi_m(0) - \xi_m(\tau)]/2\tau^{1/2}$ and $\theta_c = D\xi_m - E$ thus results in a first-order differential equation for $\xi_m(\tau)$. This first-order equation may be integrated numerically to obtain $\xi_m(\tau)$. The time at which the phase boundary reverses motion is defined as τ_R and for this approximation $\tilde{\tau}_R$ may be determined by the condition $-C\, d\xi_m/d\tau = Q = 0$. Since $\tilde{\tau}_R$ is obtained by a simple integration, the effectiveness of this method for estimating τ_R is of considerable importance.

In the above approximation, $\tilde{\tau}_R$ is a root of $Q(\xi_m, \lambda) = 0$, which defines a curve in the (ξ_m, λ) plane. Thus the intersection of a curve $\lambda(\xi_m)$ with $Q = 0$ defines $(d\xi_m/d\tau) = 0$ for the approximation of $\lambda(\xi_m)$ used. It would be useful to obtain an analytic expression for τ_R in order to gain some insight into the dependence of τ_R on the other parameters of the system. Insofar as the position of the phase

boundary as a function of time prior to reversal does not deviate greatly from the Stefan approximation, we may estimate λ by use of the characteristic equation (54) $N(\lambda, \alpha, K_2/K_1, \rho_2/\rho_1) = \theta_c(\xi_m)/C$ and $Q = 0$, resulting in an approximation of τ_R. It should be noted that this approximation is internally inconsistent.

For the case for small λ, $N \approx [\pi^{1/2}\lambda/(1 + K_2/K_1)]$, and using (35) and (56), in which only the first term in the infinite series is retained, we obtain the approximate relationship

$$\tau_R \cong \bar{\tau}_{R_1} \equiv \frac{(\xi_m - \xi_s)^2}{4 \log [-2\gamma_1\xi_s/C(\pi)^{1/2}\lambda]} \tag{57}$$

$$\bar{\tau}_{R_1} = \frac{\left\{\left[\dfrac{C(\pi)^{1/2}}{D[1 + (\gamma_1/\gamma_2)]}\,\xi_m(0) + 2(E/D)\tau_R{}^{1/2}\right] \Big/ \left(\dfrac{C(\pi)^{1/2}}{D[1 + (\gamma_1/\gamma_2)]} + 2\tau_R{}^{1/2}\right) - \xi_s\right\}^2}{4 \log \left\{\dfrac{-2\gamma_1\xi_s\left[\dfrac{C(\pi)^{1/2}}{D[1 + (\gamma_1/\gamma_2)]} + 2\tau_R{}^{1/2}\right]}{C(\pi)^{1/2}[\xi_m(0) - E/D]}\right\}} \tag{58}$$

For finite positive values of τ, we must then have $\lambda \leq -2\gamma_1\xi_s/[C(\pi)^{1/2}]$, which implies that $\theta_c \leq -\gamma_1\xi_s 2/(1 + K_2/K_1)$. For the case when $K_2 = K_1$ this simply states that the perturbation temperature at the phase boundary at the time of reversal must be less than $-\gamma_1\xi_s$, which is the perturbation temperature at the top of the sediments. The transcendental equation (58) may be solved graphically for τ_R.

Equation 58 may be too coarse an approximation, since the intersection of $Q(\xi_m, \lambda) = 0$ with $\lambda(\xi_m)$ may be very sensitive to the trajectory $\lambda(\xi_m)$. Since the determination of $(\xi_m(\tau_R), \tau_R)$ is the most subtle of the characteristics of the motion so far discussed, it appears desirable to use the set of equations most consistent with the actual problem and to integrate equation 56 directly. Nevertheless, equation 58 should not be in serious error, since it depends only logarithmically on the value of λ.

Two models that include the effects of thermal blanketing were studied, and numerical solutions were found for θ, ξ_m by solving equations 25 and 26 with the initial and boundary conditions 55. Models 12 and 13 have 3.64 km of sediments deposited on the surface, and the lower boundary condition was fixed at a depth of 95 km beneath the bottom of the sediments. Otherwise models 12 and 13 are identical to models 2 and 11, respectively.

The temperature distributions for model 13 at selected times are shown in Figure 19*b*. The time of reversal is $\tau_R = 0.019$. The temperature curves show that as the time approaches τ_R, the temperature everywhere in the region between the sediment surface and the phase boundary has risen significantly and at τ_R the temperature distribution is dominated by the effect of the sediments. Model 13 takes into account different properties of the phases and the motion of the lower boundary. Nevertheless, the essential behavior is quite similar for both models 12 and 13.

TABLE 4. Actual and Predicted Reversal Times of the Phase Boundary

Model	12	13
τ_R	0.0219	0.0192
$\xi_m(\tau_r)$	0.3175	0.3379
$\bar{\tau}_{R_1}$	0.0278	0.0284
$\tilde{\xi}_m(\bar{\tau}_{R_1})$	0.3117	0.3170
$\bar{\tau}_{R_2}$	0.0162	0.0151
$\tilde{\xi}_m(\bar{\tau}_{R_2})$	0.3022	0.3010

Estimates for τ_R were obtained from equation 58 ($\bar{\tau}_{R_1}$), and by numerically integrating equation 56 ($\bar{\tau}_{R_2}$) to find the point $Q = 0$. These values are given in Table 4, as are the corresponding $\tilde{\xi}_m$ values from equation 34*a*. The agreement of the $\bar{\tau}_R$ with the actual value of τ_R is quite good. For either model, $\bar{\tau}_{R_1}$ overestimates and $\bar{\tau}_{R_2}$ underestimates τ_R. The agreement between $\tilde{\xi}_m(\bar{\tau}_R)$ and $\xi_m(\tau_R)$ is not quite so good, although it is satisfactory. It therefore appears that the theoretical considerations provide a good estimate for the time and position of reversal, as well as a simple functional expression for this time in terms of the initial state of the system for the case of impulsive loading.

Effects of (radioactive) heat sources. The presence of sources enters the problem in two distinct ways: (1) as a term $\alpha(\sigma_1 - \sigma_2)$ in the field equations and (2) in the determination of the initial steady state $\theta(\xi, 0)$ and the final equilibrium state.

The source terms appear explicitely as the difference $\alpha(\sigma_2 - \sigma_1)$ in the field equation in region 3 but are not present in either region 1 or 2. They appear in region 3 only because of the change in spatial concentration due to the density change across the phase boundary, and they would vanish identically if $\rho_2/K_2 = \rho_1/K_1$. This region in which the source term appears comprises only the space between the phase boundary and its initial position, and, therefore, for the initial motion the region is extremely limited. However, owing to the source term, the final equilibrium value of $\partial^2\theta/\partial\xi^2$ will be nonzero, which will result in a curvature in θ in region 3 as compared with the source-free case where $\theta(\xi, \infty)$ is linear in every region. This term thus generates a transient in θ in region 3, owing to the difference between the initial state $\theta(\xi, 0) = 0$ and the curved final state, where $[\partial^2\theta(\xi, \infty)]/\partial\xi^2 = \sigma_1 - \sigma_2$. Insofar as $\alpha(\sigma_2 - \sigma_1)$ is small, as would occur for most geophysical considerations, it is to be expected that the source terms are of little significance in the field equations.

The initial steady state enters the field equations in the term $\nu\ [\partial\eta(\xi, 0)/\partial\xi]$ for convective heat. The effect of sources in making $[\partial\eta(\xi, 0)/\partial\xi]$ a linear function of ξ rather than a constant can be no greater than the effect that the term had in the case with no sources. As pointed out earlier, this term primarily compensates for the mass transport with respect to the fixed spatial coordinates and has only a minor effect.

In the boundary conditions 26*c* and 26*d*, the terms $[\partial\eta(\xi, 0)/\partial\xi]$ appear as the break in slope of $\eta(\xi, 0)$ at the location of the phase boundary due to the

change of conductivity. The effect of these terms will be the same as in the case with no sources. Some minor differences will occur, since in the source-free case the exact magnitude of this term is a constant independent of $\xi_m(0)$. However, in the case with sources, since $\eta(\xi, 0)$ is a quadratic function, the gradient will depend on the position of the phase boundary.

In the models with no sources, the reduced Clapeyron curve $\theta_c(\xi) = \eta_c(\xi) - \eta(\xi, 0)$ was a linear function, $\theta_c(\xi) = D\xi - E$, since both $\eta_c(\xi)$ and $\eta(\xi, 0)$ were linear. When sources are present, however, $\eta(\xi, 0)$ is no longer a linear function; hence $\theta_c(\xi)$ will also be a quadratic function of ξ. This may be seen in Figure 20*a*. This figure compares the initial temperature $T(x, 0)$ and Clapeyron curve $T_c(x)$ for a model with sources (model 14), with $\hat{T}(x, 0)$ and $\hat{T}_c(x)$, for a no-source model (model 11), which is used to approximate the model with sources. The Clapeyron slopes $[dT_c(x)/dx] = d\hat{T}_c/dx \equiv G\rho_1 g$ are equal for both cases, as are the initial positions and temperature gradients at the phase boundary. Making these values coincide and utilizing equations 5 to construct the source-free model required a new value of F and $J(0, 0) \equiv J_i$ in the approximation. Thus $\hat{T}_c(0)$ is less than $T_c(0)$ and $\hat{J}(0, 0)$ is less than $J(0, 0)$. In both cases the application of a pressure pulse ΔP shifts the Clapeyron curve a distance $\Delta P/\rho g$ to the left, and the temperature at the phase boundary increases by the same amount $G\ \Delta P$ for both cases. The reduced Clapeyron curves $\Theta_c(x)$ and $\hat{\Theta}_c(x)$ after application of the pressure pulse are shown on the right of Figure 20*a*. They have the same value and slope at the initial location of the phase boundary $x = M_i$. The initial motion of the phase boundary should thus be the same for both models. Owing to its curvature, $\Theta_c(x)$ diverges from $\hat{\Theta}_c(x)$ for $x \neq M_i$, and the former intercepts the x axis at a smaller value of x. Thus, for longer times the source model will depart slightly from the other, mainly owing to the different final equilibrium position of the phase boundary.

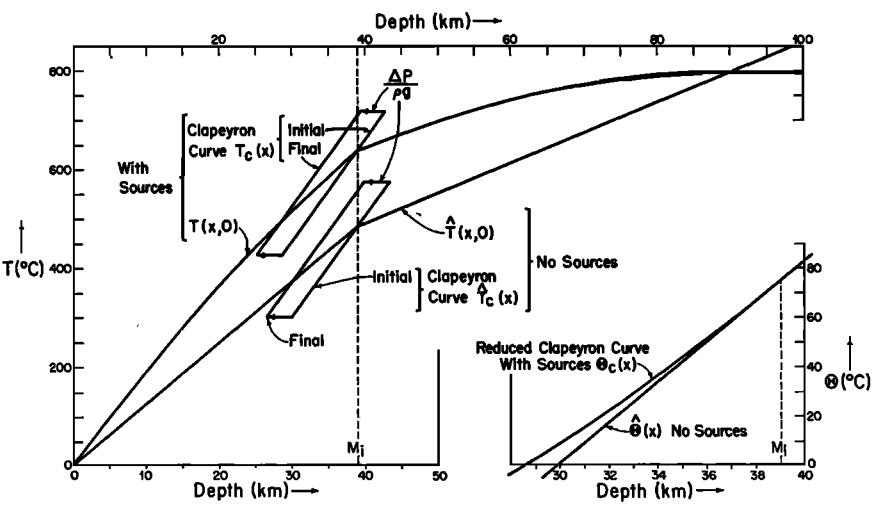

Fig. 20*a*. Initial states for a model with moderate sources and an approximation to it without sources. The shift of the Clapeyron curve is shown. The reduced Clapeyron curve for each model is at lower right. The reduced Clapeyron slopes at the initial location of the phase boundary M_i are the same for both models.

The magnitude of this difference will depend on the curvature of $\Theta(x)$, hence on the magnitude of the sources. For larger sources than those shown here, the final position of the phase boundary could be substantially different for the two models and there would be a larger long-term displacement of the phase boundary for the model with sources. The effect of the curvature per se should be quite small, and, if proper account is taken of the initial and final positions of the phase boundary, the motion of the phase boundaries for the two cases should not differ significantly.

Lastly, it should be noted that the final perturbation temperature distribution will be composed of straight-line segments except for the region between $\xi_m(0)$ and $\xi_m(\infty)$, and that only in this region will the sources directly affect the temperature distribution. Thus the dependence of the solution on the source distribution is extremely limited, and we may therefore expect to be able to represent quite adequately a model with sources by a suitable model with no sources.

In order to compare a model with sources with a 'no-source' approximation to it, a numerical solution was obtained for model 14, which has a source concentration of 3.6×10^{-14} cal/g sec in each phase. These heat sources, distributed through 100 km, are able to account for all the surface heat flux of 1.0 μcal/cm^2 sec, as may be seen in Figure 20*a*. Model 11 is a 'no-source' approximation to model 14 in the sense that both have (1) the same initial position of the phase boundary M_i; (2) the same Clapeyron slope G; (3) the same reduced Clapeyron slope at M_i; and (4) equal initial pressure pulses applied to them, and all other material properties the same. This has been achieved by adjusting the zero intercept of the Clapeyron curve F, and the initial surface heat flux $J(0, 0)$. The resultant values of the parameters are given in Table 1 and 2, and the initial states of both models may be seen in Figure 20*a*.

The motion of the phase boundary for each case is shown in Figure 20*b*. For the first half of the motion, the difference between the two cases is insignificant. Since the final position of the phase boundary is different for each model, the motion for model 14 departs slightly from that for model 11 for longer times. Nevertheless, the behavior of the model with sources is entirely predictable from the model without sources, and we conclude that the effect of sources is insignificant for such cases, except in that they partly determine the final position of the phase boundary.

Since the source concentration in model 14 was not particularly high, a numerical solution was obtained for model 15 in which the source concentration was 1.25×10^{-13} cal/g sec. These sources were distributed only in the upper 40 km of the crust, which was underlain by a layer with no sources but with thermal properties identical to those of the high-density phase. The resultant nonradiogenic heat flux was only 3% of the surface flux of 1.5 μcal/cm^2 sec. The initial state for this model is shown in Figure 21*a*.

The first curve in Figure 21*b* shows the final perturbation temperature for model 15 and illustrates the primary effects of the sources. The curve is not linear in the region between the initial position of the phase boundary M_i and the final position M_f. In addition, the discontinuities in $\partial\Theta/\partial x$ at M_i and M_f are not equal in magnitude, as they would be for a case without sources. The result is

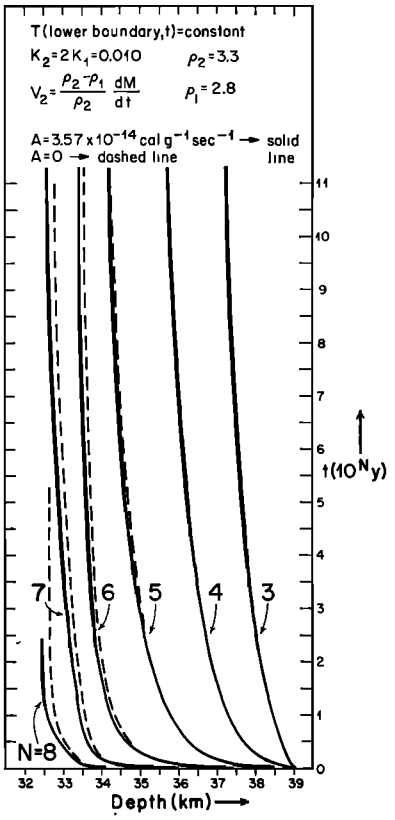

Fig. 20*b*. Motion of the phase boundary for models shown in Figure 20*a* (models 14 and 11). The difference which begins to appear at $t > 3 \times 10^5$ years is due to the different values of $M(\infty)$ for each model (cf. Θ_c in 20*a*). Apart from the difference, the two curves are almost identical.

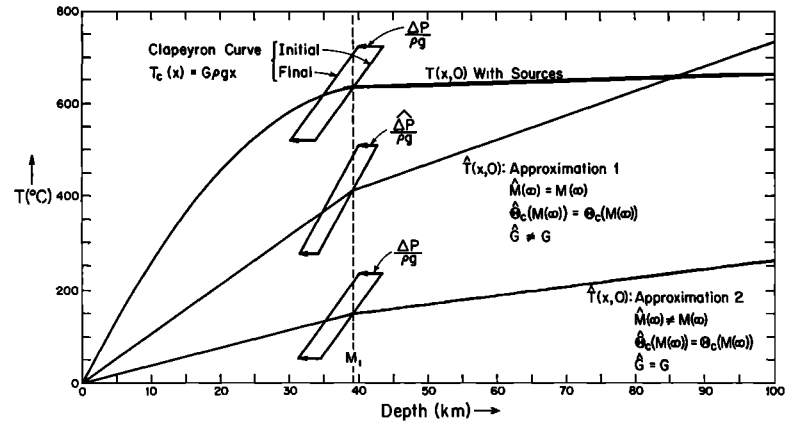

Fig. 21*a*. Initial states for a high-source model (model 15) and two no-source approximations (model 16 and 17). Model 15 has no sources below $x = 40$ km (cf. Figure 22).

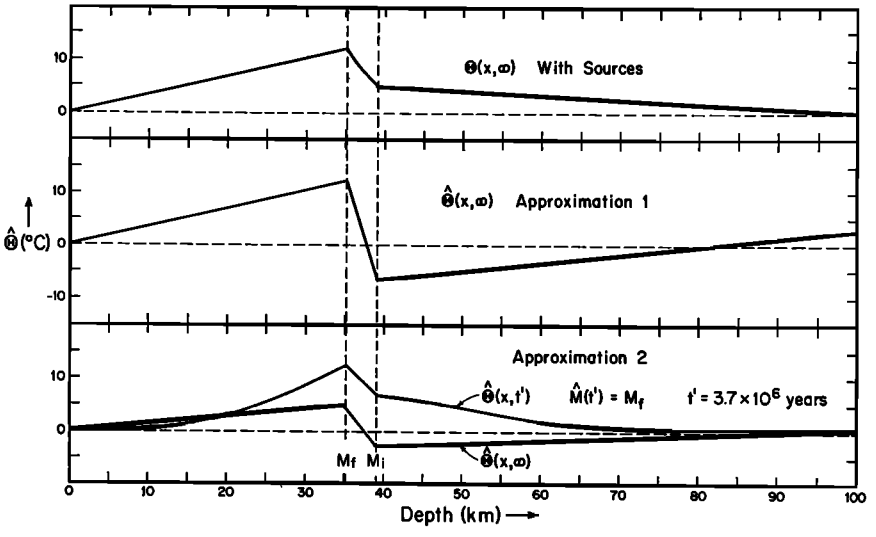

Fig. 21*b*. Final perturbation temperatures for models 15, 16, and 17. Note that $\hat{\Theta}(x, t')$ for approximation 2 comes nearest to $\hat{\Theta}(x, \infty)$ for model 15 (with sources), cf. Figure 22.

that the temperature of the final state is everywhere greater than that of the initial state. This is in marked contrast with the models without sources investigated earlier. We may expect that the result of this will be a limitation of any long-term transients in the motion. The short-term motion should remain unaffected, however, for the same reasons given for model 14.

Model 15 was approximated by models without sources in a manner analogous to the method used previously. In general, in constructing a no-source approximation, certain parameters are adjusted to make certain characteristics of the approximation coincide with those of the model being approximated. For our purpose, we wished to make the following values the same for both models: (1) the initial position of the phase boundary M_i; (2) the final position of the phase boundary M_f; (3) the initial perturbation temperature at the phase boundary $\Theta(M_i, 0)$; and (4) the final perturbation temperature at the phase boundary $\Theta(M_f, \infty)$. This was done by adjusting the following parameters in equations 5, 7, and 26*d*: (1) the initial surface flux $J(0, 0)$; (2) the zero intercept of the Clapeyron curve F; (3) the Clapeyron slope G; and (4) the pressure pulse ΔP. This resulted in model 16, or approximation 1. The initial and final states are given in Figure 21, where it may be seen that the final state differs considerably from that for model 15 in the region behind the phase boundary.

The motion of the phase boundary for each case is shown in Figure 22. Approximation 1 and the model with sources have the same final position for the phase boundary. As can be seen in Figure 21*b*, approximation 1 has a much more prominent long-term transient; hence the phase boundary approaches its final position much more slowly and lags considerably behind the phase boundary of the model with sources. The reason for this lag is that in constructing the approximation we have changed the initial temperature gradient in the vicinity

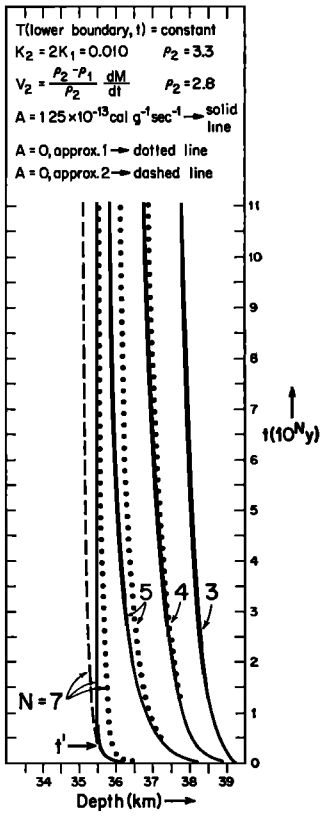

Fig. 22. Motion of the phase boundary for models 15, 16, and 17. Note that the curve for $N = 6$ has been omitted for clarity. Approximation 2 (model 17) is indistinguishable from model 15 for $t < t' = 3.7 \times 10^6$ years (cf. Figure 21).

of the phase boundary, which is obvious in Figure 21*a*. However, as was seen in the section on unmatched thermal constants, the initial temperature gradient enters the dynamic problem through the terms in $\partial\eta/\partial\xi$ in (26*c*) and (26*d*) and results in a slowing of the motion of the phase boundary, which becomes apparent for times near $\tau^{\dagger}$ and dominant for times near $\tau^{\dagger\dagger}$. The slower motion of model 16 is primarily due to the effect of the larger temperature gradient near the phase boundary for this source-free model in comparison to the high-source model. The appearance of this effect by relatively short times indicates that attempts to approximate the long-term motion (in particular the final position of the phase boundary) may seriously affect the short-term motion.

To better approximate the short-term motion, a second no-source approximation, model 17, was constructed in a manner similar to that used to construct model 14. The only difference in the two methods of approximation is that, whereas the Clapeyron curve of model 11 matches the slope of the reduced Clapeyron curve of model 14 at M_i, model 17 has a reduced Clapeyron slope which is intermediate to the reduced Clapeyron slope of model 15 at points M_i and M_f. $J(0, 0)$ and F were adjusted to make the reduced Clapeyron curves for this model and model 15 coincide at M_i and M_f, as determined from model 15. The Clapeyron slope, pressure pulse and initial position of the phase boundary are the same for both models; only the final positions of the phase boundary and

the curvatures of the reduced Clapeyron curves are different. As can be seen in Figure 21*a*, this approximation (approximation 2) is more similar to model 15 in the vicinity of the phase boundary than was approximation 1. Figure 22 shows that this model approximates the motion of the phase boundary extremely well over nearly the entire displacement for model 15. At $t = t'$, the approximation has reached the final position of the phase boundary for model 15, and at this point the two models have the same perturbation temperature at the phase boundary. The temperature distribution at this time may be seen in Figure 21*a*, where its similarity with the final distribution for model 15 is apparent. In contrast, the final distributions for both approximations differ considerably from that for model 15, although approximation 2 appears to be the better one.

These examples indicate that we cannot expect all the aspects of a model with sources to be represented by a no-source model. However, if no attempt is made to accurately model the long-term motion (e.g. by matching M_f), then nearly all of the motion may be accurately modeled so long as the slopes of the temperature and Clapeyron curves are reasonably matched, as was done in models 11 and 17. Thus the effects of sources on the dynamics of the short-term motion are extremely small. The main effect of sources is in the determination of the final steady state, which influences the long-term motion. The numerical results presented here are a clear verification of the conclusions about sources drawn previously from inspection of the field equations in terms of the perturbation temperature.

Time-dependent loading. In all the preceding discussions we have considered only the response to an instantaneous load causing a pressure change ΔP. We will now extend this treatment to the case where P is time dependent; we will determine the condition that obtains when constant sedimentation rates may be approximated by an impulse load, and the criteria that determine if the phase boundary will be in 'secular equilibrium.'

The effects of pressure enter the problem only through the Clapeyron curve $\mathfrak{I}_c(P) = GP - F$; hence the field equations and boundary conditions remain unchanged from those used so far, with the exception of the condition for the temperature at the phase boundary (26*e*), (27*d*). In dimensionless form this becomes

$$\theta_c(\xi_m(\tau)) = D\xi_m(\tau) - E(\tau) \tag{59}$$

where

$$E(\tau) = (F/T_0) - [GP(t)/T_0] \equiv E(0) - \varphi(\tau)$$

$P(t)$ is the time-dependent pressure applied at the surface. In all the previous cases with impulse loading, $P(t)$ has been a step function of magnitude ΔP:

$$P(t) = 0 \qquad t < 0$$

$$P(t) = \Delta P \qquad t \geq 0$$

We have shown that the generalized Stefan approximation is an accurate representation for impulsive loading for short times primarily because of the singular behavior. In addition, by comparison with the numerical solution, it appears

that this approximation yields a reasonable description even after significant motion of the phase boundary has taken place, as long as the effects of the upper boundary are not strong. These conclusions apply to any impulsive loading, however small. It therefore follows that the initial motion should always be of the Stefan form even for an infinitesimal ΔP. This suggests that more realistic models with finite loading rates may be approximated with a sequence of small impulsive loadings, even though the problem is nonlinear. We are thus led to apply a Stefan-type expression to approximate the temperature field for finite sedimentation rates and thus obtain an equation for $d\xi_m/d\tau$. Letting $\theta(\xi, \tau) = \tilde{\theta}_{SA}(\xi, \tau)$ as before, we obtain from (27*c*), and (29)

$$C\frac{d\xi_m}{d\tau} \approx -\frac{\theta_c(\xi_m)}{\pi^{1/2}\tau^{1/2}} \exp(-\lambda^2)\left[\frac{1}{1 - \operatorname{erf}\lambda} + \frac{1}{1 + \operatorname{erf}\lambda}\right] \tag{60}$$

where we have assumed $\rho_1 = \rho_2$, $K_1 = K_2$, $\kappa_1 = \kappa_2$ for simplicity, and $\lambda(\xi_m) = [\xi_m(0) - \xi_m(\tau)]/2\tau^{1/2}$ as before. For a sufficiently small impulsive load, λ as determined from $n(\lambda) = \theta_c/C$ is small. Therefore, for continuous loading with $P(0) = 0$, $n(\lambda)$ will be linear in λ for some time. For such a case $\theta(\xi, \tau) \approx \tilde{\theta}_{SAC}(\xi, \tau)$, where $\tilde{\theta}_{SAC}(\xi,\tau) \equiv \tilde{\theta}_{SA}(\xi, \tau)$ under the condition $\eta(\lambda) \approx (\pi^{1/2}/2)\lambda$ and $\Delta P = P(t)$. Equation 60 then becomes

$$C\frac{d\xi_m}{d\tau} \approx \frac{-2}{\pi^{1/2}}\frac{\theta_c}{\tau^{1/2}} = \frac{-2}{\pi^{1/2}}\frac{(D\xi_m - E(\tau))}{\tau^{1/2}}$$

or

$$\frac{d(\xi_m(0) - \xi_m)}{d(\tau)^{1/2}} = \frac{-4D}{C(\pi)^{1/2}}(\xi_m(0) - \xi_m) + \frac{4}{C(\pi)^{1/2}}(E(0) - E(\tau)) \tag{61}$$

The condition of secular equilibrium is defined when the left-hand side of (61) is negligible and $\xi_m \approx E(\tau)/D$. This will be the case when

$$\left|\frac{1}{[E(0) - E(\tau)]}\frac{d}{d\tau}[E(0) - E(\tau)]\right| \equiv \left|\frac{1}{\varphi}\frac{d\varphi}{d\tau}\right| \ll \frac{2D}{C(\pi)^{1/2}}\tau^{-1/2}$$

This criterion defines the conditions under which the system will respond to the loading.

Direct integration of (61) yields

$$\xi_m(0) - \xi_m(\tau) = \frac{r}{D}\exp(-r\tau^{1/2})\int_0^{\tau^{1/2}} \exp(rZ^{1/2})[E(0) - E(Z)]\, d(Z^{1/2}) \tag{62}$$

where $r \equiv 4D/C(\pi)^{1/2}$ is the natural rate constant for the system. Hence transients will decay as $\exp(-r\tau^{1/2})$, and a criterion for long times when transients will have decayed is $r\tau^{1/2} \equiv [4D/C(\pi)^{1/2}]\,\tau^{1/2} \gg 1$. If the loading rate is a linear function of time, $\varphi(\tau) = E(0) - E(\tau) = DR\tau$, where R is a constant determining the loading rate. In this case the criterion for secular equilibrium is $r\tau^{1/2} \gg 2$, and that for long times is $r\tau^{1/2} \gg 1$, which are essentially the same. This criterion is independent of the loading rate. The time over which this approximation is valid will depend on the length of time before the effects of the upper boundary become large.

For a constant loading rate as above, (62) becomes

$$\xi_m(0) - \xi_m(\tau) = R\tau + \frac{2R}{r^2} - \frac{2R}{r}\tau^{1/2} - \frac{2R}{r^2}\exp(-r\tau^{1/2}) \tag{63}$$

or equivalently

$$\xi_m(0) - \xi_m(\tau) = 2Rr\tau^{3/2}\sum_{n=0}^{\infty}\frac{(-1)^n}{(n+3)!}(r\tau^{1/2})^n$$

$$= (R\tau)2r\tau^{1/2}\left[\frac{1}{3!} - \frac{1}{4!}r\tau^{1/2} + \cdots\right]$$

The significance of the criteria for secular equilibrium and long times is apparent from these equations. In addition it may be seen that the initial velocity is proportional to $\tau^{1/2}$; hence the singular behavior that is characteristic of the Stefan problem is no longer present.

We may represent an impulsive load by requiring that the product $R\tau$ remain finite as $\tau \to 0$. The loading function is then

$$E(0) - E(\tau) = RD\tau \qquad 0 \leq \tau \leq \Delta E/RD \equiv \tau_0$$

$$E(0) - E(\tau) = \Delta E \text{ (a constant)} \qquad \tau \geq \tau_0$$

Using this in (62), we obtain

$$\xi_m(0) - \xi_m(\tau) = \frac{\Delta E}{D}\left[1 - \exp(-r\tau^{1/2})\sum_{n=0}^{\infty}\frac{2(n+1)}{(n+2)!}(r\tau_0^{1/2})^n\right] \tag{64}$$

for $\tau > \tau_0$. For an impulse, $\tau_0 \to 0$ and the infinite sum on the right of (64) approaches 1. Thus, the criterion for an impulsive load is that the terms other than the first in the sum may be neglected, or

$$\tfrac{2}{3}r\tau_0^{1/2} = \tfrac{2}{3}r(\Delta E/RD)^{1/2} \ll 1$$

Thus the time criterion for impulsive loading is independent of the loading rate, and the response to any load deposited in a time considerably less than $\tau_0 = (3/2r)^2$ will be as for an impulsive load. For the models considered here, this time corresponds to ~1 million years. In this case (64) becomes for $\tau > \tau_0$

$$\xi_m(0) - \xi_m(\tau) = \frac{\Delta E}{D}[1 - \exp(-r\tau^{1/2})] = \frac{\Delta E}{D}r\tau^{1/2}\left(1 - \frac{r\tau^{1/2}}{2} + \cdots\right)$$

and $d\xi_m/d\tau$ is initially singular and proportional to $\tau^{-1/2}$ as required for an impulse. In addition, since $\xi_m(0) - \xi_m(\infty) = \Delta E/D$, we may write the preceding equation as

$$\xi_m(\tau) - \xi_m(\infty) = (\Delta E/D)\exp(-r\tau^{1/2})$$

which agrees with (47). It should be remembered that the above results hold only when

$$[\theta_c(\xi_m)/C] = n(\lambda) \approx [(\pi)^{1/2}/2]\lambda$$

i.e., they hold only for small pulses, and not for such large pulses as we have discussed in the previous sections.

A more general result for larger λ may undoubtedly be obtained by extension of the methods given in this paper.

Numerical solutions were obtained for three models with linear pressure loading. The models (18, 19, 20) were similar to model 2 and corresponded to the gutted problem. The loading rate R was taken as 0.1, 1.0, and 10.0 in models 18, 19, and 20, respectively. These correspond to sedimentation rates of roughly 10, 100, and 1000 m/10^6 years. The motion of the phase boundary for each model is shown in Figure 23. The initial motion, as seen in Figure 23*a*, is proportional to $\tau^{3/2}$, as predicted by equation 63. The irregularities in the curves result from numerical errors due to changes in the space and time steps, which were necessary to limit the computation time. The logarithmic plot exaggerates the numerical irregularities for short times.

The motion for longer times is best seen in Figure 23*b*. Note that the time scale is different for each curve. Thus the curve for $R = 0.1$ extends up to $\tau = 1.0$ ($R\tau = 0.1$) or $t = 355 \times 10^6$ years. Long-time behavior and secular equilibrium should obtain for $\tau^{1/2} \gg 1/r \approx 0.04$. Thus, for $\tau^{1/2} \sim 0.4$ or $\tau \sim 0.1$, secular equilibrium should obtain and transients will have decayed. As can be seen, the phase boundary is in secular equilibrium after this time and follows $E(\tau)/D$ at a constant distance.

For the Stefan approximation, the lag l of the phase boundary behind $E(\tau)/D$ is

$$l = (2R/r^2)(r\tau^{1/2} - 1 + e^{-r\tau^{1/2}}) \tag{65}$$

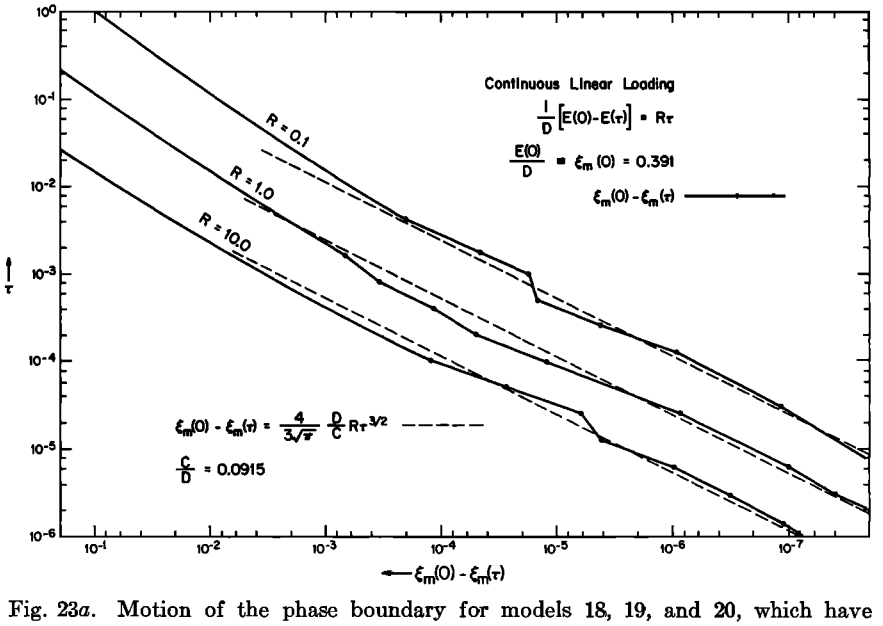

Fig. 23*a*. Motion of the phase boundary for models 18, 19, and 20, which have constant loading rates. The dashed curves show the initial motion expected from the Stefan approximation. The irregularities in the computed curves (solid lines) are due to numerical errors (see text).

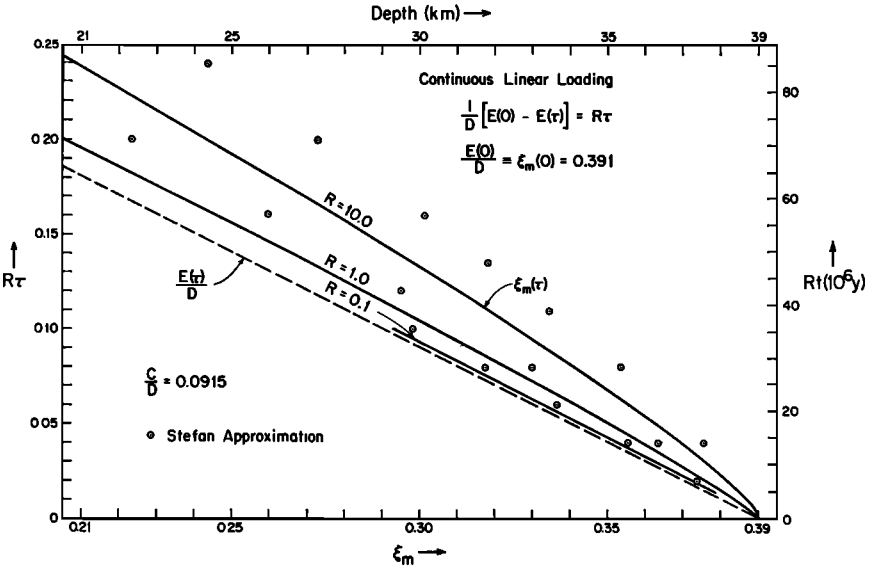

Fig. 23*b*. Linear plot of Figure 23*a* showing the motion of the phase boundary for a constant loading rate proportional to R. If secular equilibrium obtains, $\xi_m(0) - \xi_m(\tau) = R\tau$ and all continuous linear loading curves would fall on the same straight line, which is dashed. The times may be obtained from the $R\tau$ or Rt scales by dividing by R. $R = 0.1$, 1.0, and 10.0 correspond to sedimentation rates of 10, 100, and 1000 m/10^6 years, respectively. The solutions from the Stefan approximation are shown as individual points, which in each case lie above and to the right of the corresponding numerical solution. All curves lag behind $E(\tau)/D$; the Stefan approximation overestimates the actual lag.

At $\tau = 0.16$, the lag should be 0.003 in ξ or ~300 meters for $R = 0.1$. Inspection of Figure 23*b* shows that the lag remains around this value up to the time the computation was stopped when the displacement was around 10 km.

The case for $R = 1.0$ is similar. Thus the lag at $\tau \sim 0.1$ or $t \sim 35 \times 10^6$ years should be ~0.022 or 2.2 km. The actual lag is ~0.015, and the phase boundary follows $E(\tau)/D$ at this distance after this time. Similarly the lag for the case $R = 10$ at $\tau = 0.02$ is 0.055, rather than 0.08, as predicted. In both cases this is probably due to errors incurred in the linear approximation of $n(\lambda)$, which causes the Stefan approximation to overestimate the actual lag. For $\tau > 0.02$ in model 20 ($R = 10$), the lag does not increase much and the phase boundary follows $E(\tau)/D$.

The approximate solution for the position of the phase boundary without assuming secular equilibrium (equation 63) is rather good. A comparison of the computed results and those obtained from (63) are also shown in Figure 23 and indicate the accuracy of the approximation. The lag from (63) is seen to be greater than the computed lag, as mentioned before, and appears to place an upper bound on the magnitude of the lag.

The effect of the surface should become apparent for $\tau \sim \xi_m^2 \sim 0.1$ or $t \sim 35 \times 10^6$ years. The boundary condition $\theta(0, \tau) = 0$ will result in the removal of

more heat from the vicinity of the phase boundary than would be the case for an infinite medium. This in turn would tend to decrease the lag of the phase boundary behind $\xi = E(\tau)/D$. The fact that the observed lag is smaller than that predicted by (65) is undoubtedly due to the boundary effect at $\xi = 0$ in addition to the SAC approximation for the temperature field. For long times the surface effect predominates and the Stefan approximation should no longer apply.

These three models span the range of sedimentation rates that would be expected in a reasonable geophysical model, and comparison of the numerical and theoretical results indicates that it should be possible to estimate the response of most models with reasonable accuracy.

In the preceding discussion we have neglected the thermal impedance of the sediments. As discussed in the section on thermal blanketing, sediments will cause the temperature beneath them to rise, eventually stopping and reversing the motion of the phase boundary. The time at which this occurs is of paramount importance, since it signals the end of subsidence and onset of uplift, and hence also the cessation of sedimentation. Thus this will control the total amount of sediments, which in turn determine the total uplift.

As we did for impulsive loading, we approximate the temperature field by superposing the temperature due to the sediments on the temperature from the Stefan approximation. Since the thickness of the sediments, s, will in general be small compared with the depth of the phase boundary, we shall neglect it. The boundary condition of the surface is thus

$$\theta(0, \tau) \approx \theta(\xi_s, \tau) = -\gamma_1 \xi_s(\tau)$$

If s is not small in comparison with ξ_m, this case will overestimate the effect of the surface. For loading that is proportional to the time (constant sedimentation rate), the initial and boundary conditions for the temperature due to the sediments, $\tilde{\theta}_{BC}(\xi, \tau)$, are

$$\begin{aligned} \tilde{\theta}_{BC}(\xi, 0) &= 0 && 0 \leq \xi \leq \xi_m \\ \tilde{\theta}_{BC}(0, \tau) &= (\gamma_1 \rho_1 WR/\rho_s)\tau && \tau \geq 0 \\ \tilde{\theta}_{BC}(\xi_m, \tau) &= 0 && \tau \geq 0 \end{aligned}$$

where

$$W = [1 - J(0, 0)/G\rho_1 g K_1] = D(T_0/G\rho_1 g b_0).$$

ρ_s is the density of the sediments and R is the rate parameter:

$$R = \frac{1}{b_0 W} \frac{\rho_s}{\rho_1} \frac{dt}{d\tau} \frac{ds}{dt} = \frac{1}{W} \frac{\rho_s c_1 b_0}{K_1} \frac{ds}{dt}$$

We will treat ξ_m as constant in the derivation of $\tilde{\theta}_{BC}$, which is justified as long as the displacement of ξ_m is small compared with $\xi_m(0)$.

The solution to this problem is given by *Carslaw and Jaeger* [1959, p. 102]. We are concerned with the heat flux at the phase boundary, ξ_m, since it is this value that will influence the motion of the phase boundary. This is

$$\left.\frac{\partial \tilde{\theta}_{BC}}{\partial \xi}\right|_{\xi=\xi_m} = \frac{-\gamma_1 \rho_1 WR}{\rho_s} \left[\frac{\tau}{\xi_m} - \frac{\xi_m}{6} - \frac{2\xi_m}{\pi^2} \sum_{n=1}^{\infty} \frac{(-1)^n}{n^2} \exp\left(-\frac{n^2 \pi^2}{\xi_m^2} \tau\right)\right]$$

This may be added to the flux due to the Stefan approximation to determine the velocity of the phase boundary, as was done in (56).

$$-C\frac{d\xi_m}{d\tau} \approx \frac{\partial\tilde{\theta}_{\mathrm{BC}}}{d\xi}\bigg|_{\xi=\xi_m-} + \frac{\partial\tilde{\theta}_{\mathrm{SAC}}}{\partial\xi}\bigg|_{\xi=\xi_m-} - \frac{\partial\tilde{\theta}_{\mathrm{SAC}}}{\partial\xi}\bigg|_{\xi=\xi_m+}$$

This can then be integrated numerically from $\tau = 0$ to find the reversal time τ_R when $d\xi_m/d\tau = 0$. This is analogous to equation 56 for the case of impulsive loading.

Alternatively, if secular equilibrium obtains before the reversal time, then $-C(d\xi_m/d\tau) \approx RC$. But since this is proportional to the flux out of the phase boundary for the Stefan approximation, the criterion indicating the reversal of the motion may be approximated by

$$\frac{\partial\tilde{\theta}_{\mathrm{BC}}}{\partial\xi}\bigg|_{\xi=\xi_m-} + \frac{\partial\tilde{\theta}_{\mathrm{SAC}}}{\partial\xi}\bigg|_{\xi=\xi_m-} - \frac{\partial\tilde{\theta}_{\mathrm{SAC}}}{\partial\xi}\bigg|_{\xi=\xi_m+} = 0$$

or

$$\frac{\partial\tilde{\theta}_{\mathrm{BC}}}{\partial\xi}\bigg|_{\xi=\xi_m-} + RC = 0$$

Thus, at the time of reversal, the following relationship should approximately obtain:

$$\frac{C\rho_s}{\gamma_1\rho_1 W}\xi_m + \frac{\xi_m^2}{6} = \tau - \frac{2\xi_m^2}{\pi^2}\sum_{n=1}^{\infty}\frac{(-1)^n}{n^2}\exp\left(-\frac{n^2\pi^2}{\xi_m^2}\tau\right) \tag{66}$$

This may be combined with equation 63 and solved graphically for the time of reversal $\tilde{\tau}_R$. This is analogous to equation 58 for impulsive loading.

If ξ_m can be estimated, then (66) can be used alone to determine τ_R. For the parameters in models 18, 19, and 20, $\tilde{\tau}_R = 0.048$, 0.061, and 0.074 for $\xi_m = 0.25$, 0.30, and 0.35, respectively. These values correspond to times of 17, 22, and 26 million years. In each case the exponential terms have been negligible and $\tilde{\tau}_R \approx (C\rho_s/\gamma_1\rho_1 W)\xi_m + \xi_m^2/6$. If we substitute $\xi_m(\tau) = \xi_m(0) - R\tau$ in this equation, a quadratic equation for $\tilde{\tau}_R$ is obtained and the dependence on the rate R is readily seen.

Thus the reversal time depends only weakly and indirectly (through $\xi_m(\tau)$) on the sedimentation rate. It is of interest to note that it depends on the ratio C/D (since W is proportional to D).

We have not obtained numerical solutions for models including continuous sedimentation and the thermal impedance of the sediments. These will be considered in a later paper considering the more complex geophysical problem. Nevertheless, the accuracy of the above expressions for the reversal time should not be in serious error and should exhibit the dependence of $\tilde{\tau}_R$ on the parameters of the model used, if we may judge from the cases for which we have obtained numerical solutions, in particular models 12 and 13.

5. EFFECTS OF ISOSTASY

In order to consider the effect of isostasy in conjunction with a phase change, we find it convenient to consider the following model:

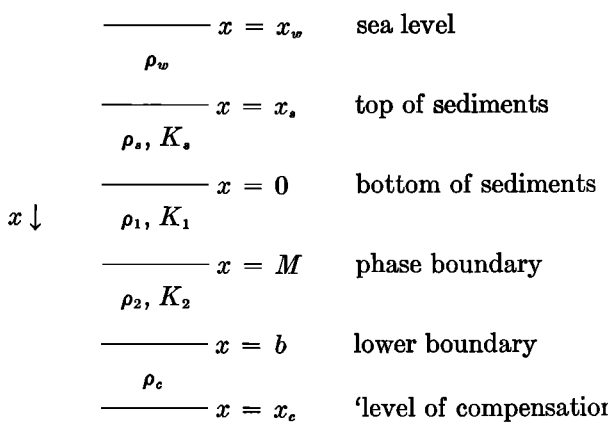

Mean sea level, x_w, is taken as a reference level, fixed with respect to the center of the earth. The depth of water is $w = x_s - x_w$; similarly, the sediment thickness is $s = -x_s$. The densities of the water and the sediments are ρ_w and ρ_s, respectively.

We shall consider isostatic equilibrium to obtain if the mass per unit area is the same after the deposition of sediments as it was before. This is equivalent to considering a crustal block floating in a denser fluid substratum.

We assume that the mass per unit area is always constant below $x = x_c$ which is fixed with respect to the center of the earth, so that $x_c - x_w$ is constant. Thus the mass per unit area above x_c will be constant if the column is in isostatic equilibrium, isostatic adjustments being made by varying the amount of matter of density ρ_c between $x = b$ and $x = x_c$ by lateral flow.

For simplicity we discuss the case with no heat sources and with constant heat flux at the lower boundary $x = b$. This is not a severe limitation, since in many cases an appropriate 'no-source approximation' can be constructed for models with sources. In addition we define

$$\rho_w(w) = \begin{cases} 1 & \text{if } w \geq 0 \\ 0 & \text{if } w < 0 \end{cases}$$

since $w < 0$ corresponds to the top of the sediments, x_s, being above sea level, in which case no water will be present. This allows generalization of the model to treat cases of deposition and erosion above sea level.

The initial state of the model will be specified by the initial depth of the water, w_0, the initial sediment thickness, which we take as zero, and the initial location of the phase boundary, which will be determined by the intersection of the Clapeyron curve and the temperature distribution in the earth. The location of the lower boundary b will depend on the total mass of material between $x = 0$ and $x = b$, which will be constant and on the position of the phase boundary.

If sediments of thickness s are deposited on the surface $x = 0$, the phase boundary will initially move only in response to the pressure load, but it will lag behind its equilibrium position by a distance l as discussed in the previous section. The resultant conversion of the low-density (ρ_1) phase to the high-density (ρ_2)

phase will result in the subsidence of the material in the region above the phase boundary. In addition, the entire block $x \leq b$ will subside, owing to the isostatic response to the load of the sediments. The exact magnitude of this subsidence will depend on how rapidly isostatic adjustments are made. Except where otherwise stated, we shall assume that the time scale of isostatic adjustments is much shorter than that of the response of the phase boundary; consequently, we assume that a state of isostatic equilibrium always obtains. If on the other hand the time scale for isostatic adjustment is much greater than the time for the phase boundary to respond (as may be determined from the Stefan approximation), then the effects of isostasy will not be important and may be neglected altogether.

For longer times the effect of thermal blanketing by the sediments will influence the motion of the phase boundary and may cause it to reverse the direction of its motion. For times less than the time of reversal, which can be estimated, the effect of thermal blanketing will be small, as was shown in the previous section on thermal blanketing and reversals. Thus we may discuss the response of the model to sedimentation for times less than the time of reversal by neglecting the thermal effect of the sediments altogether. We will include the effect of thermal blanketing later in the discussion.

The requirement that the mass per unit area be conserved in the regions $x \leq x_c$ and $J \leq x \leq b$, subject to $x_c - x_w$ constant, gives the following relation between the sediment thickness $s(t)$, water depth $w(t)$, and initial water depth w_0. At any given instant of time

$$Q_w w - Q_{w_0} w_0 + Q_s s = -l\rho_1[(1/\rho_1) - (1/\rho_2)] \tag{67}$$

where

$$Q_i \equiv \rho_i\left[\left(\frac{1}{\rho_i} - \frac{1}{\rho_c}\right) - \frac{1}{W}\left(\frac{1}{\rho_1} - \frac{1}{\rho_2}\right)\right]; \qquad i = s,\ w,\ w_0$$

and

$$W \equiv 1 - (J_M/K_1 G g \rho_1)$$

Since ρ_w is a function of w, to allow the treatment of cases involving uplift above sea level ($x_s < x_w$ or $w < 0$), we must distinguish between Q_w and Q_{w_0}. The lag of the phase boundary, $l(t)$ is defined as the distance of the boundary behind the position it would have if thermal equilibrium obtained at each instant of time. Equation 67 applies to a source-free model, in which case $J_M = J(0, 0)$. To treat a case when sources are present it is necessary to model the case with sources by a no-source approximation, as discussed in the section on radioactive heat sources. In this case, $J_M \approx K_1[T(M(0), 0) - T(M(t), 0)]/[M(0) - M(t)]$ and J_M is considered as a constant.

If $\rho_1 = \rho_2$, the phase change will have no effect on subsidence, and (67) reduces to the equation for isostatic adjustment alone [*Jeffreys*, 1962, p. 336]. Similarly, we can obtain the effect of the phase change alone in the absence of isostatic adjustment by letting $\rho_c \to \infty$ in (67). It should be noted that, when $Q_s = 0$, equation 67 is independent of s and the sediment thickness is indeterminate.

The nature of the subsidence can best be seen by differentiating (67):

$$dw/ds = -(Q_s/Q_w) - (\rho_1/Q_w)[(1/\rho_1) - (1/\rho_2)]\, dl/ds \tag{68}$$

At a given instant of time a negative value of dw/ds corresponds to a basin being filled as a result of sedimentation or, conversely, a decrease in elevation as a result of denudation. If $dw/ds = 0$, the subsidence rate will be exactly equal to the sedimentation rate and the water depth will remain the same even though sediments are deposited. If $dw/ds > 0$, the water depth will increase with sedimentation. For this case then, if the rate of sedimentation increased with the water depth, initial sedimentation would cause subsidence, which would result in even more rapid sedimentation and subsidence. Hence we shall regard the case $dw/ds > 0$ as dynamically unstable. The two previous cases we shall regard as dynamically stable ($dw/ds < 0$) and neutrally stable ($dw/ds = 0$), respectively.

Assuming $Q_w > 0$, a given model will be dynamically unstable if

$$Q_s + \rho_1[(1/\rho_1) - (1/\rho_2)](dl/ds) < 0$$

As can be seen from the definition of Q_s, this term will be negative for $(1/W)$ $[(1/\rho_1) - (1/\rho_2)] > (1/\rho_s - 1/\rho_c)$, which will be the case for sufficiently small $W\ J_M/(K_1\ G g \rho_1)$ or sufficiently close to 1.0. This condition can be attained for values of the parameters that are not outside the range of probability. (For example, for model 11, $Q_s = -0.012$ if $\rho_s = 2.4$ and $\rho_c = 3.5$.) In this case the value of dl/ds becomes critical in determining the sign of dw/ds, and hence the dynamic stability of the system. Systems that exhibit dynamic instability at one time may become stable at later times, and conversely. This is due to the time dependence of $l(t)$.

It should also be noted that the possibility of instability is not due solely to the presence of the phase change, since instability would result if $\rho_s > \rho_c$ with no phase change. The phase change does, however, permit instability to occur for $\rho_s < \rho_c$, as would generally be expected in a geophysical model. The instabilities discussed here appear to have been overlooked by previous workers.

If we consider the case of a constant sedimentation (or denudation) rate, then we can evaluate dl/ds for the Stefan approximation (SAC) from (65):

$$\frac{dl}{ds} \approx \frac{\rho_s L(1 - W)}{4J_M W^2} \left(\frac{\pi K_1}{\rho_1 c_1}\right)^{1/2} t^{-1/2} \left\{1 - \exp\left[-\frac{4J_M W}{\rho_1 L(1 - W)} \left(\frac{\rho_1 c_1}{\pi K_1}\right)^{1/2} t^{1/2}\right]\right\}$$

Values for dw/ds for models 11 and 17, taking $\rho_s = 2.4$, $\rho_w = 1.0$, and $\rho_c = 3.5$ are given in Table 5. These models are no-source approximations to models 14 and 15, respectively.

As can be seen, the lag of the phase boundary prevents model 11 from being unstable. Examination of Figure 23*b* reveals, however, that the Stefan approximation overestimates the lag by about a factor of 2. If we had used the value of the lag from the numerical solution rather than from the Stefan approximation, the model would have shown the instability, as may be seen by substituting in (67) directly. Thus the possibility of accumulating thick deposits of sediments in relatively shallow water exists for models similar to model 14.

The values of dw/ds in Table 5 should be contrasted with the value $dw/ds = -0.44$ for the case with isostasy alone and with no phase change effect. Thus the phase change has a noticeable effect on model 17, even though this model may

TABLE 5. Effect of Phase Change with Isostasy on Subsidence Due to Sedimentation

Time, 10^6 yr	dw/ds, Model 11	dw/ds, Model 17
0.2	−0.41	−0.37
1.0	−0.29	−0.32
5.0	−0.16	−0.27
10.0	−0.13	−0.26
15.0	−0.090	−0.26
20.0	−0.075	−0.26
30.0	−0.057	−0.26
50.0	−0.040	−0.26
All times (no phase change)	−0.44	−0.44

be considered conservative in terms of the magnitude of Q_s (since W is relatively large). The effect of the phase change in model 11 is very marked, as would be expected, owing to the negative value of Q_s.

If we consider a basin subject to sedimentation as long as the surface is below sea level, sedimentation will stop when either (1) the basin fills up or (2) the motion of the phase boundary reverses, owing to thermal blanketing, eventually causing the surface to be elevated above sea level. The maximum thickness of sediments that could be deposited in the basin will be attained if (1) occurs, i.e. if the basin fills completely before the phase boundary reverses; hence this maximum thickness is given by setting $w = 0$ in (67). For neutrally stable or unstable cases, this may result in a root for s that is negative and does not constitute a real physical solution. Since the time at which the phase boundary reverses motion has been estimated in the previous section, one can roughly determine whether or not this maximum thickness will be attained for a given sedimentation rate. If (2) occurs first, sediment thickness may be estimated from the sedimentation rate and the reversal time. The exact thickness will depend on the amount deposited after reversal.

After the reversal of the phase boundary, the effect of thermal blanketing will dominate the motion. Hence, since the thermal blanketing effects of the surface were completely neglected, equation 67 will no longer apply. Instead the elevation $(-w)$ will be given by

$$Q_w w - Q_{w_0} w_0 + Q_s' s = -l\rho_1[(1/\rho_1) - (1/\rho_2)] \tag{69}$$

where Q_w and Q_{w_0} are as defined in (67) and l is the lag (or lead) of the phase boundary from the position it would have if thermal equilibrium including the effects of the sediments obtained at each instant of time. This is the same definition as before; however the thermal blanketing effects are now to be included.

$$Q_s' = Q_s + (K_1\rho_1/K_s)(1/Y)[(1/\rho_1) - (1/\rho_2)]$$

where $Y \equiv (Gg\rho_1 K_1/J_s) - (J_M/J_s)$ and where J_s/K_s is the average temperature gradient in the sediments. If there are no heat sources in the sediments, $J_s =$

$J(0, 0)$. The problem of sedimentation in a basin may now be approached by considering the possible sequences of events. The maximum sediment thickness that can be accumulated in a basin will occur if the basin completely fills up before the thermal blanketing causes the phase boundary to reverse its motion. This thickness may be found by setting $w = 0$ in equation 67. The time necessary for the deposition of this thickness of sediments can then be obtained from the sedimentation rate. If this time is greater than the reversal time of the phase boundary, then the reversal of the boundary, resulting in uplift, may cause the surface to rise above sea level before the above-mentioned maximum sediment thickness has been attained. In this event the sediment thickness may be estimated from the sedimentation rate and the reversal time. In either event, once the sediment thickness is known, the maximum final elevation can be determined from (69) by setting $l = 0$, which is equivalent to assuming that the final steady-state thermal equilibrium has been attained. This maximum elevation would be attained only under the exceptional circumstance of no erosion and then only after a time sufficiently long for the region $x_s \leq x \leq b$ to approach thermal equilibrium. For a region ~100 km thick, this would be of the order of 10^8 years. Since the Stefan approximation certainly does not apply after the reversal of motion of the phase boundary, we will not attempt to estimate the uplift in the event of erosion. It should be noted, however, that, owing to isostatic compensation and the effect of the phase change (through the term dw/ds discussed above), the erosion of a given thickness of sediment will not cause a decrease in elevation of the same amount but rather less.

In Table 6 are the maximum sediment thicknesses calculated from equation 67 with $w = 0$ and the final elevations calculated from equation 69 for various values of the lag of the phase boundary for several cases. All of the cases employ the physical parameters used in model 15 (to which model 17 is the appropriate no-source approximation), but with various values for the surface heat flux (J_s) and sediment conductivity (K_s). In all cases J_M, the heat flux in the vicinity of the phase boundary, and all other relevant parameters are identical to those in model 17 (or 15). This may be considered a fairly conservative model, since, as shown in Table 5, the value of dw/ds is not especially small. If the ratio $J_M/K_1Gg\rho_1$ were greater, as would be the case if more heat originated below the phase boundary, i..e for $x > M$, then the sediment thickness and final elevation could be substantially greater. This would also be the case for denser sediments, a less dense substratum, or a greater density change with the phase change than considered here.

The first six cases are for marine deposition and later emergence above sea level. The last case, on the other hand, treats the rapid erosion to a reference level (taken arbitrarily at sea level) of a surface initially 1 km above that reference level. Since there is no water present, the ratio of the change in elevation to the sediments removed (dw/ds) is less than would be the case for a marine environment.

For all cases for the values of l given in Table 6, model 11 is unstable; i.e., the only limit to the sediment thickness is the time of reversal of the phase boundary. Since this has been previously shown to be ~20 million years, the

TABLE 6. Possible Sediment Thickness and Final Elevation Assuming No Erosion for Models (including phase change and isostasy)

J_s Average Flux in Sediments, μ cal/cm²/sec	K_s Conductivity of Sediments, cal/cm/sec/°C	w_0 Initial Water Depth, km	l Lag of Phase Boundary, km	s† Maximum Thickness of Sediments, km	$-w$ Maximum Final Elevation, km
1.0	0.005	3	0	12.6	2.3
			2	10.6	1.6
			4	8.6	1.0
1.2	0.005	3	0	12.6	2.7
			2	10.6	2.0
			4	8.6	1.3
1.2	0.0035	3	0	12.6	3.9
			2	10.6	3.0
			4	8.6	2.1
1.5	0.005	3	0	12.6	3.4
			2	10.6	2.6
			4	8.6	1.7
		5	0	21.0	5.7
			2	19.0	4.8
			4	17.0	4.0
1.5	0.0035	3	0	12.6	4.9
			2	10.6	3.8
			4	8.6	2.7
1.5	0.005	−1*	0	−6.5	−1.7*
			−1	−5.5	−1.3*
			−2	−4.5	−0.92*
			−3	−3.5	−0.50*

* Surface initially above sea level, subsequently eroded to sea level. Weight of water neglected.
† $\rho_s = 2.4$; $\rho_c = 3.5$.

sediment thickness will be just the amount that can be deposited in that time, and it will be independent of the initial water depth.

Thus, there seems to be little difficulty in accounting for thick sections of sediments that were deposited in relatively shallow water, so long as the deposition was sufficiently rapid. The long-term evolution of the surface after uplift will depend on the erosion of the surface above sea level and may be subject to an extension of the simple analysis as presented in this paper.

The possibility of a small value of dw/ds would indicate that rapid erosion rates may not substantially reduce the elevation of the eroded surface.

6. SUMMARY

The dynamic response of a phase boundary to sudden changes in pressure has been investigated by considering a one-dimensional model of two layers separated by a phase change. The problem was formulated in terms of a dimensionless perturbation temperature by subtracting the initial steady temperature distribution. In this form the simplest case, neglecting radioactive heat sources, convective heat transport, and the difference in thermal properties of the two phases, may be approximated by a simple generalization of Neumann's solution to the problem of freezing at a constant temperature. Comparison of the approximate solution with exact numerical solution revealed that the approximation very accurately described both the initial motion of the phase boundary and the temperature distribution. More complex models considering the differences in thermal properties of the two phases may also be accurately described by the approximate solution up to a time that may be determined from the approximation. In all cases, the initial motion is completely determined from (1) the ratio of the latent heat of the phase change to the difference between the Clapeyron slope and the earth's temperature gradient and (2) the product of the Clapeyron slope and the applied pressure divided by the latent heat.

The motion of the phase boundary for long times may also be accurately described from simple considerations based on the over-all geometry of the model. In addition to (1) above, the motion then depends most critically on the location of, and the boundary conditions at, the lower boundary. Since for most geophysical models the effects of the lower boundary will probably dominate the behavior for long times, the choice of this boundary condition is extremely important and is probably the most severe limitation of a one-dimensional model that attempts to describe the complete geophysical problem.

The effect of convective heat transport, which is partly estimable from the approximate solution, has been shown to be small for many geophysical cases by direct comparison of numerical solutions. Thus neglect of the convective term in the field equations is probably justified, considering the implicit limitations of a one-dimensional model and the uncertainties in the parameters.

Radioactive heat sources were shown to enter the problem only in the region through which the phase boundary actually moved. In addition, comparisons of numerical solutions indicated that the effect of sources per se on the dynamics of the motion is small. Thus a model with sources can be adequately approximated by a model without sources to which all the previous conclusions apply.

The effect of thermal blanketing by sediments has also been considered. The approximate time at which the blanketing would cause the phase boundary to reverse its motion may be determined from an analytic expression or by the integration of a first-order linear differential equation. Since the time at which reversal occurs signals the start of uplift, this criterion is especially important.

The approximate solution for impulsive loads was extended to the case of continuous sedimentation at a constant rate, and the accuracy verified by comparison with numerical solutions for sedimentation rates ranging from $\sim$10 meters/10^6 years to $\sim$1000 meters/10^6 years. It was shown that a condition of secular equilibrium would eventually obtain, where the phase boundary would follow

the applied load, and criteria were presented to determine when such a situation would obtain. In addition, the criterion determining when a continuous load would appear as an impulsive one was determined and shown to be independent of the loading rate. Similarly, the time at which the phase boundary would reverse its motion was shown to have only weak dependence on the loading rate, and an explicit expression for this time was given.

The effect of a phase change in conjunction with isostatic compensation on subsidence due to sedimentation was shown to be major. For a proper choice of reasonable parameters, the thickness of sediments that can be deposited in a basin is limited primarily by the time at which the phase boundary reverses motion, and *not* the initial depth of water. For a phase change at a depth of ~40 km, this time is ~20 million years; thus for a wide variety of cases, where the basin is not filled before reversal the sediment thickness depends almost exclusively on the sedimentation rate. The final elevation after uplift and attainment of thermal equilibrium can be substantial; the actual elevation will depend, however, on erosion rates after uplift, which have not been studied here. The proper study of the problem including erosion will depend strongly on the actual long-term behavior. Since this behavior will be dominated by the boundary conditions at depth, the problem of the proper choice for this condition must be resolved for further progress with a one-dimensional model.

The existence of reasonably accurate analytic approximations to the actual solution permits the dependence of the solution on the various parameters to be readily seen. This allows various geophysical models to be considered without the need of obtaining numerical solutions for each one. In addition, certain characteristics of the solution may be identified (e.g. long- or short-term motion), or certain aspects of the model may be characterized in terms of their effect on the solution (e.g. slow or rapid sedimentation). The problem may be separated into rather distinct physical processes with characteristic time constants. The characteristic times are determined from the initial state of the model. Insofar as the characteristic times of the various processes are distinct, the separate modes of the motion are then subject to an a priori analysis. When the characteristic times overlap, the motion may be more complicated. This allows the determination of the conditions under which the motion of a phase change will be an important geophysical process. Once this is done, the problem of whether such conditions actually exist may be treated separately.

APPENDIX 1

The gutted problem is formulated for $\theta(\xi, \tau)$, $\xi_m(\tau)$:

$$\partial\theta/\partial\tau = \partial^2\theta/\partial\xi^2 \qquad 0 \leq \xi < \xi_m, \quad \xi_m < \xi \leq 1, \quad \tau > 0 \tag{A1}$$

$$\theta(0, \tau) = \theta(1, \tau) = 0, \qquad \tau \geq 0 \tag{A2}$$

$$\left.\frac{\partial\theta}{\partial\xi}\right|_{\xi=\xi_m^+(\tau)} - \left.\frac{\partial\theta}{\partial\xi}\right|_{\xi=\xi_m^-(\tau)} = C\frac{d\xi_m}{d\tau} \tag{A3}$$

$$\theta(\xi_m(\tau), \tau) = D\xi_m(\tau) - E, \qquad \tau \geq 0 \tag{A4}$$

$$\theta(\xi, 0) = 0, \qquad \xi \neq \xi_m(0); \qquad \theta(\xi_m(0), 0) = D\xi_m(0) - E \tag{A5}$$

$$C, D, E \text{ constants}, \quad 0 < E < D, \quad 0 < \xi_m(0) < 1, \quad C \geq D\xi_m(0) - E \tag{A6}$$

We will show that these equations determine the initial motion of the phase boundary, that the phase boundary is bounded by the equilibrium position and the initial position, that the temperature to the right of the phase boundary always lies beneath the Clapeyron curve, and that the sign of $\partial^2\theta/\partial\xi^2$ immediately to the right of the phase boundary is determined.

Multiplying (A1) by θ and integrating

$$\int_0^{\xi_m} \frac{\partial}{\partial\xi}\left(\theta\frac{\partial\theta}{\partial\xi}\right) d\xi + \int_{\xi_m}^1 \frac{\partial}{\partial\xi}\left(\theta\frac{\partial\theta}{\partial\xi}\right) d\xi$$
$$= \int_0^{\xi_m}\left[\left(\frac{\partial\theta}{\partial\xi}\right)^2 + \frac{1}{2}\frac{\partial}{\partial\tau}(\theta^2)\right] d\xi + \int_{\xi_m}^1\left[\left(\frac{\partial\theta}{\partial\xi}\right)^2 + \frac{1}{2}\frac{\partial}{\partial\tau}(\theta^2)\right] d\xi$$

Carrying out the integration on the left and substituting (A2), (A4), and (A5)

$$(D\xi_m(\tau) - E)\left(-C\frac{d\xi_m}{d\tau}\right)$$
$$= \int_0^{\xi_m}\left[\left(\frac{\partial\theta}{\partial\xi}\right)^2 + \frac{1}{2}\frac{\partial}{\partial\tau}(\theta^2)\right] d\xi + \int_{\xi_m}^1\left[\left(\frac{\partial\theta}{\partial\xi}\right)^2 + \frac{1}{2}\frac{\partial}{\partial\tau}(\theta^2)\right] d\xi$$

Integrating with respect to τ and using (A5), which implies

$$\int_0^1 \theta^2(\xi, 0)\, d\xi = 0$$

we obtain

$$\int_0^\tau [D\xi_m(\tau) - E]\left[-C\frac{d\xi_m}{d\tau}\right] d\tau$$
$$= \int_0^\tau\left[\int_0^{\xi_m}\left(\frac{\partial\theta}{\partial\xi}\right)^2 d\xi + \int_{\xi_m}^1\left(\frac{\partial\theta}{\partial\xi}\right)^2 d\xi\right] d\tau + \frac{1}{2}\int_0^1 \theta^2(\xi, \tau)\, d\xi$$

This is strictly positive, since the terms on the right are positive and vanish only if θ and $\partial\theta/\partial\xi$ vanish identically on the whole interval. If the integration is carried out on the left

$$C[(D/2)(\xi_m(0) + \xi_m(\tau)) - E][\xi_m(0) - \xi_m(\tau)] > 0$$

By reductio ad absurdum $D\xi_m(0) - E > 0$ implies $\xi_m(0) - \xi_m(\tau) > 0$ and $D\xi_m(0) - E < 0$ implies $\xi_m(0) - \xi_m(\tau) < 0$. Thus the phase boundary is constrained to lie on only one side of its initial position, and the sign $(d\xi_m/d\tau)|_{\tau=0^+}$ is determined.

By applying the maximum-minimum principle, we now show that $\xi_m(\tau)$ never crosses $\xi = E/D$, which is the only equilibrium position for the phase boundary. This principle states that, if $\partial^2\theta/\partial\xi^2 = \partial\theta/\partial\tau$ on a region in space R with boundary B, that both the maximum and minimum of θ on R for $\tau_1 \geq \tau \geq 0$, where τ is some arbitrary time, will be attained for either $\xi\epsilon B$, $\tau_1 \geq \tau > 0$ or $\xi\epsilon R$, $\tau = 0$.

Hence, the extrema must lie on the boundaries

$$\xi = 0, \quad \xi = \xi_m(\tau), \quad \tau > 0 \quad \text{or} \quad 0 \leq \xi \leq \xi_m(0), \quad \tau = 0 \quad \text{in region 1}$$

or

$$\xi = \xi_m(\tau), \quad \xi = 1, \quad \tau > 0 \quad \text{or} \quad \xi_m(0) \leq \xi \leq 1, \quad \tau = 0 \quad \text{in region 2}$$

If the zero of the Clapeyron curve has not been crossed, $\xi_m(\tau) \geq E/D$. Use of the minimum principle then shows $\theta(\xi, \tau) \geq 0$. If ξ_m approaches E/D from the right, then $d\xi_m/d\tau < 0$. We now show that $d\xi_m/d\tau$ either goes to zero or reverses sign, if $\xi_m = E/D$.

$$\left.\frac{\partial\theta}{\partial\xi}\right|_{\xi_m = E/D^+} = \lim_{\epsilon \to 0}\left[\frac{\theta[(E/D) + \epsilon, \tau] - \theta[(E/D), \tau]}{\epsilon}\right] \geq 0$$

and similarly

$$\left.\frac{\partial\theta}{\partial\xi}\right|_{\xi_m = E/D^-} \leq 0$$

Hence, from (A3)

$$\left.\frac{d\xi_m(\tau)}{d\tau}\right|_{\xi_m = E/D^+} \geq 0$$

at the boundary, whereas it is negative when approaching the boundary; hence, $\xi = E/D$ is never crossed and $\xi_m(\tau) \geq E/D$.

We now show that the Clapeyron curve is never exceeded in region 2. Consider the function $\theta'(\xi, \tau) = \theta(\xi, \tau) - (D\xi - E)$ in region 2. Since obviously $\partial^2\theta/\partial\xi^2 = \partial\theta'/\partial\tau$, we may apply the maximum principle. Since

$$\begin{aligned} \theta'(\xi, 0) &= -(D\xi - E) < 0 && \xi_m(0) < \xi \leq 1 \\ \theta'(1, \tau) &= -(D - E) < 0 && \tau > 0 \\ \theta'(\xi_m(\tau), \tau) &= 0 && \tau \geq 0 \end{aligned}$$

then $\theta'(\xi, \tau) \leq 0$ or $\theta(\xi, \tau) \leq D\xi - E$. Thus the temperature to the right of the phase boundary always lies beneath the Clapeyron curve. In addition, if $\xi_m(\tau) < \xi_m(0)$, applying the maximum principle to θ shows that $\theta(\xi, \tau) < \theta(\xi_m(0), 0) = D\xi_m(0) - E$.

We now exhibit a relationship that determines the sign of $\partial^2\theta/\partial\xi^2$ at the phase boundary. This or an analogous relationship may be useful in providing insight to other problems of this type.

Since $\theta(\xi_m, \tau) = D\xi_m - E$, we obtain by the chain rule

$$D\frac{d\xi_m}{d\tau} = \left.\frac{\partial\theta}{\partial\xi}\right|_{\xi=\xi_m}\frac{d\xi_m}{d\tau} + \left.\frac{\partial\theta}{\partial\tau}\right|_{\xi=\xi_m} = \left.\frac{\partial\theta}{\partial\xi}\right|_{\xi=\xi_m}\frac{d\xi_m}{d\tau} + \left.\frac{\partial^2\theta}{\partial\xi^2}\right|_{\xi=\xi_m}.$$

Hence

$$\left.\frac{\partial^2\theta}{\partial\xi^2}\right|_{\xi=\xi_m} = \left[D - \left.\frac{\partial\theta}{\partial\xi}\right|_{\xi=\xi_m}\right]\frac{d\xi_m}{d\tau}$$

To the right of the phase boundary, θ is bounded by the Clapeyron curve; hence

$$D - \frac{\partial \theta}{\partial \xi}\bigg|_{\xi=\xi_m+} \geq 0$$

Therefore

$$\frac{\partial^2 \theta}{\partial \xi^2}\bigg|_{\xi=\xi_m+} \Big/ \frac{d\xi_m}{d\tau} \geq 0$$

Thus, if $d\xi_m/d\tau \leq 0$, then

$$\frac{\partial^2 \theta}{\partial \xi^2}\bigg|_{\xi=\xi_m+} \leq 0$$

and the shape of the temperature curve to the right of the phase boundary is always convex upward. In addition, from consideration of the initial conditions (A5), for a short enough time, say $\tau < \tau_1$,

$$\frac{\partial \theta}{\partial \xi}\bigg|_{\xi=\xi_m-} > D; \qquad \text{hence } \frac{\partial^2 \theta}{\partial \xi^2}\bigg|_{\xi=\xi_m-} \Big/ \frac{d\xi_m}{d\tau} < 0 \quad \text{for} \quad \tau < \tau_1$$

Thus, the initial shape of the temperature curve near the phase boundary is determined.

APPENDIX 2

For numerical solution, the derivatives in equations 25, 26, and 27 were replaced by standard finite difference approximations [*Forsythe and Wasow*, 1964]. The field equation $\partial\theta/\partial\tau = \partial^2\theta/\partial\xi^2$ was replaced by the implicit difference equation

$$\frac{\theta(\xi, \tau + k) - \theta(\xi, \tau)}{k} = \frac{\theta(\xi - h, \tau + k) - 2\theta(\xi, \tau + k) + \theta(\xi + h, \tau + k)}{h^2} \tag{A7}$$

where h and k are the space and time increments, respectively. This may be written, with $\mu = k/h^2$, as

$$\theta(\xi, \tau) = -\mu\theta(\xi - h, \tau + k) + (1 + 2\mu)\theta(\xi, \tau + k) - \mu\theta(\xi + h, \tau + k) \tag{A8}$$

which may be regarded as a system of simultaneous linear equations for the values of $\theta(\xi, \tau + k)$ at the net points $\xi = ih$, $i = 0, 1, 2, \cdots$. If the number of equations is finite and suitable boundary conditions are applied at the end points of the region, the above system can be solved for $\theta(\xi, \tau + k)$ in terms of $\theta(\xi, \tau)$ at the net points.

The advantage of such an implicit method is that it is stable for all values of μ; that is, it obeys the same maximum-minimum principle as does the original differential equation [*Forsythe and Wasow*, 1964, p. 102].

The above method can be applied in each of the regions $0 \leq \xi \leq \xi_m$ and $\xi_m \leq \xi \leq 1$, provided $\xi_m(\tau + k)$, and hence $\theta(\xi_m(\tau + k), t + k)$ are known. If $\xi = m_1 h$ and $\xi = m_2 h$ are the net points immediately to the left and right of the

phase boundary, and $h_1 \equiv \xi_m - m_1 h$, $h_2 \equiv m_2 h - \xi_m$, the boundary condition 27c becomes

$$\xi_m(\tau + k) - \xi_m(\tau) = \frac{k}{C}\left[\frac{\theta(m_2 h, \tau') - \theta(\xi_m, \tau')}{h_2} - \frac{\theta(\xi_m, \tau') - \theta(m_1 h, \tau')}{h_1}\right] \quad \text{(A9)}$$

where τ' may be τ or $\tau + k$. $\theta(\xi_m, \tau')$ is given by the Clapeyron curve, once $\xi_m(\tau')$ is known.

The method of solution used was: knowing $\theta(\xi, \tau)$, $\xi_m(\tau)$,

(1) $\xi_m(\tau + k)$ was calculated from (9) by letting $\tau' = \tau$. Hence, $\theta(\xi_m, \tau + k)$ was calculated.
(2) The system of equations (A8) was solved for the net points $i = 1, \cdots, m_1$ and $i = m_2 \cdots, n$ where $(n + 1)\ h = 1$, by Gauss' elimination method.
(3) $\xi_m(\tau + k)$ was recalculated from (A9), using $\tau' = \tau + k$.
(4) Using this new value of $\xi_m(\tau + k)$, steps 2 and 3 were repeated.
(5) If two successive determinations of $\xi_m(\tau + k)$ were within a certain limit of one another, the iterative process was stopped and the whole process was repeated for the next time step.

The equation A9 gives the velocity of the phase boundary at a given time; the average velocity over a time step was used to calculate the movement of the phase boundary:

$$\xi_m(\tau + k) - \xi_m(\tau) = \tfrac{1}{2}k\left[\frac{d\xi_m}{d\tau}\bigg|_{\tau=\tau} + \frac{d\xi_m}{d\tau}\bigg|_{\tau=\tau+k}\right]$$

In addition, since the velocity of the phase boundary is singular at $\tau = 0$, it was assumed in analogy with the classical Stefan problem that $d\xi_m/d\tau$ was proportional to $\tau^{-1/2}$ for short times. Thus $\xi_m(k) - \xi_m(0)$ could be calculated from $(d\xi_m/d\tau)\big|_{\tau=k}$. (For problems in which the singular behavior is of paramount importance a change of variable to $\sqrt{\tau}$ may be desirable). In order to check this assumption, the integral form of the boundary condition

$$-C\frac{d\xi_m}{d\tau} = \frac{d}{d\tau}\int_0^1 \theta\, d\xi + \frac{\partial\theta}{\partial\xi}\bigg|_{\xi=0} - \frac{\partial\theta}{\partial\xi}\bigg|_{\xi=1}$$

was used in the computer program, performing the integral numerically by the trapezoidal rule. In this way the displacement of the phase boundary is determined directly for each time step rather than the velocity. Thus it was found, using this form of the boundary condition:

$$\frac{\xi_m(2k) - \xi_m(0)}{\xi_m(k) - \xi_m(0)} = 1.44$$

Using the differential form including the assumption on $d\xi_m/d\tau$ gave a ratio slightly closer to $2^{1/2} = 1.414$, which was the expected value. Considering the inherent difficulties in treating such a singularity numerically, the results were considered acceptable.

The singularity in velocity at $\tau = 0$ also made it desirable to use an extremely fine space net and small time steps. The retention of such a fine net, however, would have required a prohibitively long execution time for the solution to proceed to large enough values of τ. Therefore, provisions were made in the program both for making the space net coarser and for varying the time step. The space net was made coarser at times chosen so that θ would be sufficiently smooth to be relatively unaffected by the change. The time step k was doubled whenever $|\xi_m(\tau + k) - \xi_m(\tau)|$ was less than a predetermined minimum. A maximum step was set, though, beyond which k was not increased. Comparisons in trial cases showed no significant differences between cases where the maximum k resulted in $\mu = 3.2$ or where μ reached 102.4. In the solutions used in this paper, μ varies from 0.1 initially to a final value of 51.2.

Comparisons of trial solutions with different net spacings and time steps indicated: (1) refinement of the space net caused the phase boundary to move faster, especially for small τ; and (2) a smaller time step caused the phase boundary to move more slowly, especially for small τ. The maximum difference between any two trial solutions for the location of the phase boundary at a given time was 300 meters, and this difference appeared during the first 15% of the 9 km of total movement of the phase boundary, the difference decreasing slowly during the last 85%.

Thus, the finite net spacing and time steps seem to cause errors of opposite sign that are significant only during the initial phases of the solution. These errors may be attributed primarily to the singularity in velocity at time $\tau = 0$. The solutions presented in this paper have all been performed with the same net spacing and initial time steps; comparisons among them should therefore be subject to relatively little error.

Acknowledgments. We wish to acknowledge helpful discussions with M. Lees who suggested the method of numerical solution in appendix 2 and some of the mathematical results in appendix 1. Some of the initial investigations of the steady-state aspects were done by A. Ramo. We wish to thank C. Chase for his careful efforts in the calculation and tabulation of the special functions used in this work.

This work was supported by the National Science Foundation.

REFERENCES

Carslaw, H. S., and J. C. Jaeger, *Conduction of Heat in Solids,* 510 pp., Oxford University Press, 1959.

Forsythe, G. E., and W. R. Wasow, *Finite Difference Methods for Partial Differential Equations,* 444 pp., John Wiley & Sons, 1964.

Jeffreys, Harold, *The Earth, Its Origin, History and Physical Constitution,* 438 pp., Cambridge University Press, 1962.

Kennedy, G. C., The origin of continents, mountain ranges, and ocean basins, *Am. Scientist, 47,* 491, 1959.

Lovering, J. F., The nature of the Mohorovicic discontinuity, *Trans. Am. Geophys. Union, 39,* 947–955, 1958.

MacDonald, G. J. F., and N. F. Ness, Stability of phase transitions within the earth, *J. Geophys. Research, 65,* 2173–2190, 1960.

Neumann, Franz, Lecture (mentioned in Riemann-Weber: *Die partiellen Differentialgleichungen der mathematischen Physik*, vol. 2, p. 121, 5th edition, 1912), 1860.

Ringwood, A. E., and D. H. Green, Experimental investigations bearing on the nature of the Mohorovicic discontinuity, *Nature, 201,* 566–567, Feb. 8, 1964.

Wetherill, G. W. Steady-state calculations bearing on geological implications of a phase-transition Mohorovicic discontinuity, *J. Geophys. Research, 66,* 2983–2993, 1961.

(Manuscript received May 8, 1967; revised July 12, 1967.)